

# MOON: ORIGIN AND EVOLUTION OF MULTI-RING BASINS

W. K. HARTMANN and C. A. WOOD

*IIT Research Institute, Tucson, Ariz. U.S.A.*

and

*Lunar and Planetary Laboratory, University of Arizona, Tucson, Ariz. U.S.A.*

(Received 14 January, 1971)

**Abstract.** This paper summarizes current data and new observations on lunar basin systems. Parts 1–4 review earlier literature and give new crater-counts used to reconstruct basin histories. Among the results are: basin rings are defined by faults, hills, craters, and/or wrinkle ridges; all of these are inter-related;  $\sqrt{2}$  plays a special role in the ratios of ring diameters; flooding occurred in many basins prior to the formation of the familiar front-side maria; 3 km is a typical depth of lava flooding in basins. Parts 5–11 interpret these results in terms of origin and evolution of basins. Polar concentrations of basins and old, large craters are found (Figures 28 and 29). Basins originated by impacts of very early planetesimals left over from or created during formation of the Moon (6). Concentric fractures were produced by the impacts. Concentric rings developed along fractures during subsequent sagging of the basin into partially melted substrata, along the lines of theory and experiments by Lance and Onat (1962) (Figures 36 and 37). There is marginal empirical evidence that some rings formed significantly after their basins (8). The structure of specific rings depended on the nature of volcanic products extruded. Wrinkle ridges, 'peak-rings', rings of craters, concentric graben, and central peaks are all consequences of basin-forming evolutionary processes (9, Figure 41). Flooding by lava was a final stage in basin evolution. Lava extruded from concentric ring-faults, wrinkle ridges, and crater and basin rims (10). Mascons are directly correlated with the amount of mare lava, but not correlated with basin age or morphology (11). Section 12 summarizes the results and compares them to those of other authors.

## 1. Introduction

The purpose of this paper is to describe newly-identified multi-ring basin systems on the far side of the Moon, review our current knowledge of all the basin systems, and discuss new data bearing on the origin of basins and associated features. A number of new basins have been discovered and measured by use of enhanced Orbiter positive transparencies supplied by NASA. Since these photographs are significantly better than the widely circulated unenhanced Orbiter prints, some of them are reproduced here.

Stuart-Alexander and Howard (1970) have recently described some farside basins in a review of basin and mare distribution; we will extend and supplement, not duplicate, their work.

## 2. Nomenclature

There has been both semantic and substantive confusion over the nomenclature of basins. With the 1959 discovery by Lunik 3 that the lunar farside was deficient in maria, some authors erroneously stated that the farside was deficient in larger craters,

or the large circular, crater-like depressions which some of the frontside maria occupy. This error still persists, in spite of various findings that there is no evidence for a difference between front and backside terrae in pre-mare crater or basin densities (Hartmann, 1966a; Stuart-Alexander and Howard, 1970; etc.). The confusion arises because of insufficient distinction between the *mare material* and *structural depressions* it occupies. The backside is deficient in *maria*, but not in circular-basins.

In 1962, when the Orientale system was first recognized, the term *basin* was introduced to denote circular depressions with remarkable *concentric rings* and *radial lineaments* (Hartmann and Kuiper, hereafter denoted H/K, 1962). Basins are obviously not comparable to mare material and are distinguished from ordinary craters by the ring-and-lineament systems. It was found that many basins could be recognized on the frontside, all in a more damaged state than Orientale, but all with concentric and/or radial structure which distinguished them from craters. They were larger than all but the largest craters and usually stratigraphically old. The term basin was used not to imply a genetic distinction from craters, but only as a convenient way to note the peculiar morphologic distinction.

The nomenclature was unfortunately expanded when the Soviet analysts of Zond 3 photographs introduced the term *thalassoid* to refer to large, unflooded, crater-like depressions on the farside (Lipsky, 1965). Lipsky compared them to *maria*, adding to confusion between surface deposits (*maria*) on the one hand and structural features (*basins*) on the other. The original definition of *maria* was purely colorimetric: they were the dark patches which Galileo's contemporaries took to be oceans. We now know them to be plains of basalt-like composition showing numerous evidences of volcanic emplacement; evidently they are lava flows. The new 'thalassoids' should have been compared not with *maria*, but with large craters and basins. This was subsequently done and it was found that they were indistinguishable from craters, or unflooded basins, and that there were examples of them on the front side, and that they fit onto the diameter distribution of frontside craters (Hartmann, 1966a). Therefore, we propose to discard the term 'thalassoid'.

Cartographic nomenclature is also somewhat confused. Traditionally, *maria* are named after metaphysical influences or states of mind supposedly caused by the Moon. Craters are named after men. On the front side, since most basins are flooded, they were given only mare-names,\* e.g., the Crisium basin. Some, however, were originally identified as craters, e.g., the Grimaldi basin. On the backside most basins are not flooded, and at the 1970 meeting of the *International Astronomical Union*, most were named as craters – scientists' names – e.g., the Schrödinger basin. The minor inconsistency – mixing surnames and metaphysical names among the basins – is a necessary consequence of the traditional nomenclature system.

Two further inconsistencies are now in the official IAU nomenclature. One multi-ring basin was named Apollo, and one mare occupying a multi-ring basin was named after Moscow – presumably not intending to indicate a state of mind.

\* The recognition of the assigning of underlying structural basins being much more recent than the front-side nomenclature.

TABLE I  
Nomenclature

Term	Definition	Recommendation
Mare material	Relatively smooth and dark material of the sort originally thought to be oceans by contemporaries of Galileo. Can occur in basins, craters or irregular depressions.	Use to refer to the smooth dark material without genetic implication.
Mare	A large deposit of mare material, whether in a circular basin or irregular depression. <sup>a</sup>	Use only to refer to dark material; never to be used to refer to basin structures or other depressions.
Basin	Used to designate the largest circular depressions, resembling craters but having concentric rings and radial structures. Basins may or may not be flooded by mare material	Use only to distinguish depressions with large concentric-radial systems from ordinary craters. Flooded basins, if unnamed, can be designated by the accompanying mare name, e.g., 'Orientale basin'.
Thalassoid	Used by Lipsky (1965) to designate large, crater-like circular depressions lacking mare material on their floors. Some are ordinary craters and some are 'dry' or 'unflooded' basins.	The term thalassoid is unnecessary.
Crater	Circular structures with raised rims and depressed interiors, whether flooded or unflooded by mare material, but lacking the characteristic concentric and radial structures of the basins. Craters are usually but not always smaller than basins. Includes impact and endogenic structures.	Use without genetic implication.

<sup>a</sup> In this paper we conclude that certain light-toned, flat plains are old mare material thinly covered by high-albedo debris. These are not properly called maria because of the albedo.

In this paper we have adopted the definitions summarized in Table I. Since many of the circular maria of the front side happen to occupy unnamed basins, we use the name of the mare to refer also to the basin (e.g., 'Orientale' or the 'Orientale basin'). There remains an unavoidable inconsistency: some of the smallest basins have been assigned names of men while others have only metaphysical names (e.g., the Grimaldi basin; the Nectaris basin).

### 3. Review of Observations and Hypotheses

Many of the early selenographers recognized the systems of scarps and parallel lineaments that make up the concentric and radial families of various basins, but they did not recognize the consistent appearance of these features as diagnostic of a *class* of structures. Gilbert (1893) was first to recognize that 'furrows' and 'sculpture'

widespread on the Moon constituted a pattern of radial lineaments centered on Mare Imbrium. Gilbert's was the most comprehensive study until the 1940's. Baldwin (1949) described a number of mountain rings and depressed zones surrounding certain lunar maria. An extensive review of the pre-1960 literature on basin systems is given by Hartmann (1963).

A widespread class of basin systems was recognized by H/K (1962) with the application of rectified photography. This revealed the Orientale 'bull's-eye' for the first time and a number of other concentric ring systems too close to the limb to be well-studied without rectification. When the new basins were studied as a group, the following observations were made:

- (1) The ratio of successive ring diameters is usually about  $\sqrt{2}$  or in some cases 2.
- (2) The rings (often excepting the inner ring) have the morphology of fault scarps, with steeper inner faces. Innermost rings are frequently composed of isolated peaks instead of continuous scarps.
- (3) Flooding by mare material occurs preferentially at the centers of the basin systems and sometimes along the bases of major scarps.
- (4) The central maria often exhibit concentric wrinkle ridge and rille systems, extending the axial symmetry expressed in the terrae.
- (5) There were substantial and variable intervals between basin formation and subsequent flooding. This rules out the oftstated hypothesis that the mare material was entirely impact-produced.
- (6) The basins with the best-developed concentric ring systems are stratigraphically youngest.

Hartmann (1963, 1964) extending this work to radial systems of lineaments around basins. Further observations included:

- (7) Radial systems are a systematic feature of basins, but are best-developed only in the stratigraphically youngest.
- (8) Around some basins, the radial lineament systems are most pronounced in the NE- and NW-trending directions, as if enhanced by the global grid systems which run in those directions. Some basins show a deficiency in E-W trending lineaments.
- (9) Orthogonal patterns, *en echelon* arrangements, and crater-form segments of lineaments indicate that the large-scale lineaments (width >2 km) are primarily the result of faulting, not scouring by flying ejecta.
- (10) Large-scale radial lineaments are best displayed outside the outermost concentric ring. Inside this ring, they are displayed in regions of partial flooding.

From these observations it was hypothesized that the lunar basins are giant impact craters, consistent with the views first set forth in modern form by Gilbert (1893) and Baldwin (1949). The impact hypothesis was extended by inferring that impact-caused stresses produced concentric and radial fractures outside the largest craters' rims. The heating and resulting expansion of the Moon due to internal radioactivity led to faulting along the concentric fractures, producing the prominent concentric scarps. The overlying crust subsided into a more plastic interior as lava extruded and flooded the inner floors of the basins. In some cases, exemplified by the Orientale

basin, lava gained access to the surface not only through the fractures under the central basin, but also along the concentric faults, producing arcuate maria at the base of the fault scarps. At the same time, tectonic activity along the radial fractures produced faults, graben, and crater chains.

From the same observations, it was hypothesized that tectonic activity at the time of the mare flooding also led to the production of faults, grabens, and crater chains along the radial fractures. These were identified with the *multikilometer-width* radial lineaments visible from the Earth. This view of endogenic evolution of the radial lineaments contrasts with a school of thought which describes the radial valleys as grooves gouged out by flying fragments blown from the central basin (Steavenson, 1919; Urey, 1952; Fielder, 1961). After the Orbiter pictures showed high resolution views, several authors described the *hectometer-width* lineaments as furrowed ground scoured by nuee-ardente-like fluidized ejecta clouds or 'base surges' (Masursky, 1968; Hartmann and Yale, 1968; Guest and Murray, 1969). It now appears that multi-kilometer-width lineaments are associated with faulting while hectometer-width lineaments are produced by fluidized clouds.

Fielder (1963) hypothesized that the concentric ring systems and the basins themselves were endogenic. He referred to theoretical and experimental work by Lance and Onat (1962) that suggests that circular plates sagging into a fluid medium below will fracture with the characteristic  $\sqrt{2}$  radius ratios found in lunar basin systems. Because of the experimental results, Fielder hypothesized that the outer rings were oldest and the inner rings, youngest. We will return to the Lance-Onat paper, which is perhaps the best available laboratory analog to basin systems.

Baldwin (1963) proposed a different view of the rings' origin. He described them as ring anticlines and synclines and proposed that when the inner basin formed by impact, a radiating concentric shock wave was frozen at some distance from the inner basin rim. This amplified Baldwin's 1949 description of mountain rings around basins as ripples generated by basin-forming impacts.

Johnson *et al.* (1964), who reported two outer rims around the Ries crater at radii 1.4 and 1.9 times the inner crater radius, criticized Baldwin's concept of a frozen shock ring and attributed the rings to beat interference between compression and shear waves.

Baldwin (1966) reiterated his concept of a frozen shock wave by comparing the impact-produced shock to a tsunami. He described a tsunami-like wave which would propagate outward, deforming rock layers out to the point where the peak pressure declined to a value below the rupture modulus of the lunar crust. At this point the tsunami-like motion would cease and the wave would dissipate at lower energy densities through the rock. This point was supposed to correspond to a frozen anticline surrounding an inner damaged zone.

Van Dorn (1968) quantitatively dealt with Baldwin's hypothesis of frozen tsunami-like waves. Van Dorn used the equation for wave disturbances in an inviscid liquid layer and shows that it can be fitted to the sequence of five rings around the Orientale basin. The equation predicts a series of waves with ratios averaging 1.4. When the

equation was fitted to the Orientale system for a fixed time  $t$  after the impact, it was found that the depth of the inviscid layer was 50 km and time  $t$  was 1.0 h after the impact. Van Dorn pointed out that the actual viscosity and rigidity conditions in the Moon will probably not alter these results greatly. Van Dorn (1969) identified 40 lunar multi-ring maria as homologous structures of similar origin and that the 50 km crust was a universal lunar layer. He further showed that an impacting body could produce the necessary energy and that the estimated altitudes of the rings are consistent with the wave equation predictions. Some questions raised by the theory are: (1) if the rings are frozen waves, it is not clear why they 'freeze', in the observed position; (2) the theory calls for a fluid crust and rigid basement, while most authors and Van Dorn's Figure 3 (1968) call for a solid crust overlying a more plastic or partially molten basement; (3) the lunar rings do not have wave-form profiles, but rather appear to be sharply asymmetric fault scarps as shown in Van Dorn's cross-section through the system. These questions suggest the possibility that the wave-geometry of the initial shock was only one factor in an ultimate faulting and subsidence of the basin system.

Chadderton *et al.* (1969) introduced still another idea which ultimately comes full-circle back to the idea of collapse-faulting along fractures produced by impact. Chadderton *et al.* theorized that standing waves, rather than frozen tsunamis, were set up on the Moon by impacts. The idea is supported by both theoretically predicted and observed Chladni figures on the surfaces of vibrating self-gravitating spheres. The Chladni figures are arrangements of nodal lines in the vibrating system, and the lines take the form of latitudinal and/or concentric longitudinal arrays centered on the impact point. Chadderton *et al.* predicted that impacts will produce 'free vibrations of long period (up to the order of 15 min)', a prediction perhaps supported by Apollo seismic results. Chadderton *et al.* criticized the Baldwin 'frozen shock waves' on the grounds that they would not be expected to freeze simultaneously. However, they pointed out that the Chladni figures would have constant wavelength unless complications were invoked. Hence they suggested that the standing waves might be only partially responsible for causing the concentric rings by creating stationary wave forms later exploited during lunar evolution as the sites of faulting.

Two papers by Soviet authors have claimed further significance for the  $\sqrt{2}$  radii ratios, mentioned above in connection with basin ring systems. Zabelin *et al.* (1968) finds that lunar and possibly Martian crater diameter distributions show second-order departures from the long-known  $-2$  power law distribution function. The successive maxima in the departures are reported to occur at crater diameters in the ratio  $\sqrt{2}$ . Shemyakin (1969) finds a tendency among lunar crater chains for neighboring craters to decline in size along the chain. The successive craters are reported to have diameter ratios of integral multiples of  $\sqrt{2}$ . These conclusions probably warrant further study but their application to our present topic is questionable.

We conclude from this review that all of the suggested theories of basin system formation can be accommodated in the statement that stresses will be set up in the Moon by the violent dissipation of energy during basin formation; all authors agree

that these stresses are likely to produce a series of concentric ring fractures surrounding the basin, though the detailed theoretical models differ.

#### 4. Measurements of Basins

This section briefly describes the basins and the raw data and may be skipped by readers interested only in the final interpretation of the data.

*Theory.* Figure 1 shows a time-sequence of crater diameter distributions for a given spot on an evolving Moon. If there were ever an initial period when no craters existed, the crater population would soon begin to build up, as in the first diagram.

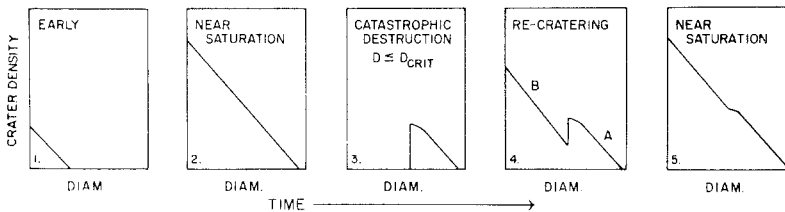


Fig. 1. Time sequence of crater diameter distributions, starting with a nearly-uncratered surface (1) which accumulates craters, undergoes an event which destroys small craters, and then is re-cratered.

Since the frequency of crater diameters  $D$  goes as  $D^{-2}$ , equal areas are covered by craters of different sizes; therefore the saturation crater distribution will by coincidence have the same slope.  $-2$ , as the non-saturated distributions. In the second diagram saturation is being approached. This must have been the situation in most regions of the moon more than 4 aeons ago when Mare Tranquillitatis was forming (the early cratering chronology is reconstructed in a separate paper in press in *Icarus*, 1970). If a local catastrophe occurred, such as deposition of a basin ejecta blanket or flooding by mare lavas, all craters up to a certain size  $D_{crit}$  would be buried. Larger craters would survive, as shown in the third figure. Later the area would be re-cratered as shown in the fourth diagram, a stage exhibited near many basins, as we will show. Segments A and B represent ages of different units – pre-basin saturated surface, basin ejecta blanket, or recent mare flooding – depending on the example. Ultimately, as in the fifth figure, the discontinuity will disappear as the surface resaturates with craters. The last stage is shown by the oldest basins.

In earlier papers we have used a relative chronology based on crater density, with density 1.00 assigned to the mean density for maria on the front side. The most heavily cratered upland regions have a density about 32 which is near saturation. The young crater Tycho, for comparison, has a density only 0.1. (Hartmann, 1968a). These densities are *not* directly proportional to age because of variations in the cratering rate; they establish only relative ages. Henceforth in this paper we will use the terms ‘crater density’ and ‘relative age’ interchangeably.

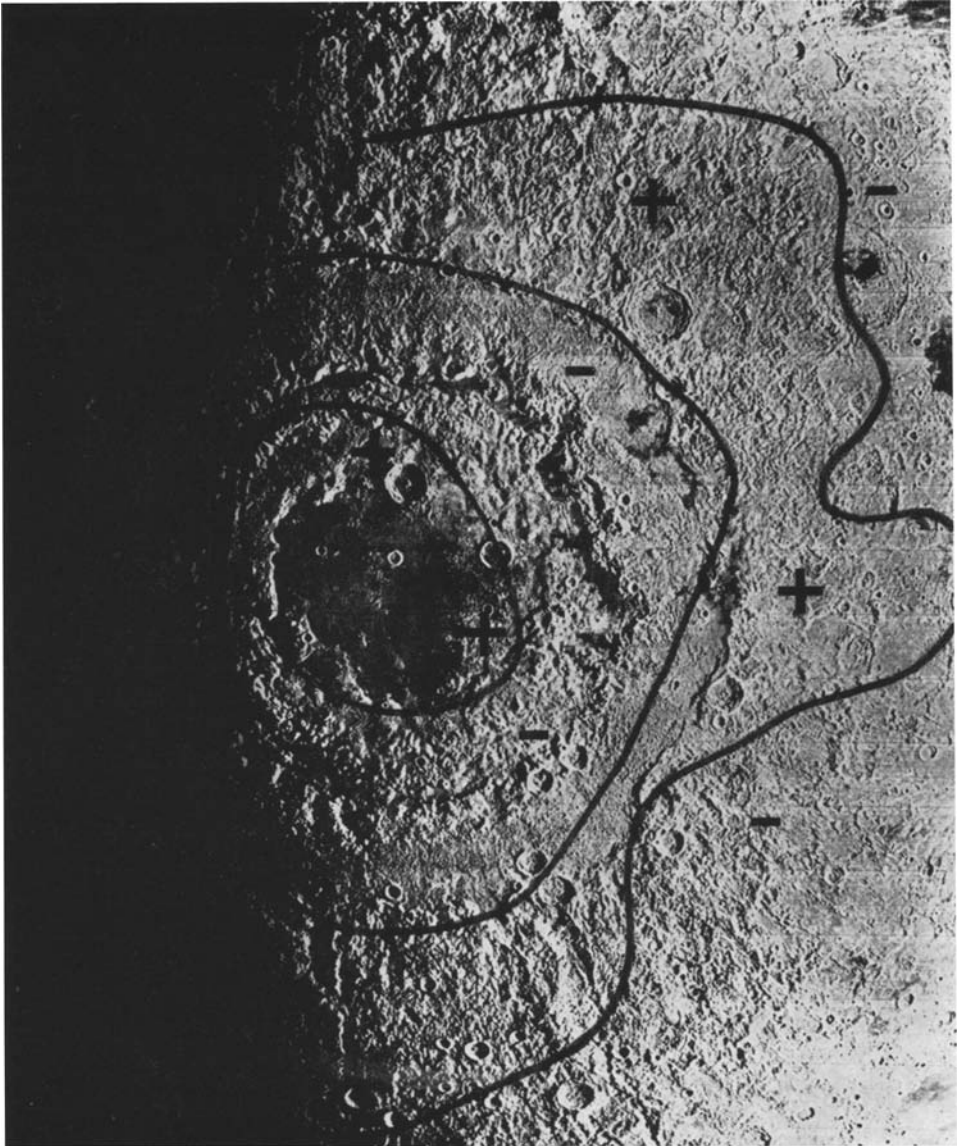


Fig. 2. Orientale basin, with contours showing positive and negative gravity anomalies, after data given by Booker (1970). NASA Orbiter 4, M187.



The basins will be described here in order of increasing relative age. Positions are given in Table 1.

*Orientele*. The youngest basin is *Orientele*; its ejecta blanket has a crater density  $2.4 \pm 0.2$  (est. PE) and its central mare has a crater density  $1.0 \pm 0.1$ . These counts have been discussed in detail elsewhere and so will not be reviewed here (Hartmann and Yale, 1968). A new result due to Booker (1970) deserves note. Subsequent to

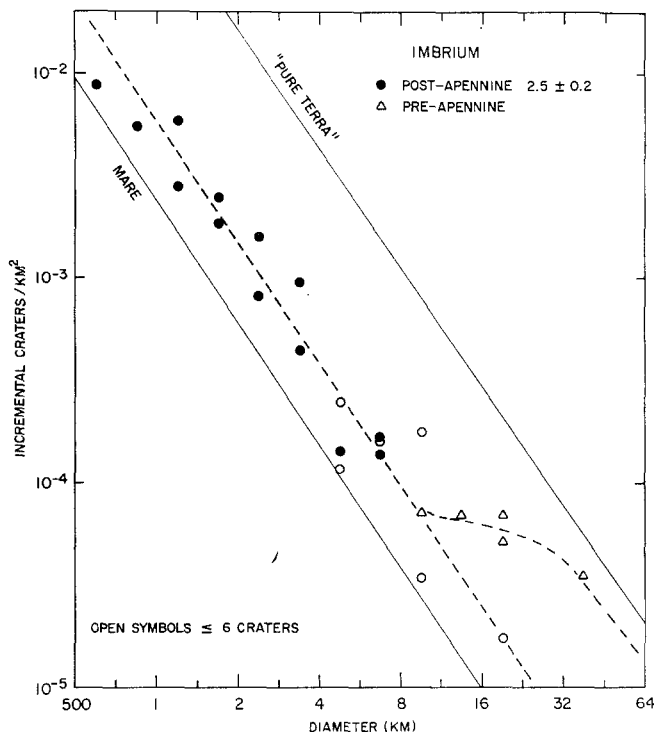


Fig. 3. Crater diameter distribution on Apennine ejecta blanket of Imbrium basin. In all following crater curves, open symbols represent lower-weight points based on  $\leq 6$  craters.

Sjogren's announcement of a mascon in the *Orientele* basin, (cf. Booker, 1970) Booker mapped *gravity anomalies near Orientele showing concentric ring structure*, with a central positive mass excess surrounded by a negative, a positive, and an outer negative ring. The positions of these rings are shown in Figure 2.

*Imbrium*. Figure 3 shows crater counts in the Apennine Mountains, the best-preserved part of the Imbrium ejecta blanket. On all of the crater count diagrams we have added comparison lines for the mean mare and for the 'pure terrae'. For the Imbrium ejecta we find a density of  $2.5 \pm 0.2$  as shown by the straight dashed line. Emphasis is given to intermediate-sized craters (2–8 km) in drawing this line to meet the criteria of (1) absence of contamination by secondaries and endogenic craters,

(2) completeness in counting, and (3) significantly large sample. In the lower right is shown a segment defined by ancient, pre-Apennine craters, equivalent to segment A in Figure 1. Most pre-Apennine craters smaller than about 32 km have been obliterated. This corresponds to a mean ejecta blanket depth of some 3 km, consistent with extreme mountain peak heights in the Apennines of about 7 km (Baldwin, 1963). The probable errors of the Orientale and Imbrium dates overlap, but in defense of the older age for Imbrium, we note that its radial system seems less clear than Orientale's and that even 1 km diam craters on the Imbrium ejecta are typically smoothed by a regolith. The 'relative age' of 2.5 is a revision of an earlier-published value of 6, estimated from a survey of large craters on the Imbrium periphery (Hartmann, 1968b).

The Imbrium mare surface has a crater density  $0.9 \pm 0.1$  (Hartmann, 1968b). The

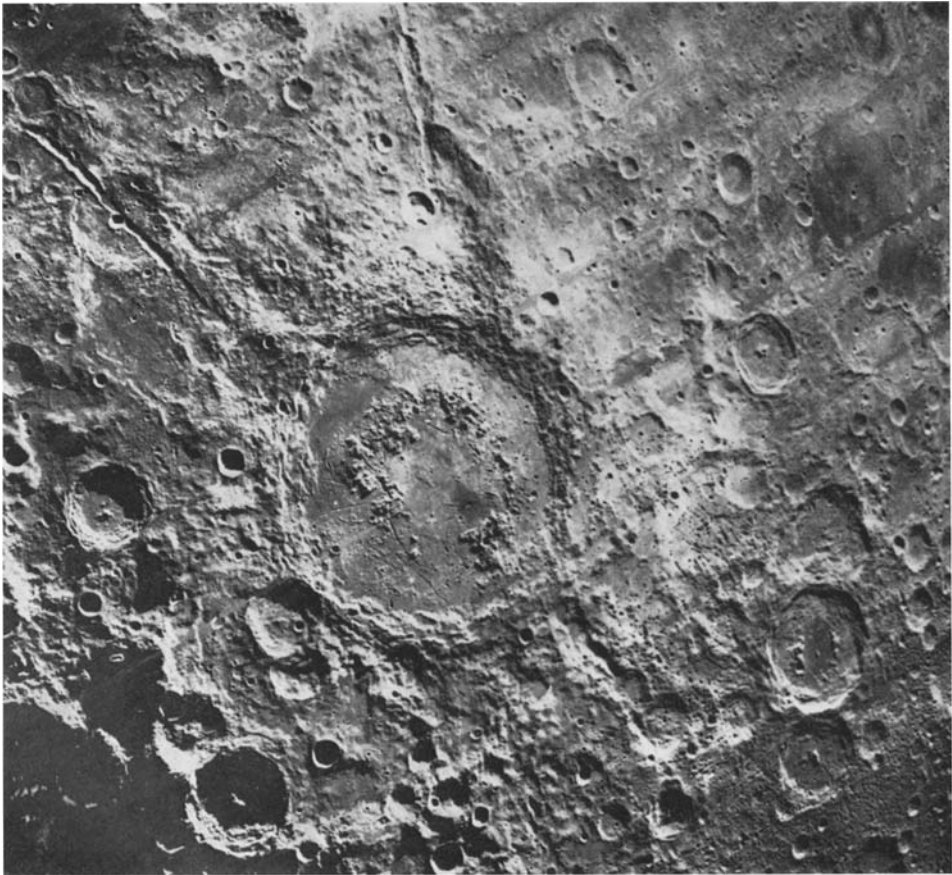


Fig. 4a. Schrödinger basin and Antoniadi. Schrödinger contains an inner ring of peaks, and Antoniadi appears intermediate between a double-ring basin and an ordinary crater. Antoniadi lies at lower right, at about '4 o'clock' from Schrödinger. NASA Orbiter 4, M8.

sequence of flow structures has been diagrammed in detail by Strom and Whitaker (Kuiper, 1966).

*Schrödinger and Antoniadi.* Schrödinger (Figure 4a) is a fresh, double-ring basin near the far side south pole. Because the basin is small there are not enough large post-basin craters to give an accurate age or density. (Small craters are not used

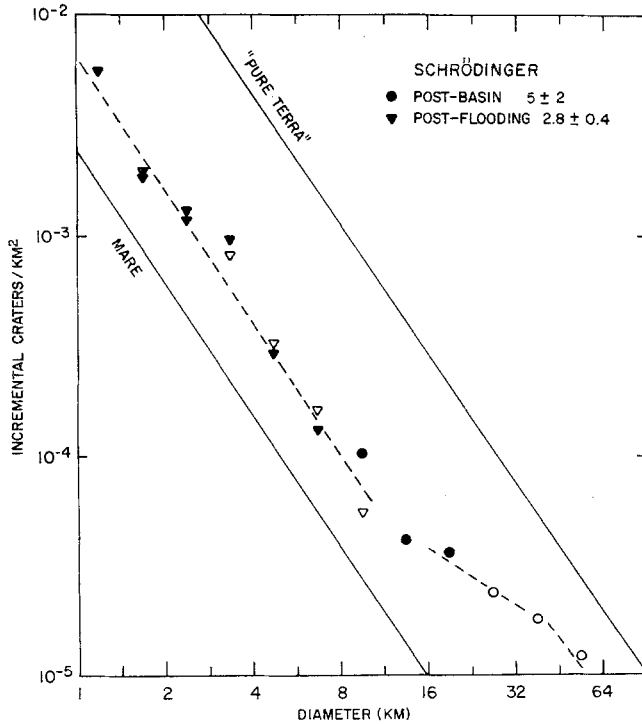


Fig. 4b. Crater diameter distribution near Schrödinger.

because most regions are contaminated by secondaries and endogenic craters). Above  $D=20$  km, pre-basin craters apparently 'show through' the ejecta. Craters near  $D=10$  km suggest a crater density  $5 \pm 2$  (Figure 4b).

The interior of Schrödinger is flooded with rather light-toned mare material and contains one prominent, large dark-halo crater. This surface has a crater density of  $2.8 \pm 0.5$ , unusually high for maria. Tranquilitatis, the oldest of the major maria, has a value of about 1.6 (Hartmann, 1968b). This is the first of several evidences in this paper for mare flooding much older than the familiar maria.

Schrödinger has a remarkable inner ring which has more of the characteristics of central peaks of craters than of a crater rim. It suggests a transition between inner rings and central peaks, which we will discuss in Section 9. A radial lineament system is well-expressed by three long, prominent grooves plus minor lineaments.

Antoniadi lies in the lower right in Figure 4A. It is a small, crater-like basin containing a ring of peaks on its floor. The inside of this peak-ring is flooded, and contains a small central peak isolated by mare material. Hitherto, no double-ring basin of this size or with a central peak was known.

*Milne.* Milne is partially covered by ejecta and secondaries from a nearby young crater (Figure 5a). The two authors independently counted craters larger than  $D = 2.8$  km; the resulting diameter distributions give ages concordant within about 20%. This is a characteristic error for crater density determination. The resulting relative age inside the basin is  $6 \pm 1$ ; this may represent the age of an overlying ejecta or plains-forming unit (Figure 5b). The largest craters suggest a greater basin age of about  $10 \pm 5$ , more consistent with the basin's battered appearance.

Instead of a single, well-defined inner ring, Milne has a series of three arcs composed of mountain masses individually resembling central peaks of craters. The configuration again suggests something intermediate between a crater rim (typical of many basin rings) and a symmetric mountain mass (typical of central peaks).

*SE Limb Basin.* Using rectified Earth-based photography, H/K (1962) described



Fig. 5a. Milne basin. The inner ring shows three arc-segments. NASA Orbiter 3, M121.

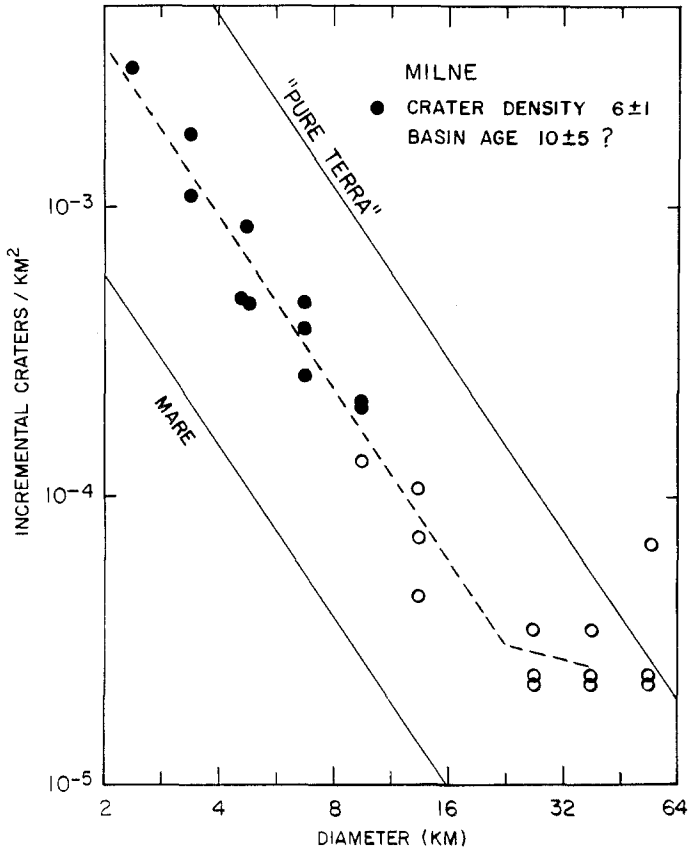


Fig. 5b. Crater diameter distribution in and about Milne.

this basin. It is on the limb and partially obliterated by Orientale ejecta (Figures 6a and 6b). The relative age of the SE limb basin is  $12 \pm 1$  based on counts in the unblanketed southern half of the basin. The highly battered appearance, which suggests a much older age, is largely a result of the thick blanket of Orientale ejecta. The small patch of dark mare material in the southern part of the inner ring appears to have covered the ejecta and thus is younger than the Orientale 'age' of 2.4.

*Apollo.* This farside basin contains some patches of dark, fresh mare, but to the south are some light-colored plains with radial lineaments or ejecta associated with the Orientale basin (Figure 7a). We estimate that the basin has a relative age about  $12 \pm 4$  but as seen in Figure 7b the slope of the crater count curve is rather shallow, reflecting a series of progressive stages as shown in Figure 1 – stages independently evidenced by the appearance of flooding. By examining the crater counts, we can reconstruct the history: Long ago, the background in the vicinity of the basin was nearly saturated with craters the largest of which are still seen at  $D > 32$  km. The basin then formed at relative age about 12. Craters in the range 12–32 km appear

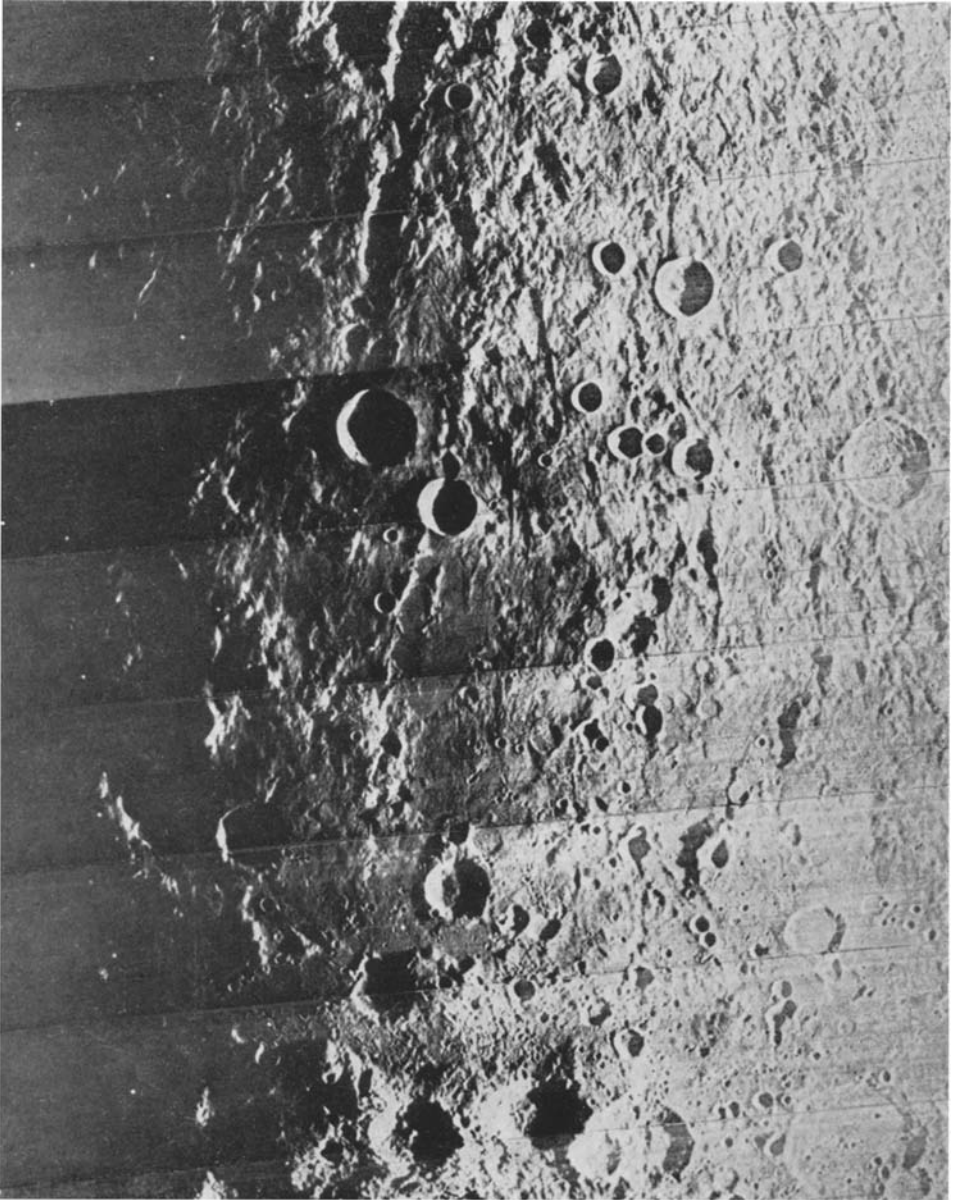


Fig. 6a. Unnamed 'SE Limb' basin, partially obscured by ejecta from Orientale, to the north (top).  
NASA Orbiter 4, M193.

to be post-basin craters. A light plains-forming unit (lava flows?) then appeared, and then the Orientale event spread ejecta across this unit at age 2.4. Lava erupted still later to form the dark maria at the base of the outer wall and in the center. Craters smaller than 12 km have been depleted by this complex flooding history. Because the mare patches are small and the resolution limited, we have no separate age determination for the mare in the Apollo basin.

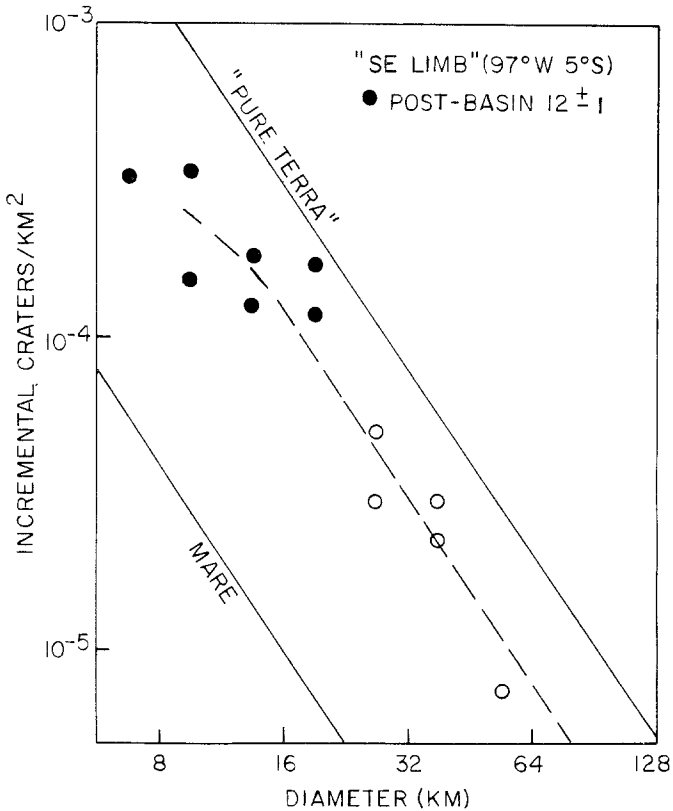


Fig. 6b. Crater diameter distribution in the southern part of the 'SE Limb' basin, an area with minimal contamination from Orientale ejecta.

*Bailly.* Bailly, which has been considered a normal crater, is a basin system: there is an inner ring (Figure 8a) now battered by overlying craters and what appears to be some ancient plains-forming fill. Outside to the east, part of a third ring can be traced. The large craters of the interior and outside rim suggest a basin age about  $12+9/-4$  (Figure 8b), but the interior craters of  $D < 45$  km suggest an age for the plains-forming fill of about  $8 \pm 2$ . There is evident contamination by secondary ejecta and craters from Hausen and probably endogenic craters of  $D < 16$  km, as confirmed by the upward curve of the diameter distribution.

*Moscoviense*. The first photographs of the Moon's far side obtained by Lunik 3 in 1959 revealed the Mare Moscoviense. Orbiter photographs (Figure 9a) show that this is a basin with only shallow flooding. Densely cratered pieces of the original basin floor protrude above the mare. The flooding is deepest to the east and here has partially destroyed the rim of the inner ring. The post-mare crater density is not well established but appears to be about 4 (Figure 9b). This is higher than the normal

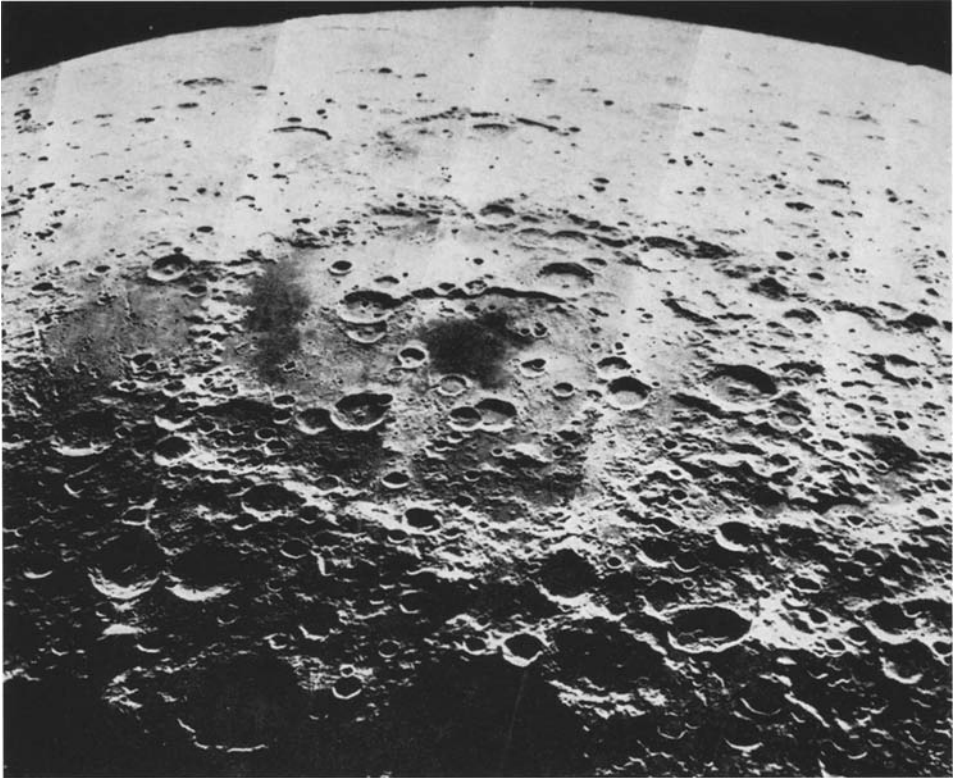


Fig. 7a. Apollo basin. Area contains radial lineaments and ejecta from Orientale, out of frame in foreground. NASA Orbiter 5, M30.

post-mare crater density. We suspect some of the excess to be endogenic and possible pre-mare craters, not distinguished in the counts. The basin itself shows a post-basin crater density of  $14 \pm 2$ , fairly well-defined by terra surfaces within the outer ring.

*Korolev*. This basin apparently has had a comparatively simple history – Figure 10b shows that since the basin was formed at  $15 \pm 2$ , there has been insufficient flooding to affect the slope of the diameter distribution. The inner ring is mountainous on the east and a few peaks define the remainder of its course (Figure 10a). There is an unusually high crater density along the line of the inner ring, and one crater



on the SW edge of this ring tops a well-formed cone about 8 km diam. A third ring of smaller radius is hinted at by a nearly continuous concentration of craters on the western segment of the basin's interior. Volcanic production of the inner rings is thus indicated. The W and SW floor, especially near the outer ring base, shows evidence of localized flooding.

*Humboldtianum and Compton.* Photography of the Humboldtianum basin remains poor. Lying near Humboldtianum and shown in Figure 11a is the interesting crater Compton, which contains an inner ring of hills surrounding a central peak on a light-toned mare floor. Except for the central peak, Compton is reminiscent of a

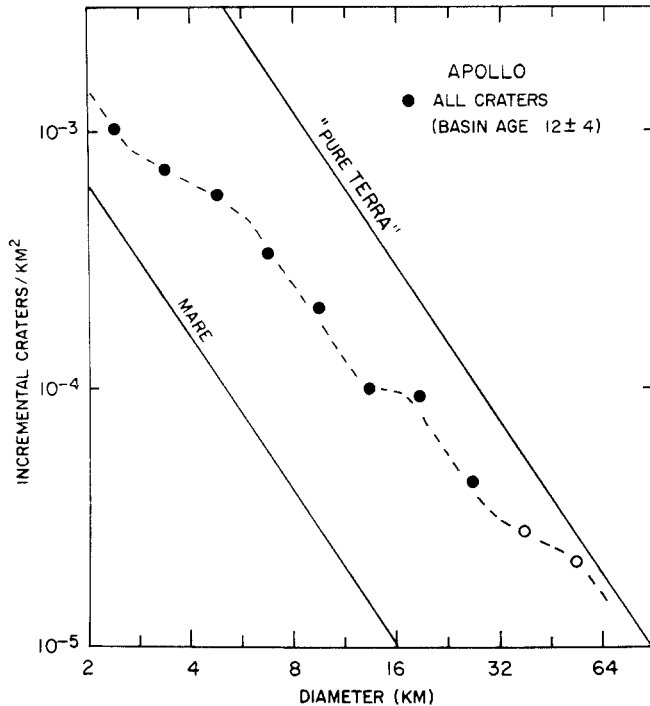


Fig. 7b. Crater diameter distribution in unflooded portions of Apollo basin.

scaled-down Schrödinger, but about half as big. Compton is the best example of transition between craters and basins. Compton is much younger than Humboldtianum, but the photography is inadequate for good crater counts. Counts on the flooded interior of Compton suggest a crater density typical of mare, about  $1.0 \pm 0.4$ .

H/K (1962) contains rectified photos of Humboldtianum. The post-basin crater density of Humboldtianum is  $15 \pm 3$ , with craters less than 16 km diameter being depleted, probably by tectonic and flooding activity (Figure 11b).

*Hertzprung.* Orientale ejecta – including linear arrays of craters – overlay both



Fig. 8a. Bailly basin, containing a faint inner ring partly obliterated by craters.  
NASA Orbiter 4, M166.

the rim structure and the mare filling in the center of Hertzprung (Figure 12a). This is consistent with the crater densities: Hertzprung was formed with relative age  $15 \pm 2$  (Figure 12b). The inner ring area was flooded subsequently and the Orientale ejecta was deposited at  $2.4 \pm 0.2$ . This flooding does not appear to be dark on Zond 3 photographs. It has the other characteristics of maria, however, and may be old mare material overlain by a veneer of light-toned ejecta, including that from Orientale.

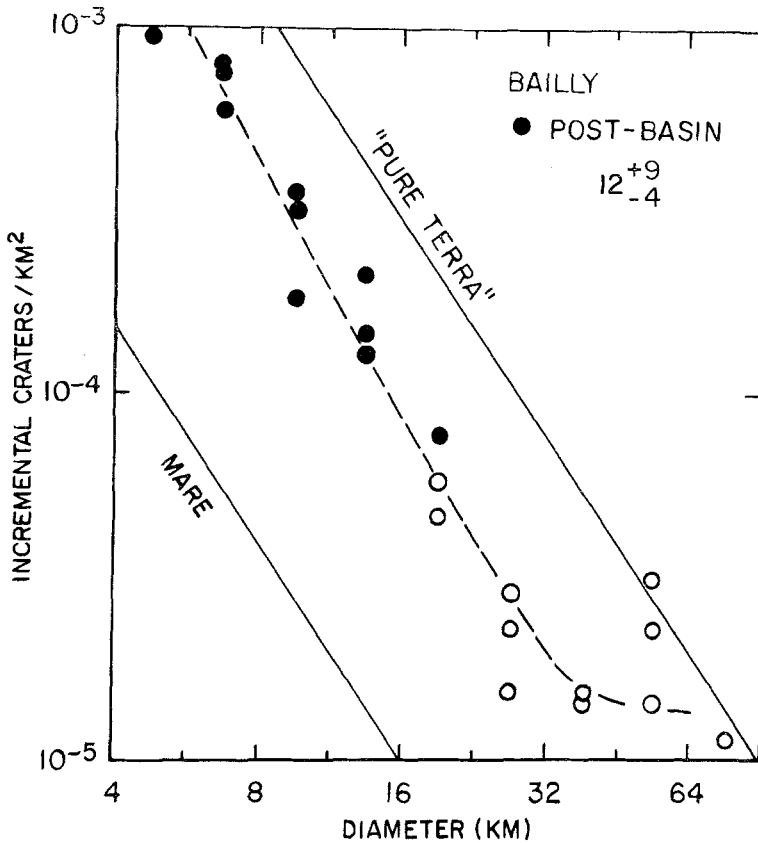


Fig. 8b. Crater diameter distribution in and about Bailly. Steep slope at  $D < 16$  suggests contamination by secondaries from Hausen, immediately to west (left).

In places, the Orientale ejecta is thick and clustered with secondary craters, illustrating how flooded basin surfaces can be transformed into terra-like surfaces.

*Nectaris*. In its center, the Nectaris basin contains obvious mare material dated in Figure 13 at  $0.9 \pm 0.3$ , a slight revision of an earlier value 1.0 (Hartmann, 1968b). The basin itself is dated in Figure 13 at relative age  $16 \pm 2$  by counts near the Altai scarp and inter-ring zone inside the Altai scarp. We note, however, that the inter-ring zone shows clear signs of early flooding and destruction of surface detail, complicating

the interpretation of the counts. Post-basin craters of  $D < 16$  km have apparently been depleted. Such inter-ring destruction and tectonic activity is common to most basins (Hartmann, 1963, 1964; McCauley, private communication, 1970).

*Grimaldi*. Figure 14b shows the crater counts, from which a post-basin crater density of  $16 \pm 4$  is deduced. Figure 14a shows the eastern portion of the Grimaldi



Fig. 9a. Moscoviense basin. NASA Orbiter 5, M103, rectified.

rim (left) and outer ring (right). The crater marked D is Damoiseau A. A significant fact is that the outer ring of Grimaldi does not cut through this crater but rather appears to detour continuously around the eastern rim of Damoiseau A. The crater does not appear to be a post-ring impact; its southern rim is marked by isolated hills and there is no evidence of a young ejecta blanket. Thus it is either a pre-ring crater, or a post-ring caldera, which suggests that *the Grimaldi outer ring is a fault feature which utilized a pre-existing weak zone under the rim of Damoiseau A*. The arrow

indicates an interesting shelf in the small crater Damoiseau D, apparently too high to be a rebound feature of the sort discussed by Gault (1969) and possibly an outcrop. The mare inside Grimaldi was dated at  $0.75 \pm 0.1$  and counts on the inter-ring chaotic zone gave an effective mean age of about  $3.5 \pm 1$  for the inter-ring flooding and destruction.

*Planck*. Photography of this basin is poor, but Figure 15a shows what appears to be part of an inner ring. The limited crater counting that can be done gives a post-basin crater density of  $16 \pm 7$ , with craters smaller than 16 km being depleted.

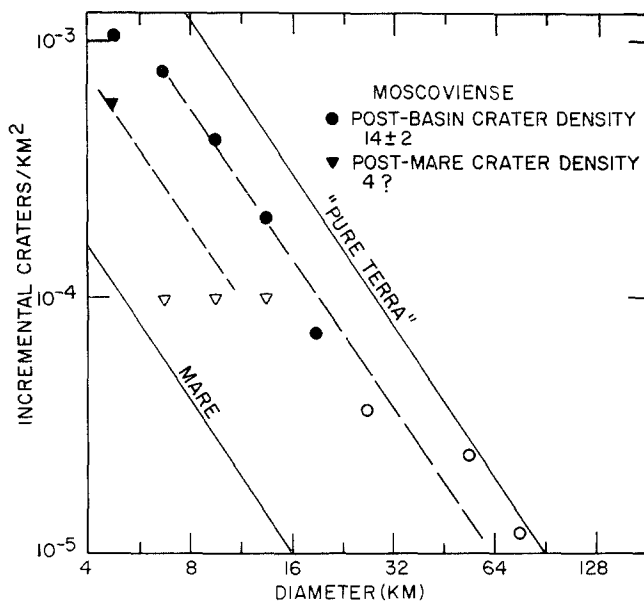


Fig. 9b. Crater diameter distributions on unflooded and flooded surfaces in Moscoviense basin.

*Poincaré*. This farside basin is partly flooded and appears to have had a complex history, including multistage flows (Figure 16a). What appears to be a late flow is in the left half of the large central foreground crater. The post-basin crater density was found from counts on the inter-ring zone. Figure 16b shows that at  $D > 8$  km these define a post-basin density of  $17 \pm 2$ , but the inter-ring zone has been depleted in craters of  $D < 8$  km, which have a density about 7. Counts on the central mare give a post-mare density of  $2.6 \pm 0.9$ . This is rather large for true mare, and Figure 16a suggests that the mare cover is thin and that there may be contamination from unrecognized pre-mare craters or endogenic or secondary craters. Orbiter 4 photograph M8 shows the SE part of the floor and an annulus along the inner fragmentary ring to be darker than the rest of the center. This indicates (1) multi-phase flooding and (2) that the inner ring may contain extrusion sites.

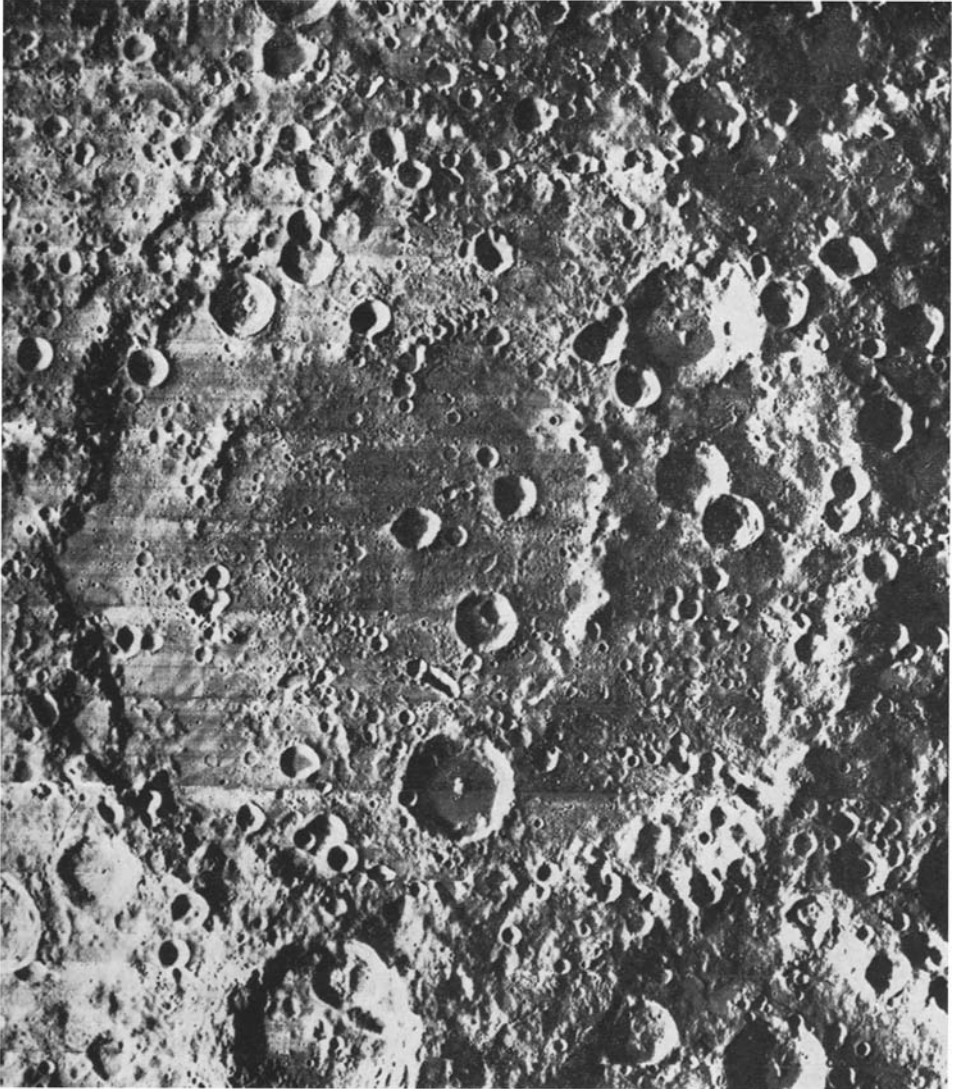


Fig. 10a. Korolev basin. Inner ring is extended on west side by ring of densely-packed craters, and a third innermost ring of craters is also suggested. NASA Orbiter 1, M40.

*Crisium*. Counts along the outer rim of Crisium give a post-basin crater density of  $17 \pm 4$  (Figure 17). The inter-ring zone has been severely depleted in craters of  $D < 16$  km, consistent with the abundant morphological evidence for partial flooding and lineament-forming tectonic activity (Hartmann, 1963; Binder, 1967). The mare gives some further evidence for multi-phase flooding activity, as discussed under Poincaré above. Counts of all craters in the entire mare, especially craters of  $D > 8$  km,

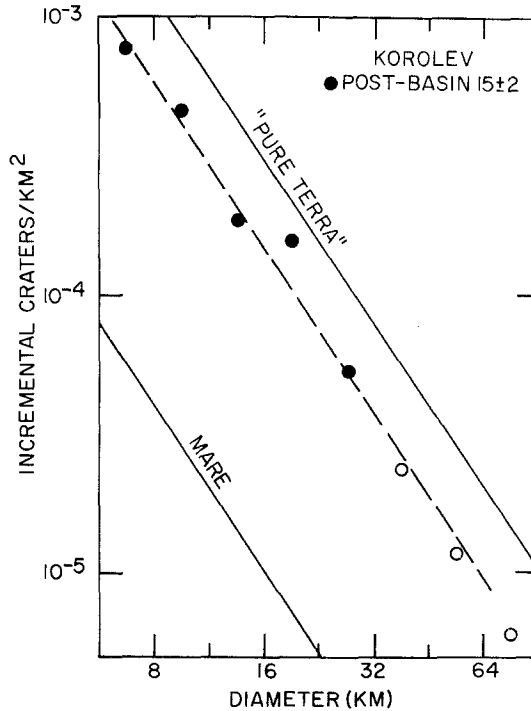


Fig. 10b. Crater diameter distribution in and about Korolev.

give a density somewhat greater than 1.0, the average mare density. However, counts of craters of  $D < 16$  km in the central mare inside the wrinkle ridges indicate that this is one of the youngest extended mare areas on the Moon, with a density 0.4.

*Birkhoff*. Figure 18a shows that Birkhoff, although it is overlain by a number of large craters has a sharp, well-defined outer rim, suggesting a moderate age. The crater counts (Figure 18b) show a well-defined crater density of 18 for craters of  $D < 22$  km. Our inference is that the larger craters are simply statistically overabundant and that  $18 \pm 6$  represents the basin relative age. The inner ring has been partly obliterated by post-basin craters. The large overlapping crater to the north, with a mare-flooding floor, exhibits a wrinkle ridge that occupies the original position of the Birkhoff rim. This observation shows that the basin rim is the site of some

underlying structure that – *even after the rim is destroyed* – contributes to its resurgence in the form of a wrinkle ridge. Our inference is that deep-seated fractures underlie the basin rims and serve as later sites for extrusive or intrusive activity. Two additional justifications for this interpretation are (1) the fact that differential isostatic stresses are greatest along the wall – the boundary between an excavated hole

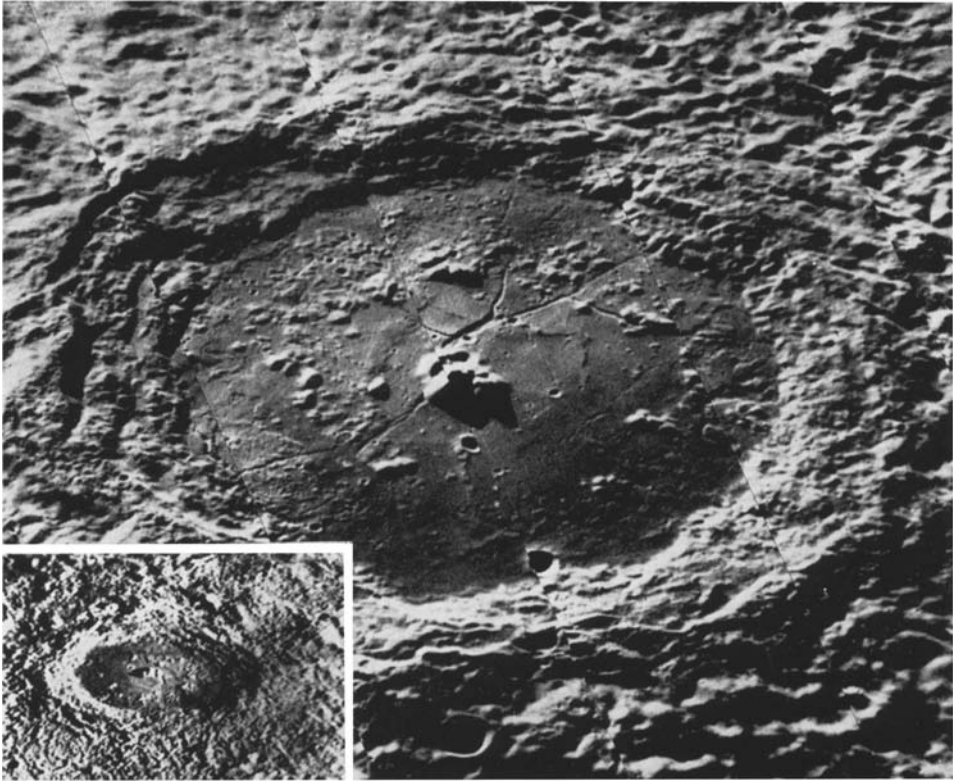


Fig. 11a. Compton, which contains *both* a well-developed central peak and an inner ring of peaks, is the best example of a transition between craters and basins. Insert shows a second view from a different direction. NASA Orbiter 5, M181; Orbiter 4, M140.

and piled-up ejecta, and (2) the detailed work of Strom and Fielder (1970), establishing that large craters such as Tycho and Aristarchus have complex post-crater eruptive activity on their rims. This evidence also marks the wrinkle ridges as extrusive or intrusive, a point to which we will return in Section 9.

*Unnamed Basin (A)*. This is the most questionable basin in our list. It is overlapped by Schrödinger (Figure 4a) and one of its major radial valleys. Comparing various Orbiter photos of the region, we find some evidence for a weak outer ring and possibly a broad central ring or elevation. The crater counts (Figure 19) indicate the presence



of Schrödinger ejecta in the SE part, destroying craters of  $D < 45$  km and having an age of  $5 \pm 2$ , confirming the value 5 found for Schrödinger. Figure 19 shows some evidence for the older age of 'A', estimated to be  $21 \pm 6$  based on the larger craters.

*Janssen.* Crater counts for this battered front-side basin (Figure 20) suggest a basin age of  $22 \pm 8$ . Craters of  $D < 32$  have been depleted and there is suggestion that the southern floor contains mare material covered by a thin veneer of light, pulverized ejecta, probably rays from Tycho and Stevinus B which intersect at Janssen.

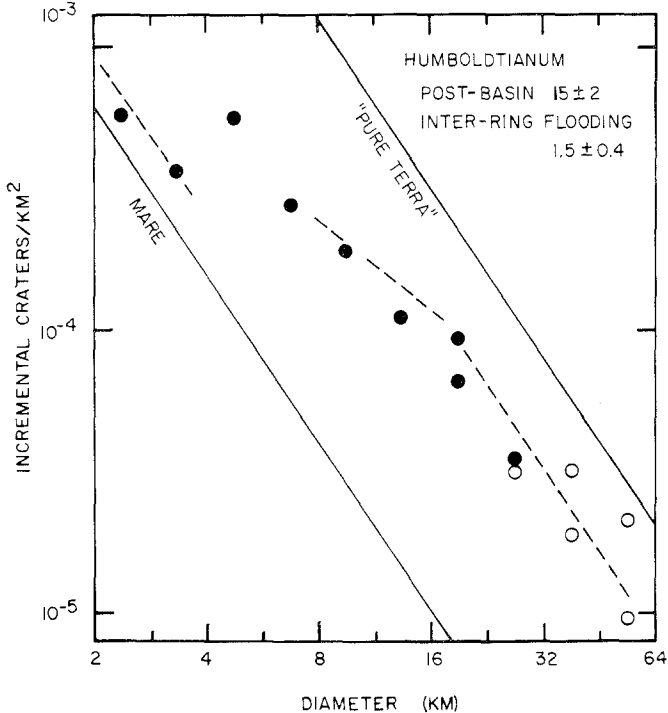


Fig. 11b. Crater diameter distributions on inter-ring zone, Humboldtianum basin.

*Lorentz.* Lorentz (Figure 21a) is very similar to Birkhoff except apparently older, for the outer walls are weaker and two large craters overlie it. The crater density,  $23 \pm 3$ , confirms high relative age (Figure 21b). Light-colored flooding occurs on the floors of the two large craters and in patches within the outer ring. A peculiar locale of flooding is a high plateau confined between the two large craters and the NE sector of the outer ring. Since this flooding appears higher than the neighboring flooded regions, the lava there could not have been in hydrostatic equilibrium with the lower flooding. It may have tapped a separate source of magma or utilized separate channels of access to the surface. In this case, as in others above, the access may have been through faults under the basin's outer ring.

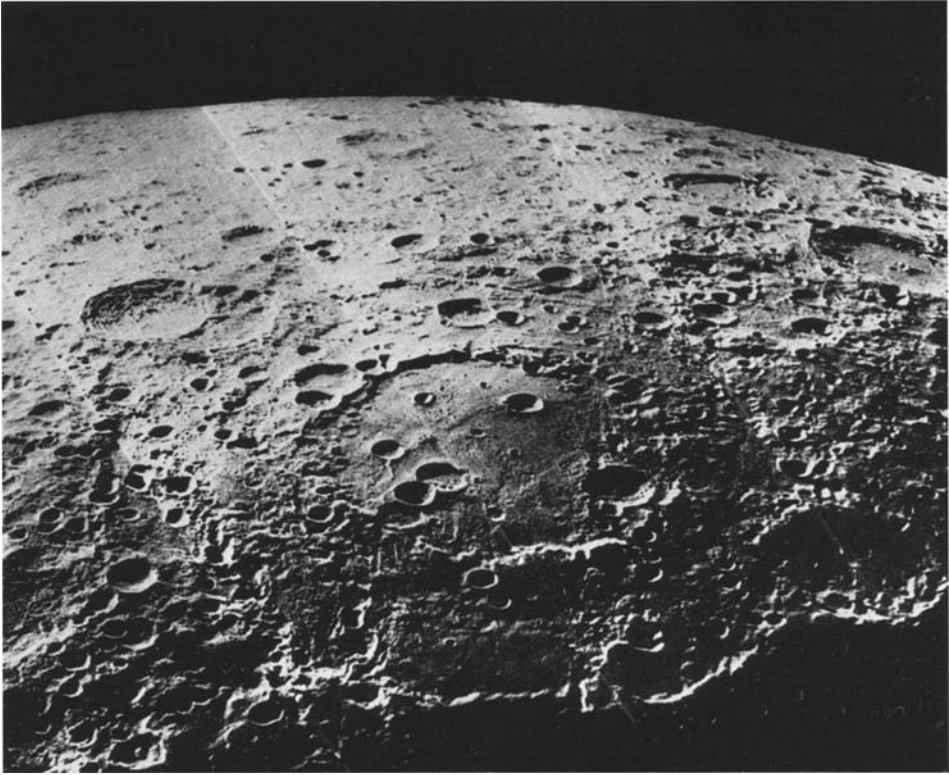


Fig. 12a. Hertzprung basin, thinly overlain by ejecta and radial lineaments from Orientale (out of frame, foreground). NASA Orbiter 5, M26.

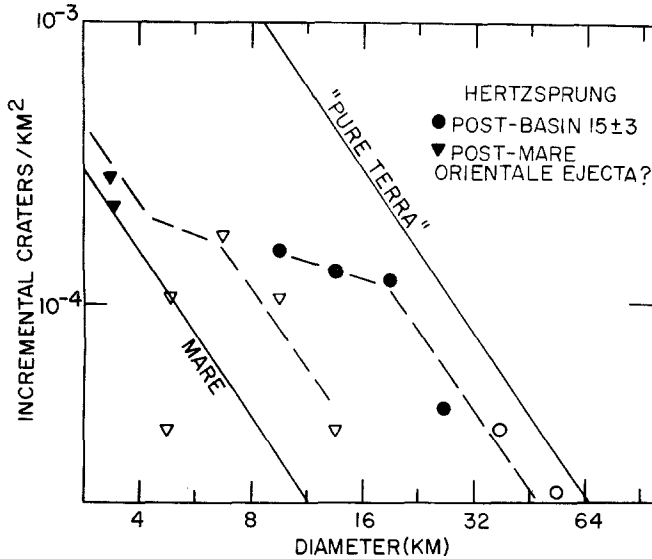


Fig. 12b. Crater diameter distributions on unflooded and flooded surfaces in Hertzprung basin. Largest craters appear to date basin-forming event, but smaller craters, the Orientale ejecta.

*Humorum.* Although this front-side basin is familiar, its basin rings are highly battered, indicating great relative age. This is confirmed by counts of post-basin craters along and beyond the inner ring. These give a crater density of  $25 \pm 2$  (Figure 22). The mare gives a crater density of  $0.85 \pm 0.1$ .

*Unnamed Basin (B).* This ancient, nearly destroyed basin (Figure 23a) was detected by comparison of two Orbiter photos. A faint outer ring can be traced and the inner ring is low-walled and thinly flooded. Counts of the basin surface, excluding the inner mare, give a post-basin crater density of  $25 \pm 4$  (Figure 23b).

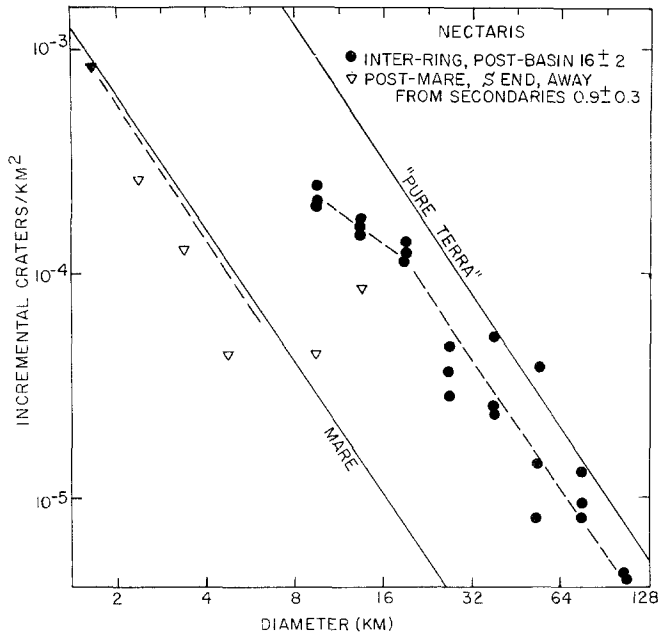


Fig. 13. Crater diameter distributions on unflooded and flooded surfaces in Nectaris basin.

*Pingré.* This battered formation was originally considered an ordinary crater, but there is evidence of an outer ring. Crater counts give a well-determined density of  $13 \pm 4$ , but the true basin age is presumably reflected by the more abundant large craters, with a very roughly estimated relative age of  $25 \pm 9$  (?) for the basin (Figure 24). If this is the true basin age, as we infer, then the relative age of 13 must refer to an old plains-forming unit within Pingré.

*Basin near Schiller.* The entire interior of this basin is covered by smooth flooding; mostly light in hue (Figure 25a) but an annulus of darker flooding apparently occurs within and eccentric to the inner ring, reminiscent of Poincaré. Figure 25b shows a discontinuity in the diameter distribution: craters of  $D > 32$  km show that the basin was formed about  $26 \pm 6$ , but that at  $5 \pm 2$  the flooding we see now occurred with a

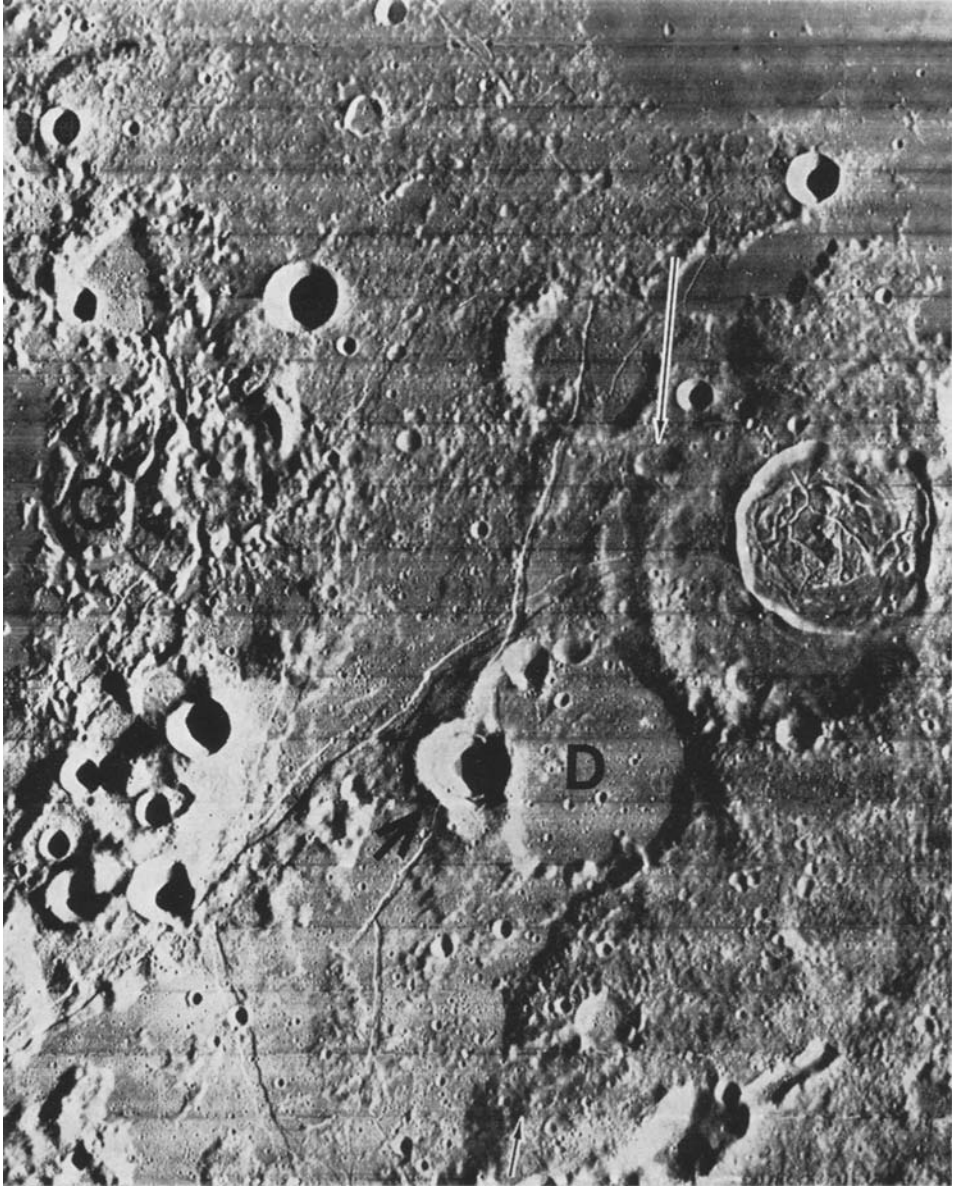


Fig. 14a. Detail of outer ring (white arrows) around Grimaldi basin (G). D marks crater Damoiseau A, around which the ring appears to detour in the manner of a fault utilizing a zone of weakness. Black arrow marks a good example of an inner ring in an intermediate-size crater ( $D = 16$  km). NASA Orbiter 4, H161.

depth about 3 km, inferred from the destruction of craters  $<32$  km. Structural features such as wrinkle ridges confirm the mare nature of the interior; the light tone would seem to be due to a thin veneer of ray material. The flooding episode is a good example of the theory in Figure 1. The long axis of the perplexing feature Schiller follows the rim of the basin, indicating Schiller may be endogenic. Linear arrays of secondary craters and tectonic patterns of fracture-lineaments in terra just N of the Schiller basin align with the Orientale (Figure 25a) radial lineaments.

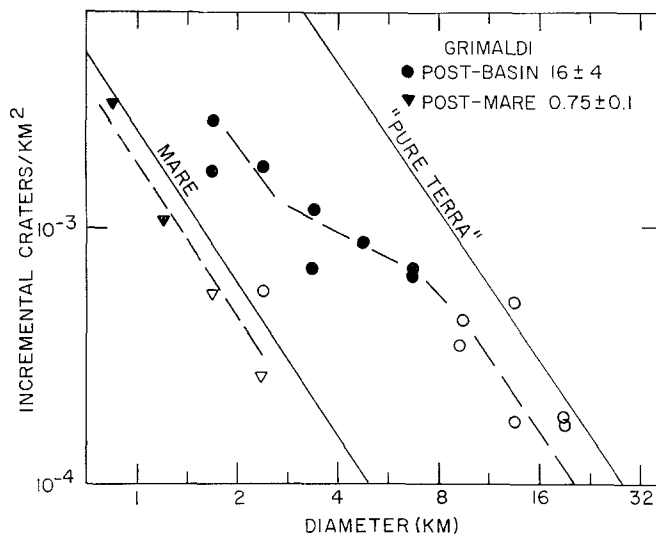


Fig. 14b. Crater diameter distributions on flooded and unflooded surfaces in Grimaldi basin.

*Smythii*. The outer rim of the basin is low and discontinuous, and the shelf inside the outer rim is noticeably less densely cratered and smoother than the surrounding continental region, indicating inter-ring flooding and/or tectonic activity. Figure 26 shows that the basin has apparently had a two-stage cratering history. The basin itself formed at  $27 \pm 7$ . Counts on the central dark area show a two-phase history. Original craters larger than 32 km are all detectable, but craters of  $D < 8$  km define a flooding period at  $1.9 \pm 0.2$ . The depth of this flooding is estimated to be of the order 3 km, the depth of the 32 km craters which begin to show obliteration by flooding. Many craters in the north part of Mare Smythii have peculiar inner-ring structures resembling basin systems. Perhaps this indicates a layered structure in the lunar crust in this region, or perhaps these are caldera-like collapse craters.

*Conclusions*. Table II shows a collection of the data on all known basins (i.e., multi-ring structures), arranged by estimated relative age. The following observations are made.

TABLE II  
Data on basins (arranged by estimated age)

	Long.	Lat.	Est. ring diameters <sup>a</sup> (km)	Data on basins (arranged by estimated age)		Relative 'age' <sup>b</sup> (relative crater density)		Mare	Morphology <sup>c</sup>			
				Est. ring diameters <sup>a</sup> (km)	Basin	Flooding or blanketing	Amt. of mare		Conc. syst.	Radial syst.		
											Basin	Flooding or blanketing
Oriental	96W	21S	320	480	620	930	1300	2.4	1.0	<i>g</i>	<i>vs</i>	<i>vs</i>
Imbrium	19W	38N	670	970	1340			2.5	0.9	<i>vg</i>	<i>vs</i>	<i>vs</i>
Antoniadi	172W	69S		65	140			?		<i>m</i>	<i>s</i>	<i>m</i>
Compton	104E	56N		80	175			?	1.0	<i>m</i>	<i>s</i>	<i>m</i>
Schrödinger	132E	75S		155	320			5	2.8	<i>m</i>	<i>s</i>	<i>vs</i>
Milne	113E	31S		120	240			10	6	<i>vl</i>	<i>m</i>	<i>w</i>
SE Limb Basin	94W	49S	220	330	480	640		12	2.4	<i>l</i>	<i>m</i>	<i>w</i>
Apollo	153W	36S		235	435			12	2.4+	<i>m</i>	<i>m</i>	<i>w</i>
Bailly	68W	67S		145	300	480		12	8	<i>l</i>	<i>w</i>	<i>w</i>
Moscoviense	147E	26N	205	305	410	700?		14	4?	<i>g</i>	<i>s</i>	<i>m</i>
Korolev	157W	4S		200	405			15		<i>m</i>	<i>m</i>	<i>w</i>
Humboldtianum	82E	58N		300	600			15	1.5	<i>m</i>	<i>s</i>	<i>s</i>
Hertzprung	129W	1N		400	285	440	550	15	2.4	<i>m</i>	<i>m</i>	<i>m</i>
Nectaris	34E	15S		600	840			16	0.9	<i>g</i>	<i>s</i>	<i>s</i>
Grimaldi	69W	67S		220	220	410		16	0.75	<i>m</i>	<i>m</i>	<i>vw</i>
Planck	135E	58S		190	325			16		<i>l</i>	<i>w</i>	<i>vw</i>
Poincaré	161E	58S	70	180	335			17	1.6	<i>m</i>	<i>s</i>	<i>m</i>
Crisium	59E	16N		170	450	670	1060	17	0.5	<i>g</i>	<i>m</i>	<i>m</i>
Birkhoff	147W	59N		320	320			18		<i>l</i>	<i>w</i>	<i>w</i>
Unnamed (A)	108E	68S		285	285	580?		21	?	<i>l</i> ?	<i>vw</i>	<i>vw</i>
Janssen	39E	43S		160	160	350	540	22	0.8	<i>l</i>	<i>w</i>	<i>w</i>
Lorentz	97W	34N		160	330			23		<i>m</i>	<i>m</i>	<i>w</i>
Humorum	39W	24S		410	410	560	700	25	0.85	<i>g</i>	<i>w</i>	<i>w</i>
Unnamed (B)	123W	53N		135	410			25		<i>l</i>	<i>vw</i>	<i>vw</i>
Pingré	78W	56S		300	300	660?		25?	13	<i>l</i>	<i>vw</i>	<i>vw</i>
Near Schiller	45W	56S		180	350			26	5?	<i>m</i>	<i>m</i>	<i>vw</i>
Smythii	87E	1S		450	450	810?		27	1.9	<i>g</i>	<i>vw</i>	<i>vw</i>

<sup>a</sup> Most prominent ring is in italics.

<sup>b</sup> Estimated probable errors, given in text, average about 25%. Flooding and mare ages were not measurable in some cases.

<sup>c</sup> *v* = very

*s* = strong

*g* = great

*l* = little

*m* = moderate

*w* = weak

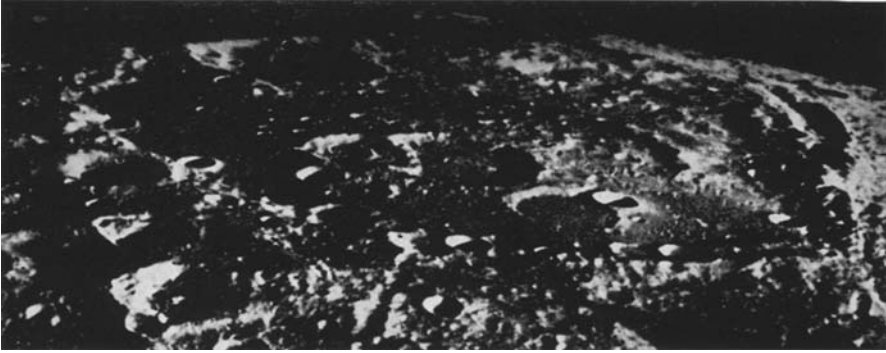


Fig. 15a. Planck basin. NASA Orbiter 3, M121.

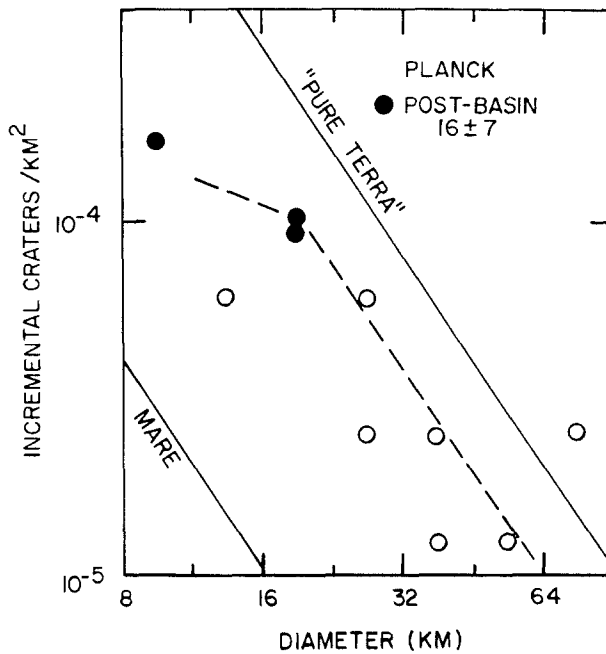


Fig. 15b. Crater diameter distribution in and near Planck.

(1) The special role of  $\sqrt{2}$  in ring diameter ratios is confirmed by Figure 27, which shows a histogram of ring ratios within each basin, measured with respect to the most prominent rings.

(2) There is repeated evidence for early flooding or destructive episodes at crater densities 3 to 8 in the stratigraphic column, after the basins formed but before most of the present-day maria.

(3) Most present dark maria have crater densities 0.5 to 1.9 (based on craters of  $D > 2$  km). A few have crater densities greater than 2, and are generally lighter in tone or show evidence of patchy overlying ray material.

(4) Radial systems disappear relatively quickly with increasing age. This occurs because these systems are primarily surficial, of low relief, and easily blanketed by ejecta and regolith.

(5) Concentric systems last longer, presumably because they have greater relief and perhaps because they have deeper-seated structural control.

(6) A flooding depth of the order of 3 km appears to be evidenced in various basins. This is considerably shallower than many authors have assumed in discussions of mascons, but is consistent with isostatic flattening of the basins before flooding.

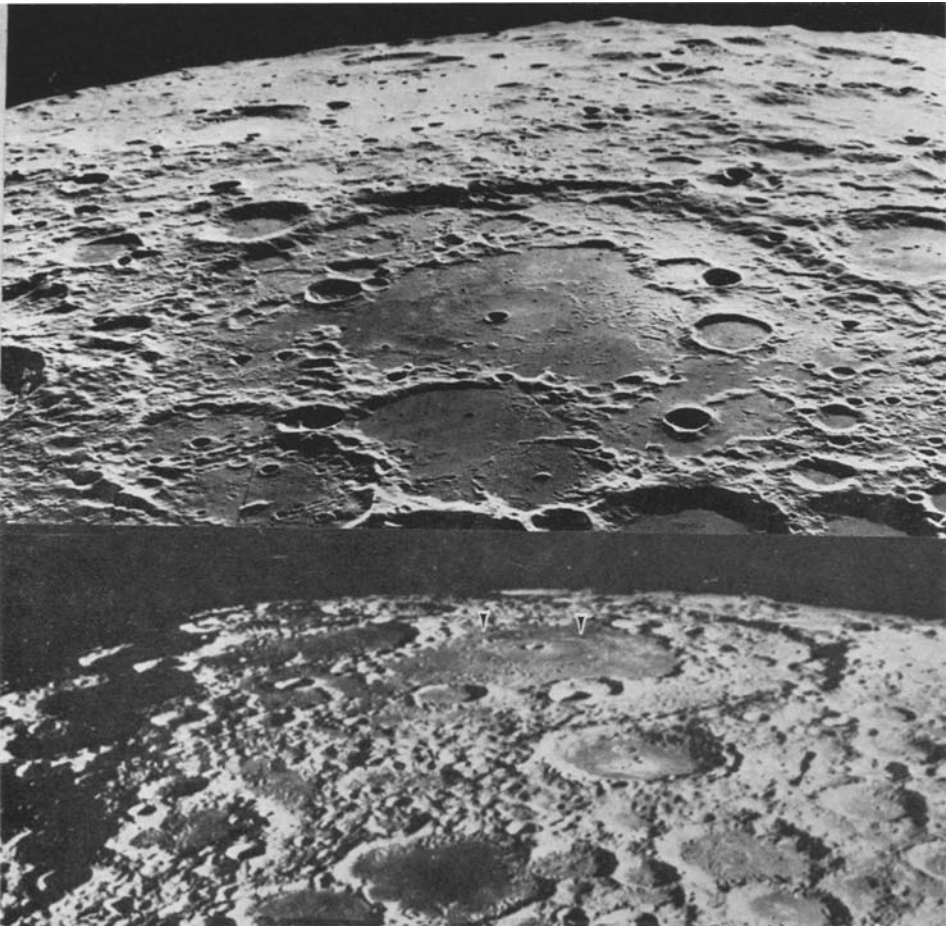


Fig. 16a. Poincaré basin. Second view shows more clearly the annular dark mare hue (arrows) just inside the innermost ring, suggesting extrusive activity along the inner ring.  
NASA Orbiter 5, M65; 2, M75.



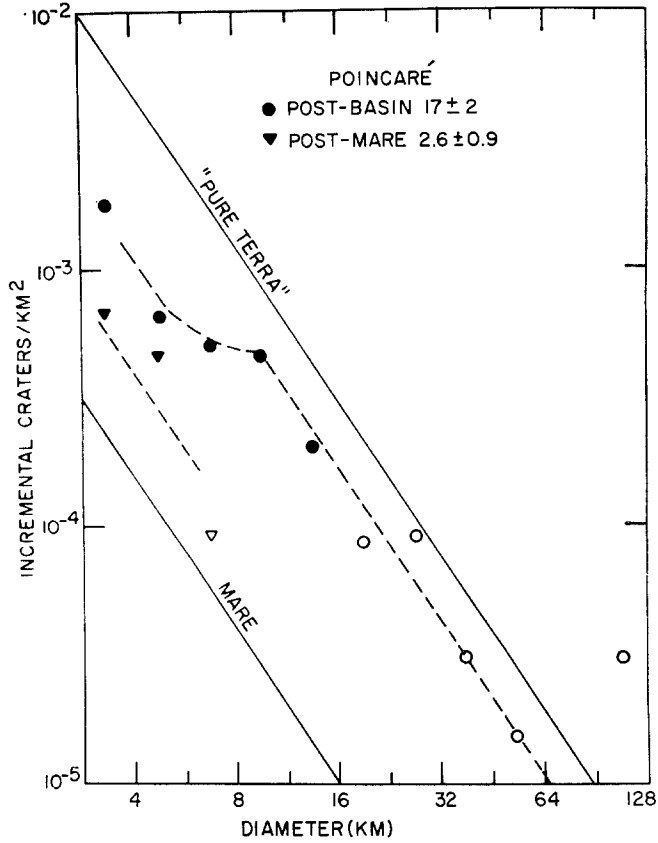


Fig. 16b. Crater diameter distribution on unflooded and flooded portions of Poincaré.

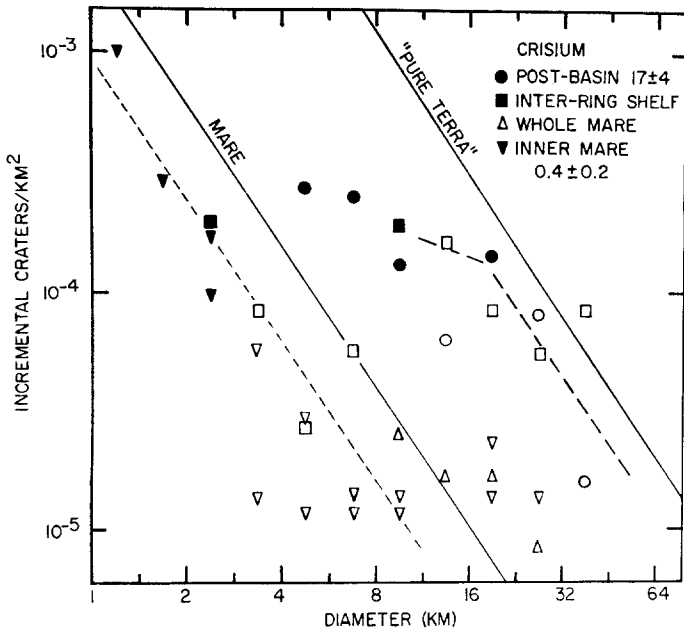


Fig. 17. Crater diameter distributions on unflooded and flooded surfaces of Crisium. Inner Mare Crisium gives evidence of being an unusually young mare surface.

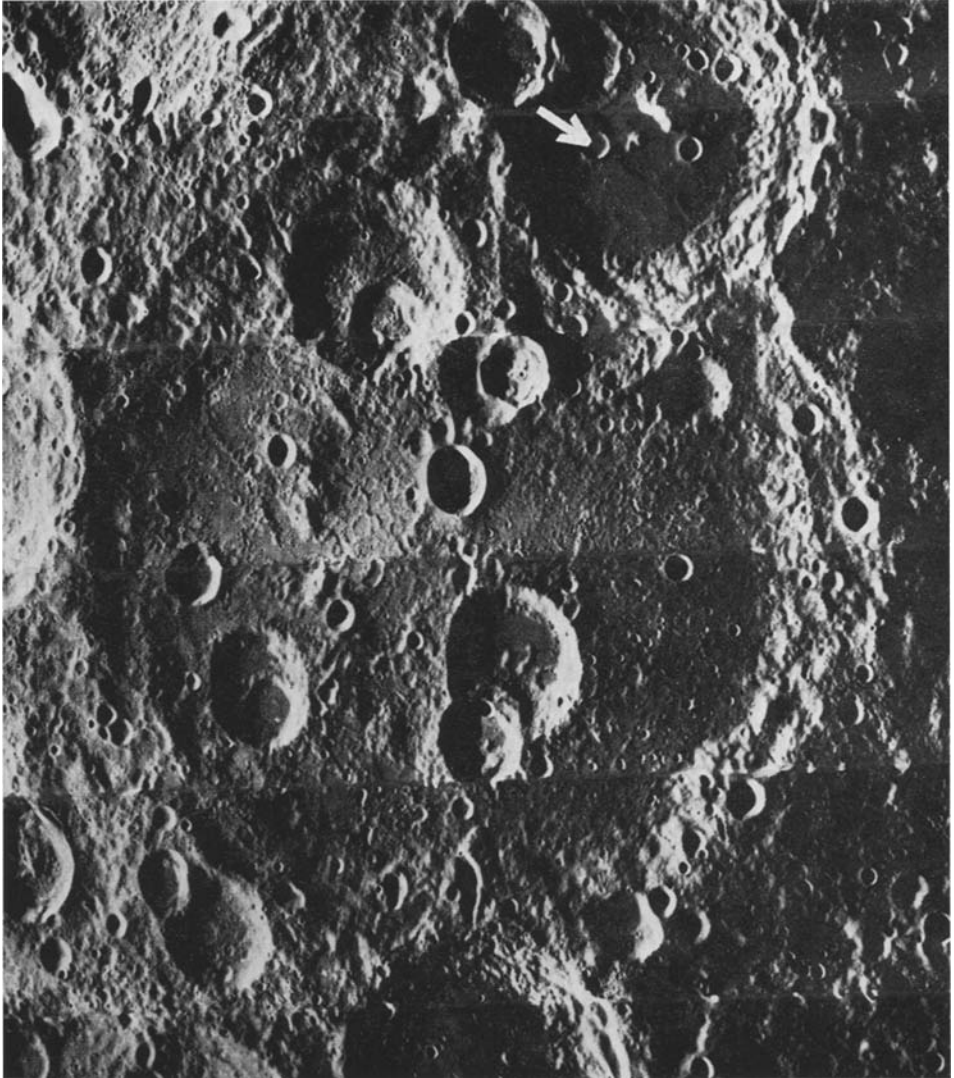


Fig. 18a. Birkhoff basin. An inner ring, nearly obliterated by craters, is visible. On the floor of a post-basin crater in the NNE (arrow), the continuation of the rim of Birkhoff is expressed in a wrinkle ridge, suggesting extrusive or intrusive activity on faults under basin rims. NASA Orbiter 5, M29.

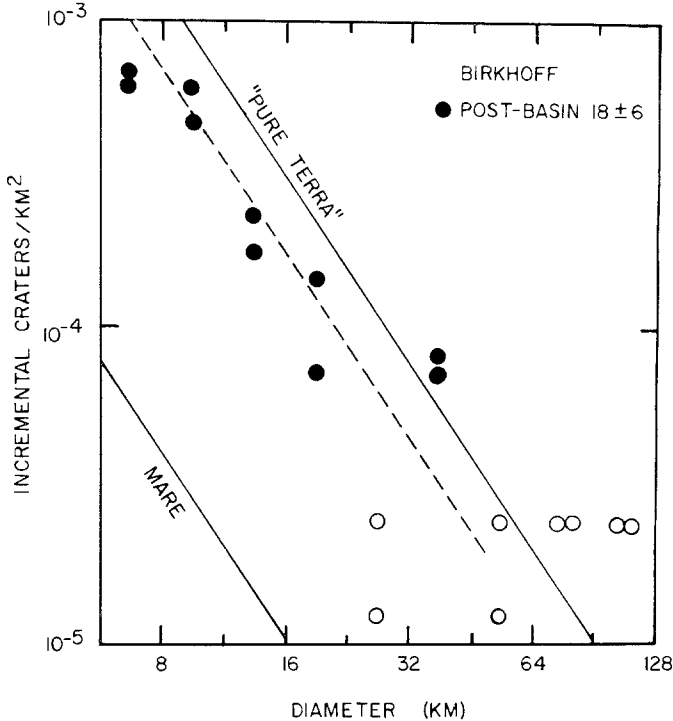


Fig. 18b. Crater diameter distribution in Birkhoff.

### 5. Latitude Distribution of Basins and Large Craters

A polar concentration of old craters of  $D > 40$  km was found by Hartmann (1968c) in terra areas on the front and back sides; post-mare craters did not show such a strong polar concentration. One hypothetical explanation was that the earliest bodies to strike the Moon struck preferentially in the polar regions for unknown reasons, possibly involving proximity to the Earth of the early Moon. Possible alternative explanations were preferential formation of very large volcanic craters near the poles, or destruction of impact craters by volcanism or tectonism preferentially near the equator.

Theoretical support for the first alternative comes from calculations of impact positions by Barricelli and Metcalfe (1969) indicating that certain families of circumterrestrial planetesimals exterior to the Moon's orbit can be perturbed into lunar collisions with non-random latitude distributions. For example, a family of 23 planetesimals with inclinations to the Moon's orbit of  $4^\circ$  to  $5^\circ$ , but depleted in inclinations of  $0^\circ$ , gave 61% of all impacts in the half of the Moon within  $30^\circ$  of the poles. Further calculations of this sort are needed before any rational explanation of a polar concentration can be offered.

We have extended the evidence for a polar concentration. Figure 28 shows the

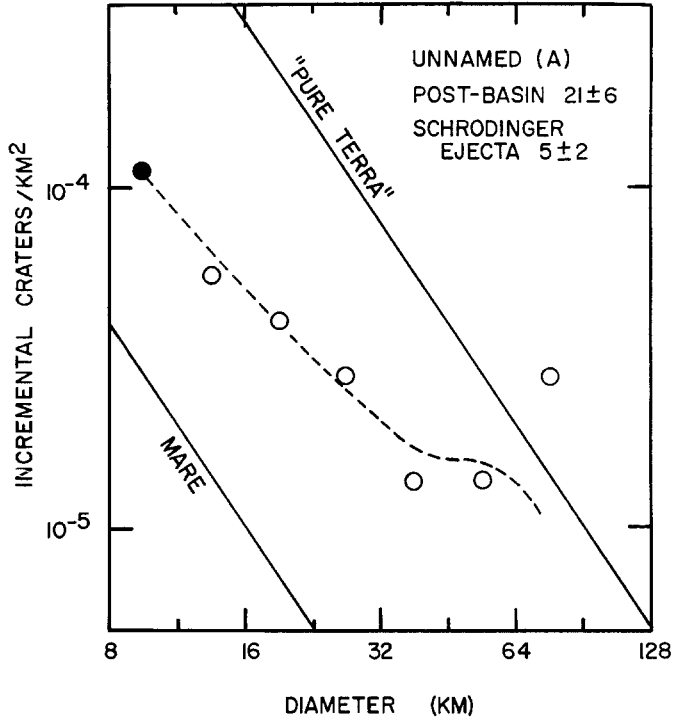


Fig. 19. Crater diameter distribution in unnamed basin '(A)'.

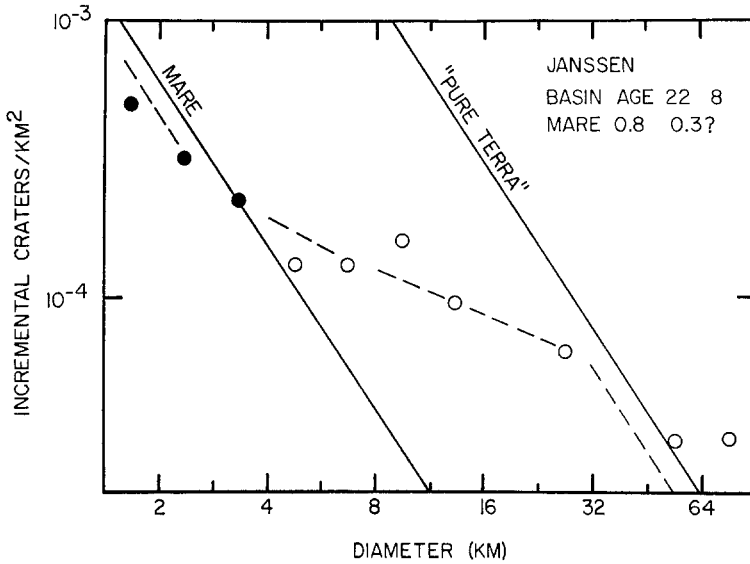


Fig. 20. Crater diameter distribution in and about Janssen.

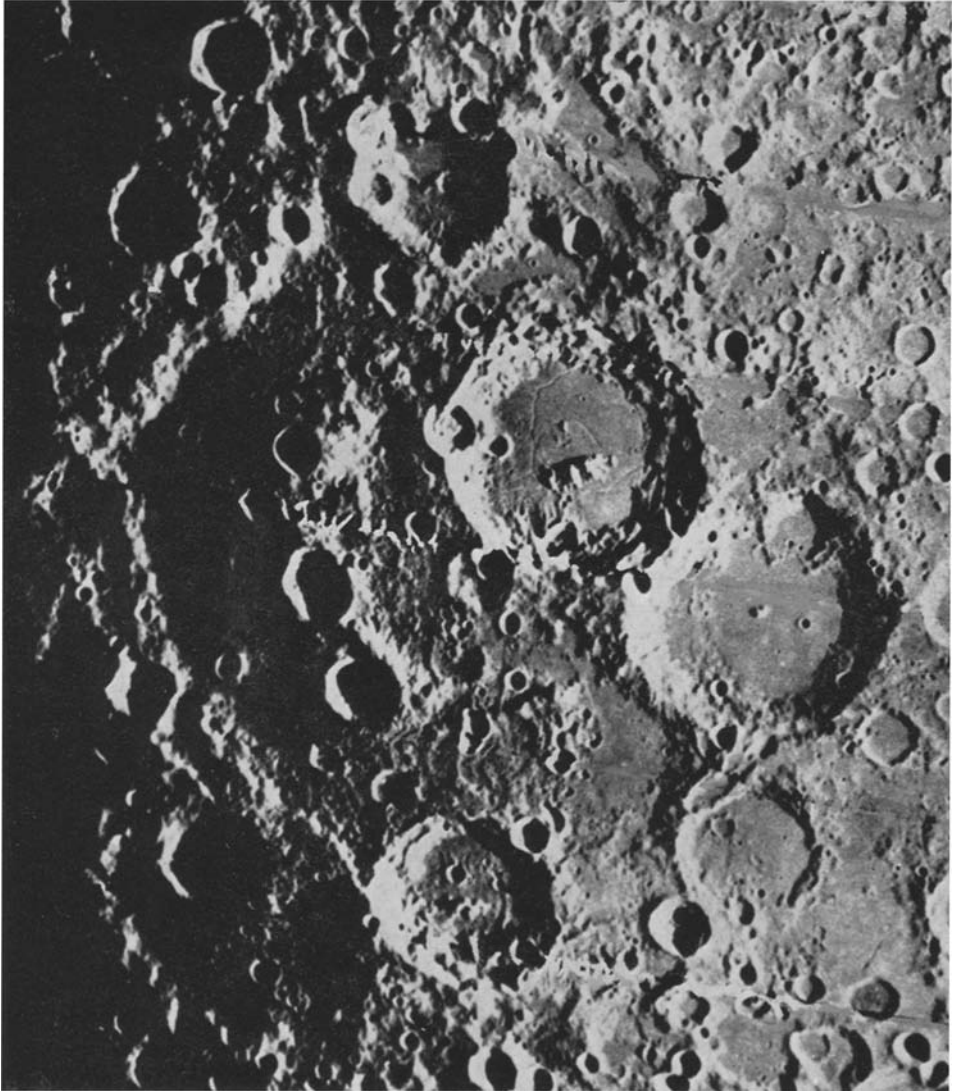


Fig. 21a. Lorentz basin. A well-defined inner ring is partly obliterated by craters.  
NASA Orbiter 4, M189.

latitude distribution of the 27 multiple-ring basin systems listed in Table II, plotted by equi-area latitude zones. In spite of the small statistical sample it is noted that 70% of the basins occur in the polar half of the Moon exceeding 30° latitude.

As an independent check, we have tabulated for the *far side only* all craters and basins of diameter  $D > 181$  km. Table III lists the resulting 42 structures. Figure 29

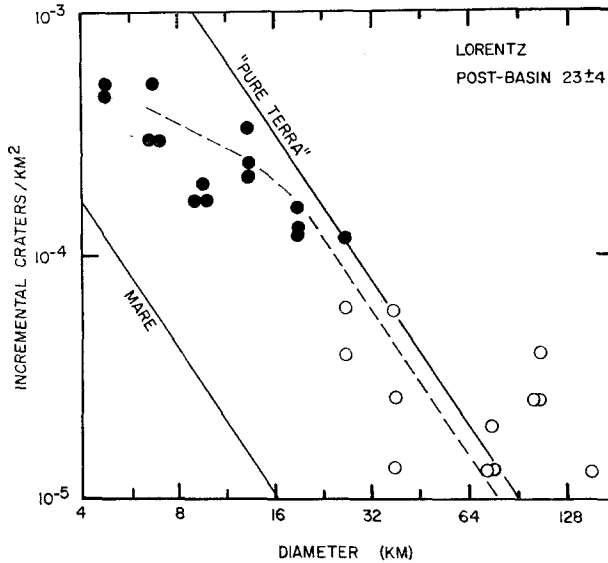


Fig. 21b. Crater diameter distribution in Lorentz basin.

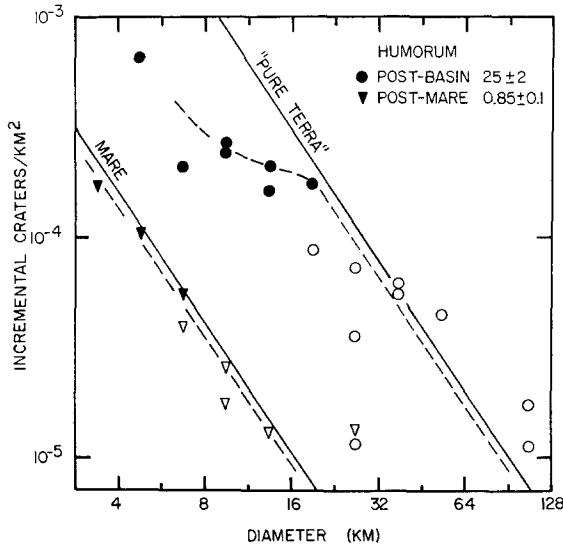


Fig. 22. Crater diameter distribution on unflooded and flooded surfaces in Humorum basin.

shows the latitude distribution of these features. Again, a polar concentration is found, with 64% of the structures falling in the polar half of the Moon exceeding 30° latitude. Since the far side of the Moon is almost entirely terrae, and since we have used only the largest structures, we can be sure that mare flooding is not effective

TABLE III  
Farside basins and large craters and basins  
( $D \geq 181$  km)

Name	Long.	Lat.	Diam.
Joliot-Curie	94E	26N	182
Riemann	95E	40N	195
Fabry	101E	43N	195
Compton	104E	56N	185
Pasteur	105E	12S	235
Unnamed (A)	108E	68S	285, 580
Milne	113E	31S	120, 240
Schwarzschild	120E	70N	205
Fermi	123E	19S	241
Unnamed (VI)	124E	81S	335
Tsiolkovsky	129E	21S	198
Schrödinger	132E	75S	155, 320
Planck	135E	58S	190, 325
Mendeleev	141E	6N	330
Moscoviense	147E	26N	205, 305, 410, 700
Gagarin	149E	20S	270
Campbell	151E	45N	235
Poincaré	161E	58S	70, 180, 335
Unnamed (a)	162E	6N	192
Ingenii	163E	33S	320
D'Alembert	164E	52N	220
Unnamed (b)	171E	20S	190
Unnamed (c)	175E	48S	240
Von Karman	176E	48S	240
Leibnitz	178E	38S	250
Unnamed (d) <sup>a</sup>	167E	18N	600
Oppenheimer	166W	36S	215
Korolev	157W	4S	209, 405
Apollo	153W	36S	235, 435
Galois	152W	14S	205
Mach	149W	18N	205
Birkhoff	147W	59N	170, 320
Fowler	145W	43N	185
Zeeman	134W	75S	201
Chebyshev	133W	34S	182
Hertzprung	129W	1N	285, 440, 500
Unnamed (B)	123W	53N	135, 410
Landau	119W	42N	220
Boltzmann	115W	55S	200
Lorentz	97W	34N	160, 330
Oriente	96W	21S	320, 620, 1300
SE Limb	94W	49S	220, 480

<sup>a</sup> First described by R. Baldwin (1969).

in biasing the data. A tabulation of the 42 structures by longitude revealed no non-randomness in longitude distribution.

McCauley (1970, private communication) has pointed out that the terrae are not homogeneous, but made up of distinguishable provinces, some of which have been rejuvenated by constructional volcanic activity (not simple mare flooding). Therefore the question of whether the polar concentration of old craters and basins is due to internal effects or celestial mechanical external effects remains an open research topic. If celestial mechanical influences can be confirmed, the polar concentration gives a powerful indicator of the origin of the bodies causing the basins – probably favoring a circum-terrestrial source, as indicated by the papers quoted above.

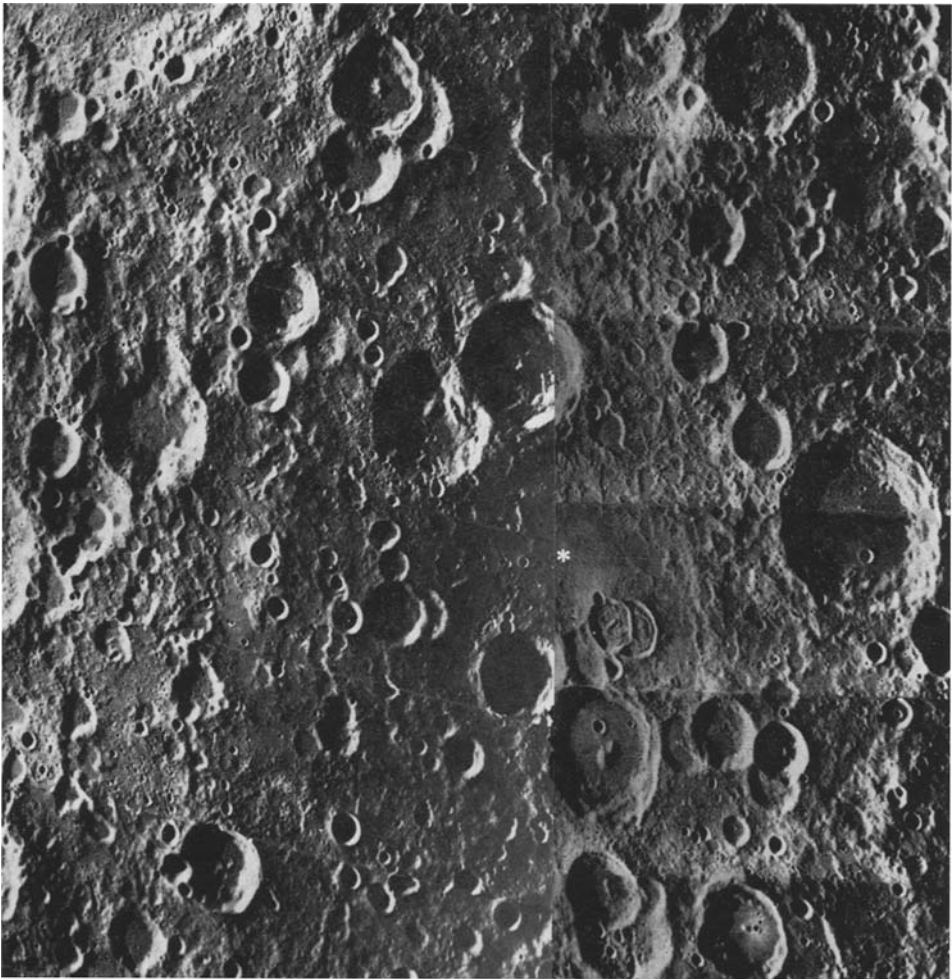


Fig. 23a. Unnamed basin '(B)', an ancient basin revealed under low lighting by a depressed patch (star) with some flooding and traces of outer arcs. NASA Orbiter 5, M25; 5, M5.



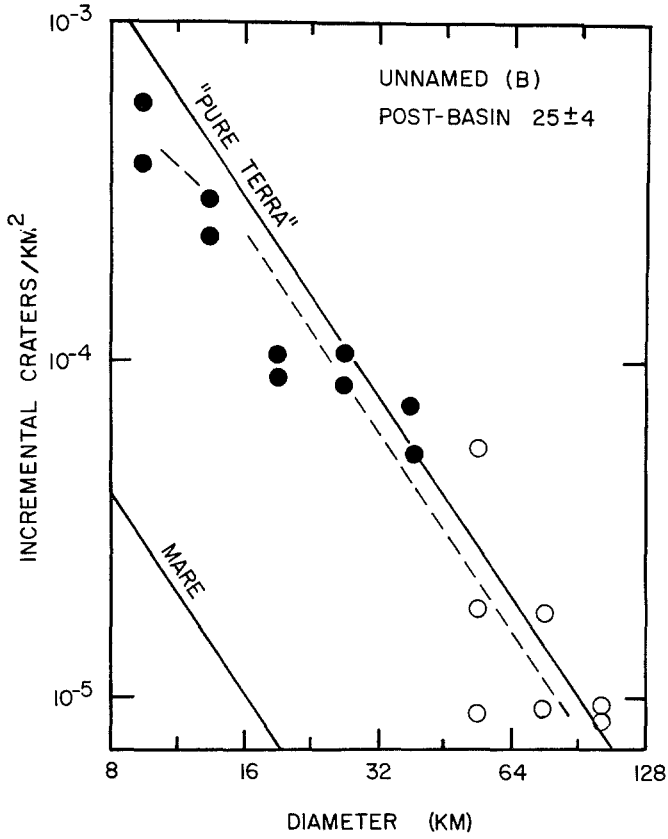


Fig. 23b. Crater diameter distribution in and about unnamed basin '(B)'.

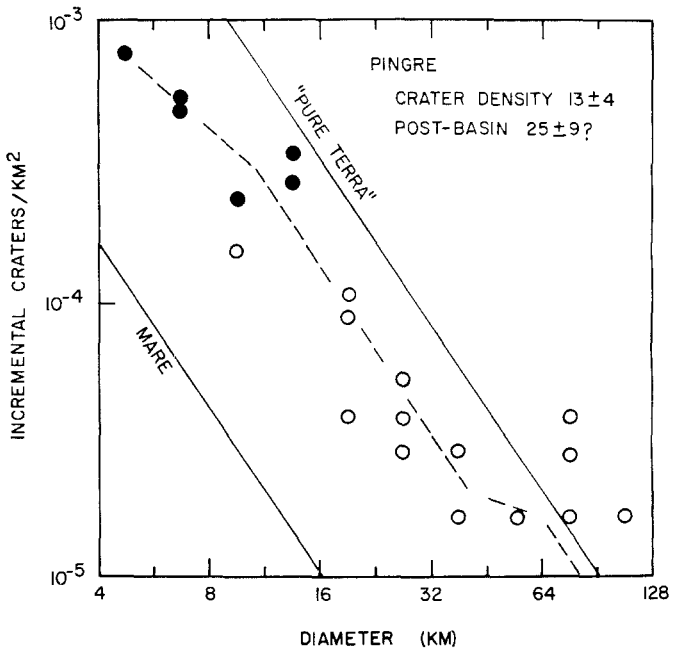


Fig. 24. Crater diameter distribution in and about Pingré basin.

## 6. Diameter Distribution and Origin of Basins

Figure 30 shows the diameter distribution of the basins plotted along with the mare crater distribution and that of the terrae for which data points ('*T*') are given. Defining the basin diameter distribution is not simple. First, one must decide whether to use the diameter of the largest, smallest, or most prominent ring. In addition, one is faced with the possibility that mare lava flooding seriously depleted the number of visible basins. In Figure 30 we plotted diameters of most prominent rings for both the whole Moon and the back side alone, thus avoiding mare contamination. For comparison we also made plots using the outer and inner ring diameter over the whole Moon and back side but in no case could we conclude that the basin distribution fell on the same straight line as the terra craters, '*T*'. Rather, the basins were

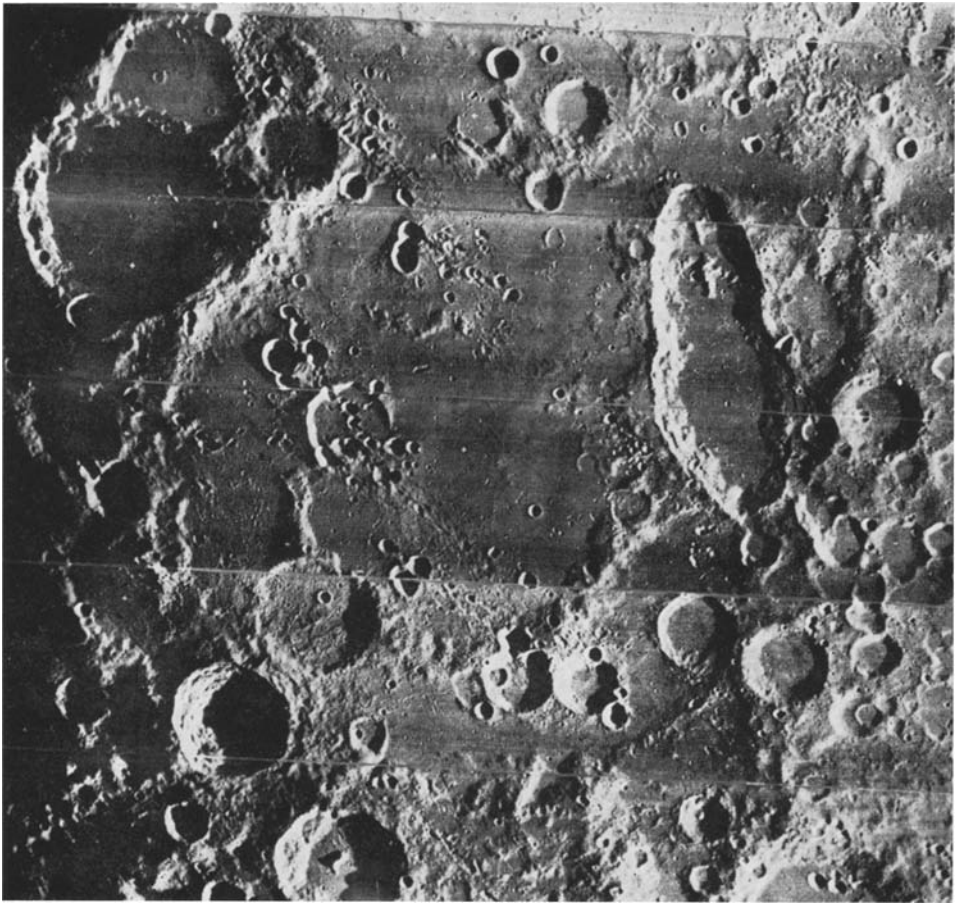


Fig. 25a. Unnamed basin 'Near Schiller'. Floor shows all morphological characteristics of mare flooding, but is high in albedo, probably due to thin veneer of ray material. Darkest is an annulus near center, suggesting extrusive activity along innermost ring. NASA Orbiter 4 M142.

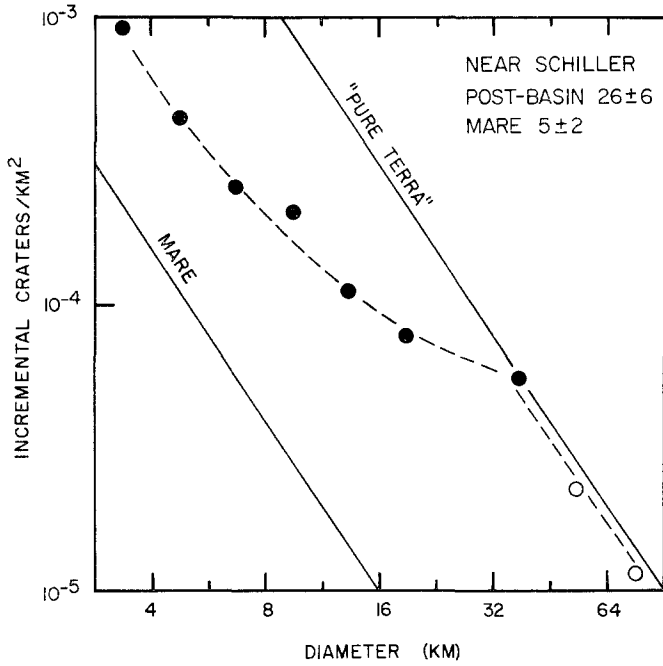


Fig. 25b. Crater diameter distribution in and about basin 'Near Schiller'.

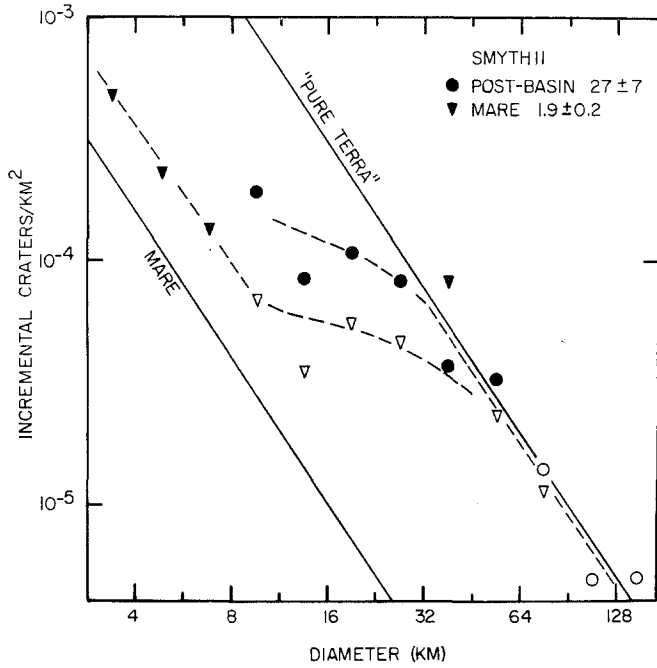


Fig. 26. Crater diameter distributions on unflooded and flooded surfaces in Smythii basin.

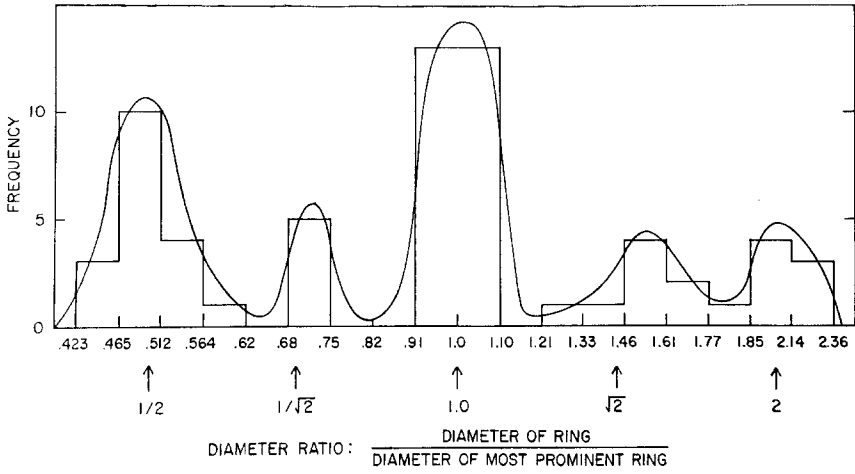


Fig. 27. Histogram of ring diameter ratios among all lunar basins, showing significance of  $\sqrt{2}$  relationship.

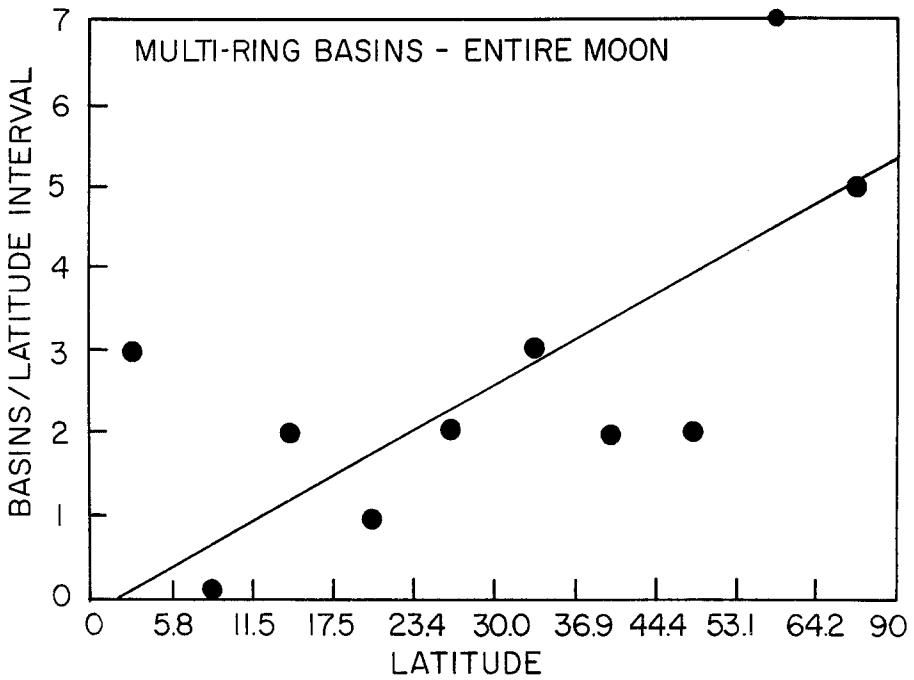


Fig. 28. Latitude distribution of all lunar basins (Table II), showing indication of polar concentration.

deficient with respect to this line, and fitted a well-defined line joining the terra crater distribution with different slope. This revises a conclusion by one of us (W.K.H., 1966a) based on preliminary counts from far-side Zond photographs that the basins did extend the straight terra crater distribution.

We will next consider possible explanations for the deficiency of basins and large craters.

In the remainder of this section we will assume that the basins were initiated by impact events. The justification for this is: The basins are certainly point-source explosion sites, as evidenced by their massive ejecta blankets and the high degree of radial and concentric symmetry in surrounding structure. Therefore, if they are endogenic, they cannot be explained as simple caldera-like collapse features, although

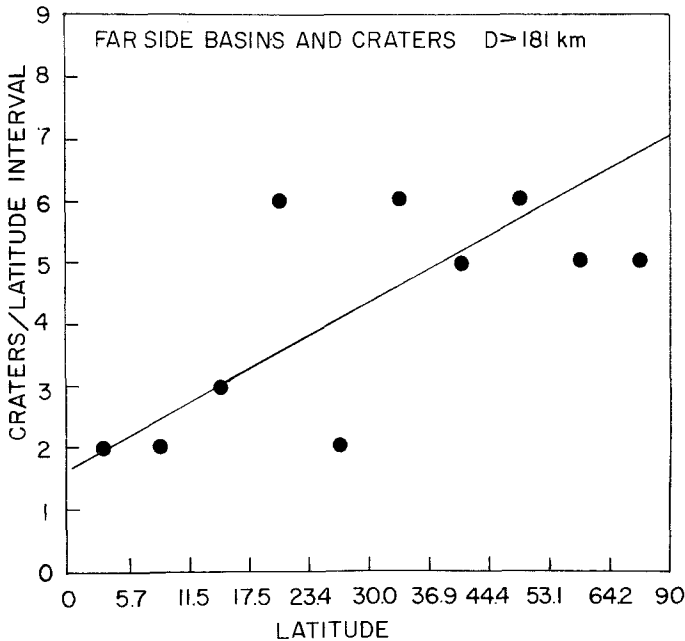


Fig. 29. Latitude distribution of basins and large craters on lunar farside (mostly terra), showing indication of polar concentration.

caldera-like collapse apparently played a role in forming the outer rings. The energy required to throw the ejecta blanket of a typical large basin out of the inner basin is of the order of  $10^{31}$  erg. This is nearly a million times the energy released in the largest recorded earthquakes and is about  $10^5$  times the annual earthquake energy released in the entire planet Earth (Jeffreys, 1962, p. 107). On these grounds, it appears unlikely that an internal tectonic mechanism of the Moon would produce enough explosive energy to form a basin.

Having ruled out endogenic collapse or explosive mechanisms, we are left with impacts. The impact mechanism is reasonable since an impact by one of the larger asteroidal bodies would release  $10^{31}$  erg and create a basin-size crater.

The question now remains, can we convert the observed diameter distribution of basins into a reasonable mass distribution for the impacting bodies? We will consider

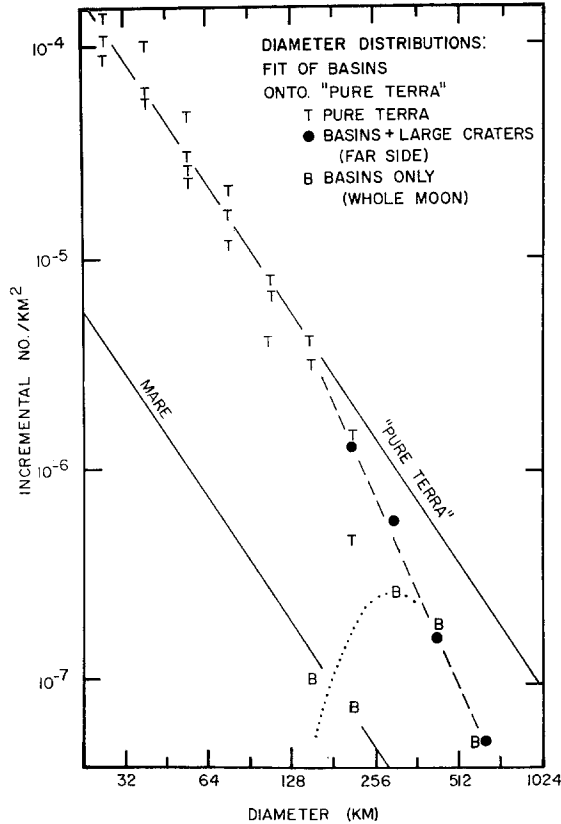


Fig. 30. Diameter distribution of lunar basins. Solid lines are references (mare and 'pure terra'). Dotted line shows diameter distribution among multi-ring basins only. Dashed line includes both basins and large craters and is the accepted empirical curve, which incidentally fits onto the crater counts 'T' from pure terra surfaces.

three hypotheses. Hypothesis 1: The observed distribution is the normal mass distribution of the meteorites that formed the terra craters (Figure 30). Under the normal laws governing meteorite mass distribution (Marcus, 1965; Hartmann, 1969) any meteorite population that produced the terra craters 'T' would also produce the dotted extension of line 'T', because such bodies are fragmented according to a fixed power-law mass distribution. Therefore, hypothesis 1 fails. Hypothesis 2: The basins reflect not a normal meteorite mass distribution but rather the mass distribution of

the original, ancient planetesimals being swept up by the Moon. Anders (1965) gave some evidence that the initial mass distribution of the unfragmented planetesimals was different from that of the present-day, fragmented meteorites. Models of the mass distribution among them, however, (Anders, 1965; Figure 4; Hartmann and Hartmann, 1968, Figures 1 and 3) suggest that the large planetesimals would be

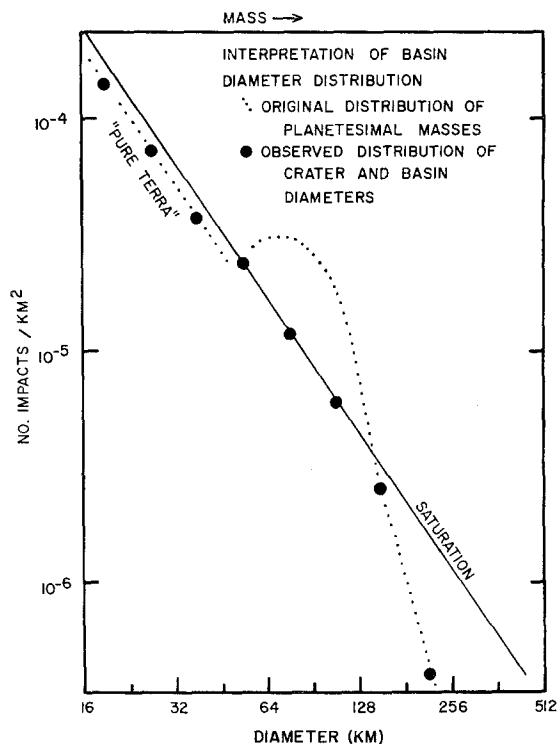


Fig. 31. A possible interpretation of the diameter distribution of lunar basins and large craters (Hypothesis 2: see text).

overabundant, not underabundant. Due to near-saturation or saturation cratering in most of the uplands, we could still argue that such an overabundance might not be detected. The data could thus be interpreted as in Figure 31. Hypothesis 3: While we have not ruled out hypothesis 2, another interesting possibility is that the difference between the basin curve and the upland 'U' curve is not a deficiency in *number*, but rather a deficiency in crater *diameter*. This means that the basins represent the same original population of objects as the upland craters. but that the larger objects impacted at *lower velocities* than the smaller objects. This idea may seem at first sight far-fetched, but could be interpreted plausibly as follows. The offset in diameter from the basin curve to curve 'T' is a factor about 1.9 in diameter. By using the scaling law

between the crater diameter  $D$  and the energy  $E$ , we have

$$D = kE^{1/3.3} = \frac{k}{2} M^{1/3.3} V^{2/3.3},$$

which converts the diameter difference to a velocity difference of a factor about 3.

Now consider a catastrophic event in the circum-terrestrial, cis-lunar neighborhood. This event could be fission of the Moon from the Earth, or a major impact on the Earth or Moon, etc. The event would produce fragments with some degree of equipartition of energy. The low-velocity, large masses thus could be bound in the Earth–Moon system and could impact the Moon at its escape velocity, 2.4 km/sec. The higher-velocity small masses preferentially escape the Earth–Moon system and go into solar orbit. Arnold (1965, Figure 8) and Öpik (1966, p. 322) have shown that in such a situation many of the particles are eventually swept up again by the Moon. The bulk of these ( $\sim 80\%$ ) strike the Moon again within  $10^7$  years at mean impact velocity of 5 km/sec. The last particles to strike, however, impact up to  $10^8$  years later and because they have suffered multiple perturbations they impact from more eccentric orbits with higher velocities ranging in extreme cases up to some 20 km/sec. Thus the typical velocity of the last impacts in this early epoch would be greater than 5 km/sec, the modal velocity of the last half of Arnold's impacts being approximately 9 km/sec. We can thus assert that a separation of high-and-low mass objects produced catastrophically in the early Earth–Moon system would produce just the observed impact velocity range of about a factor 3.

If this hypothesis be accepted, it is evidence not only for low impact velocities among the early basins, but also for a catastrophic event within the Earth–Moon system some  $10^8$  years before the formation of the most recent basins. This event could have been associated with the formation of the Moon.

Although we cannot choose between hypotheses 2 and 3 we note that in both cases the basins must be interpreted as formed by *very early planetesimals* that were left over from or created during the formation of the Moon. This accords with the fact that ages of Apollo 11 and 12 samples place the formation of the basins prior to 3.9 aeons ago, i.e., during the first few  $10^8$  yr of the Moon's history.

## 7. Mechanics of Ring Production

We will now consider the evolution of the basin systems in the next few sections, which are arranged in a chronological sequence from basin-formation to basin-filling by lava.

The review of the literature, Section 3, left us in an unsatisfactory position, because the hypotheses involved only a diversity of possible mechanisms. At best, it can be said that the hypersonic basin-forming impact initiates shock phenomena that result in concentric ring fractures. Whether this happens by wave interference, or wave reflection from crustal layers, etc., is uncertain.

*Possible Terrestrial Analogs.* We will now consider additional evidence. Table IV



TABLE IV  
Possible terrestrial analogs

Crater	Ref.	Ring Feature	Est. diam.	Ratio	
Clearwater Lake (W) Impact?	Dence (1964)	Original rim	32 km	1.00	
	Dence <i>et al.</i> (1964)	Original inner ring crest (est.) Faults at edge of central uplift (est.)	17 km 8.6 km	0.53 0.27	
	Dence <i>et al.</i> (1968)	Original rim Islands and breccia annulus	12.5 km 5.3 km	1.00 0.42	
Deep Bay Impact	Innes (1964)	Original rim Concentric fault	19 km 9.5 km	2.00 1.00	
	Wilshire and Howard (1968) Howard and Offield (1968)	Original rim Upturned edge of central uplift	4.9 km 1.38 km	1.0 0.54	
Flynn Creek Impact?	Roddy (1965)	Original rim Sediment hills Orig. edge of central uplift	3.5 km 1.9 km 0.77 km	1.00 0.54 0.22	
	Physics 8 Collapse over underground nuclear explosion	Los Alamos, private communication (1969)	Outer cracks Main flexure Initial flexure	69 m 46 m 33.5 m	1.50 1.00 0.73
		Sukharov (1968)	Outer anticline Main rim (?) Inner anticline Innermost anticline	61 m 42 m 23 m 14.2 m	1.45 1.00 0.54 0.34
Prairie Flat (Dres) Explosion of 500 T TNT at surface					

lists some possible terrestrial analogs of lunar basins. These are diverse craters: five probably impacts, a collapse, and surface explosion. All show multiple rings and some tendency to follow the  $\sqrt{2}$  or factor 2 spacing law.

Innes (1964) shows that the Deep Bay structure is very probably an impact crater, originally of about 9.5 km diam. Innes maps an outer fault ring whose diameter is 2 times the original rim diameter. The outer ring is shown in Innes' cross-section as a normal fault with subsidence into the central crater, and finds its present expression in a depressed zone containing at least one accurate lake. This is the closest terrestrial analog to the outer rings of lunar basins. Innes makes the important point that the fractured and shocked zone under the crater continues *out* beyond the main rim to about the position of the outer ring. This accords with lunar experience in which inter-ring zones outside the main rim are found to be faulted and crossed by orthogonal lineaments.

Innes also notes that a 1962 impact experiment by Shoemaker and Gault produced a 5 cm crater surrounded by an 'almost completely circular fracture' of diameter 11 cm, a 2.2 ratio.

Figure 32 shows inferred original cross-sections of three probable impact craters: Deep Bay (after Innes, 1964) and the double-ring feature Clearwater Lake (W) (after

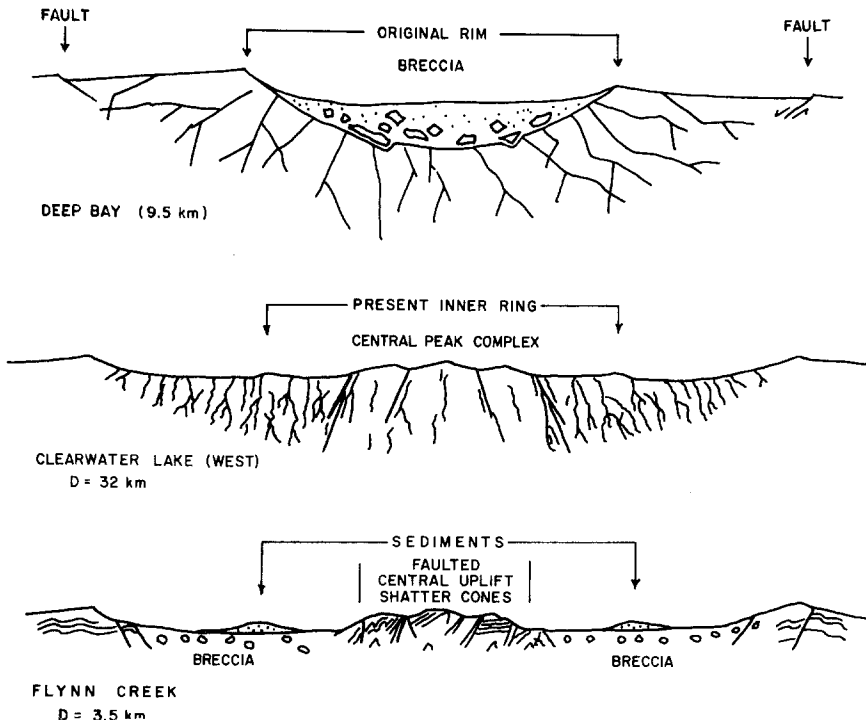


Fig. 32. Cross-sections of terrestrial impact craters, showing possible analogs to inner rings and central peaks of lunar features. Top: Deep Bay, after Innes (1964). Middle: Clearwater Lake (W), after Dence *et al.* (1968). Bottom: Flynn Creek, after Roddy (1965).

Dence *et al.*, 1968) and Flynn Creek (after Roddy, 1965). Dence *et al.* do not indicate an anomalous structure underlying the pronounced inner ring of Clearwater Lake, but they do show major faults bounding the central uplift. These faults lie at approximately  $\frac{1}{4}$  the crater radius. Clearwater Lake (W) appears the best terrestrial analog in scale and form to basin inner-ring structures.

Dence *et al.* consider Nicolson Lake to be a deeply eroded impact crater, and they note an 'annulus' of coherent breccia outcropping on islands which suggest an inner raised ring at about  $\frac{1}{2}$  the radius of the crater. Mistastin Lake, identified as a 20 km impact crater, also has an inner, arc-shaped island (Taylor and Dence, 1969). Roddy's (1965) analysis of the Flynn Creek structure (Figure 32, bottom) shows the edge of the central uplift in a position similar to that found in Clearwater Lake (W). Hills or a ring lie at  $\frac{1}{2}$  the crater radius, but Roddy maps these as sediment remnants overlying the breccia-filled floor, in which case they would not be tectonically significant.

Twenty-three minutes after the Physics-8 underground nuclear test, a collapse crater formed within an interval of a few seconds. Figure 33a shows the state of this crater during its first instants, before the crater was complete (blurred jets of dust are escaping from cracks in the center). Two distinct radii are of interest: a point of flexure where the railroad tracks break, and the outer cracks. When the cratering was complete, new outer cracks defined a third position (arrows). These three radii have the same relative values commonly found for lunar basin rings. These cracks are reminiscent of the kind of  $\sqrt{2}$ -spaced fractures postulated by Fielder (1963) for lunar collapses, based on the work of Lance and Onat (1962), to which we will return.

A different phenomenon appears in the Canadian Prairie Flat (DRES) explosion crater (Figure 33b). Here are a series of ring anticlines and synclines. Of all known terrestrial and lunar examples, these are closest to the sort of frozen waves postulated by Baldwin (1963) as the origin of lunar basin rings. They do not give as good a fit as the Physics-8 fractures to the lunar  $\sqrt{2}$  spacing law, however, and the wave-like appearance does not truly resemble the lunar basins. It is interesting that, as Hope (see Sukhanov, 1968) remarks, water extruded from fractures in the low zone and formed annular lakes (black in photo), resembling the annular extrusive maria around Orientale and some other basins.

Dence *et al.* (1968) make the following generalization about the structure of the Canadian impact craters, based on drilling and geophysical measures:

... craters formed in plutonic rocks can be classified as either simple craters or complex craters. Simple craters have a lens of mixed breccias thickest in the center; complex craters have a central uplift of weakly to moderately shocked autochthonous gneisses, a blanket of shocked ejecta in an annulus around the center of the uplift, and a peripheral depression.

The transition from simple to complex structures occurs with increasing diameter between 4 and 9.5 km diameter, according to Dence *et al.*, but Flynn Creek (3.5 km) appears to have complex structure. We infer that this transition corresponds to the lunar transition from craters without central peaks to craters with central peaks and the first traces of ring structure. Wood (1968) found that in well-preserved lunar craters, noticeable central peaks begin to appear at a diameter about 10 km (in a



Fig. 33a. Artificial collapse crater forming over site of the underground 'Physics-8' nuclear blast. Arrows show positions of outer cracks at completion of crater-forming process. b. Artificial explosion crater – Canadian Prairie Flat (DRES) experiment. The crater is surrounded by a series of ring anticlines and synclines. Water (arrows) extruded in ponds in main syncline.

few percent of the craters) and increase in frequency, reaching a maximum of 100% in craters larger than about 60 km. It would thus appear that the brecciated, faulted, shocked central uplifts of terrestrial craters are related to lunar central peaks, but occur at smaller sizes on Earth than on the Moon.\*

At lunar crater diameters exceeding 140 km, the multi-ring structure diagnostic of basins begins to appear strongly. In the spirit of Dence *et al.*, we suggest that another transition of uncertain nature appears in the crater-forming process at this diameter, producing multiple rings.

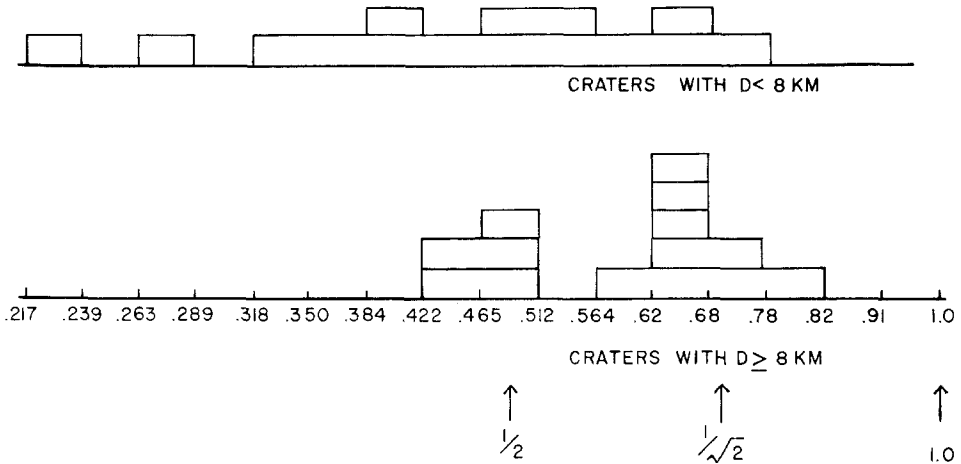


Fig. 34. Histogram of ring diameter ratios among small (top) and intermediate-size (bottom) double-ring lunar craters. The latter group shows significant  $\sqrt{2}$  clustering, reminiscent of relations among basin rings (Fig. 27).

*Double-Ring Lunar Craters.* Central uplifts in terrestrial and lunar craters are sometimes detected at diameters smaller than that at which lunar central peaks are commonly detected. In the same way, the structures associated with major basin systems may sometimes be detectable in craters smaller than full-fledged basins. In this way we can perhaps account for familiar examples of small, double-ring craters, not normally considered to be basins.

Table V lists an incomplete selection of double-ring craters. Even this short list of examples shows clustering about radii ratios of about 0.46 and 0.70, as in basins (cf. Figures 27 and 34). Close examination of these rings suggests that they are extrusions inside the rims of normal craters (Figure 35). Certainly the intimate relation between ridges and graben-like rilles (e.g. Posidonius) indicates that faulting plays a role in the production of these rings. In this section we will go no further than to

\* Work in progress shows that Martian craters commonly contain central peaks at crater diameters about 15 to 30 km, intermediate between the lunar and terrestrial cases. Homology relations based on planetary scale may be involved.

TABLE V  
Possible transitions from lunar craters to lunar basins

Crater	Rim diam. (Arthur Catalog)	Concentric structure	Ratio
Gassendi	110	Ridge, flooded boundaries	0.72
Posidonius	101	Peaks and ridge changing into rille	0.66
La Condamine	37	Hills and rilles	0.51
Lavoisier C	31	Ridge changing into rille (Inner edge of graben?)	0.79
Kunowsky	18	Discontinuous ridge, central peak-ring	0.63
Damoiseau D	16	Continuous ridge or shelf	0.72
Hesiodus A	15	Continuous rim	0.48
Pontanus E	12	Continuous rim in old crater	0.59
Lagrange T	11	Continuous rim	0.45
Crozier H	11	Continuous bulbous rim	0.47
Lavoisier	10	Continuous rim	0.67
Damoiseau BA	9	Continuous rim	0.64
SSE of Lehmann C	9	Continuous rim	0.44
Repsold A	8	Raised 'shelf' on rim	0.64
Gambart J	7	Continuous low ridge	0.45
Gruithuisen K	7	Merging hills, continuous ring	0.53, 0.23
S of Markov	7	Continuous bulbous ring	0.37
Archytus G	7	Continuous low ring	0.66
Between Atlas and Endymion	6	Broken hilly ring, continuous ring	0.65, 0.40
W of Bouguer B	6	Raised 'breadcrust' hill	0.40
Marth	6	Continuous ring, hilly	0.48
NW of Herschel M	5	Continuous ring, foot of wall	0.27
W of La Condamine F	5	Continuous ring, foot of wall	0.35
Mersenius M	4.4	Continuous, bulbous ring	0.51
In Fraunhofer	4	Raised 'shelf' on rim	0.70
Between Rocca F and Q	1.9	Merging hills	0.53
Between Cruger and Cruger E	1.5	Continuous ring (?)	0.62

suggest a relation between double-ring craters and the larger features we have called basins.\*

We have seen repeated evidences of faulting: (1) in the shape of outer scarps, such as those around Orientale; (2) in the lava extrusions at the base of such scarps; (3) in the orthogonal radial-concentric patterns associated with such scarps in Orientale, Imbrium, Crisium, and elsewhere; (4) in the association of grabens with rings inside

\* It should be clear that the double-ring craters we refer to here are different from the smaller craters studied by Gault (1969) in which a subsurface resistant layer causes deformation of the crater floor. Craters with shelves along the lower inner wall were explained in this way as being affected by the interaction of the shock wave with the strong substrate. Lunar craters so affected are usually smaller than a kilometer. However, we do not rule out interactions between shock waves and stratified inhomogeneous subsurface layers as an influence in forming multiple rings. Indeed, such a cause has been suggested for the rings found in the Canadian DRES explosion crater and various suspected impact craters (McCauley, 1970, private communication).

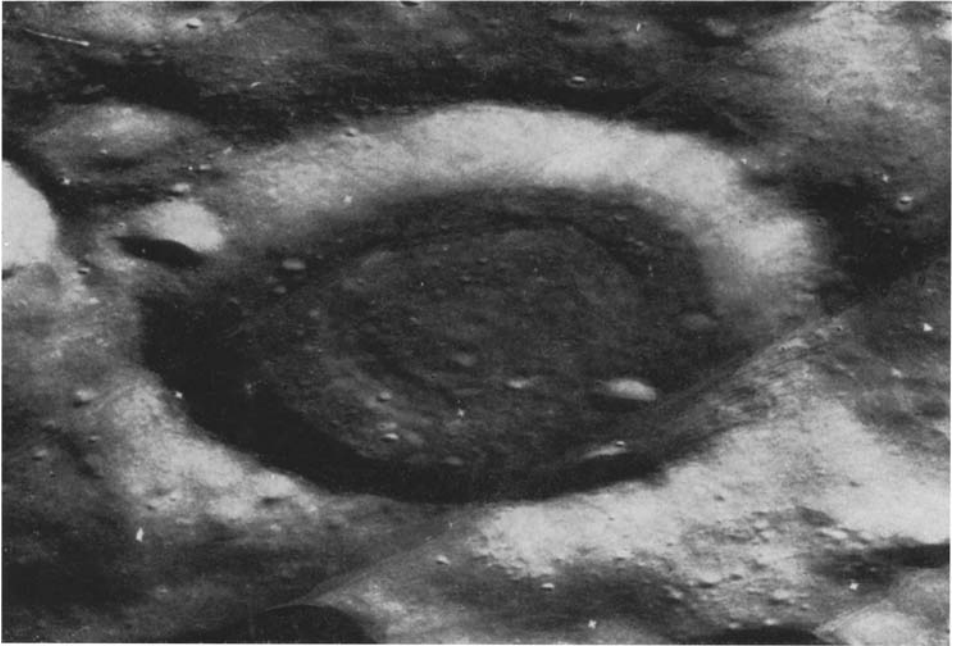


Fig. 35. Gambart J ( $D = 7$  km), showing inner ring with features suggesting an extrusive origin. NASA Orbiter 3, H-120.

small craters; (5) in the mapping of faults around concentric uplifts in terrestrial craters; and (6) in the work of Lance and Onat (1962) on sagging plates, quoted by Fielder (1963) as a possible mechanism for basin fracturing.

The connection between double-ring craters and the concentric rings of basins may indeed be that such faulting is a first step in the production of the rings.

*Lance-Onat Mechanism.* In view of these evidences for faulting, let us review in greater detail the faulting mechanism proposed by Fielder (1963), based on the theoretical and experimental work of Lance and Onat (1962). Figure 36 is adapted from Lance and Onat. It shows a section through a disk-shaped steel plate with firmly held edges but subjected across its upper surface to a uniform, downward hydrostatic pressure. The plate was then cut, polished, and etched with acid to show the stress marks drawn in Figure 36. As theoretically predicted, the portion of the plate beyond  $0.73 R$  has stress lines roughly in the form of logarithmic spirals, while inside this zone the stress lines are radial\*. At and near  $0.73 R$  is a concentration of shear fractures resembling those found in a steel specimen under pure bending.

This remarkable theoretical and experimental result has several similarities to what is found in lunar basins and double ring craters. First, the inner basin ring (zone of shear?) lies near  $0.73 R$  where  $R$  is the basin radius. Second, scarps or extrusions

\* The inner part of the plate, incidentally, resembles another experimental plate with a single vertical, thin bearing pushing down in the center.

could consistently be interpreted as the expression of shear fractures leading to either a fault or extrusive site. Third, the usual confinement of circular rilles (graben) to the zone between the inner ring and the basin rim would be explained by the presence of Lance-Onat fractures tending toward concentricity in that zone. Such rilles are

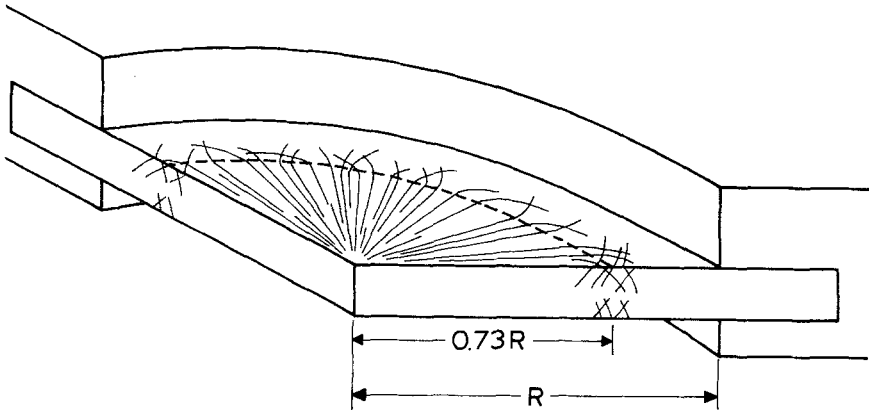


Fig. 36. Schematic diagram of the Lance-Onat experiment and theory. An iron plate is subjected to downward hydrostatic (uniform) pressure. Subsequent etching shows radial stress lines inside  $0.73 R$ , a concentration of fractures at  $0.73 R$ , and spiral stresses outside  $0.73 R$ , tending toward a concentric pattern. Similar relations are observed in lunar basins.

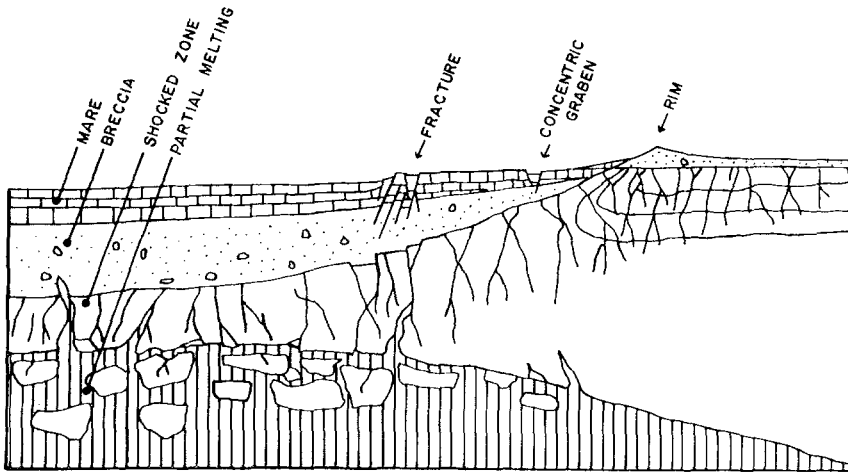


Fig. 37. Hypothetical cross-section of lunar basin shortly after flooding begins, based on the Lance-Onat mechanism. Sagging of the basin into a soft, partially molten subsurface causes fractures at  $0.7 R$ . Magma gains access to the surface through subsurface fractures in the highly-shocked central basin or along the ring fractures at  $0.7 R$ ,  $1.0 R$ , ... Concentric graben between  $0.7 R$  and  $1.0 R$  are equivalents of Lance-Onat stress lines in this zone. (Incidental note: In several interpretations of lunar anorthosites, basins are shown as 'cookie-cutter' holes punched entirely through the anorthositic crust with the maria diagrammed as continuous lava columns extending into a lunar mantle. The present diagram appears more realistic and accounts for numerous surface features better, without conflicting with the essential anorthositic-crust theory.)



rare in mare centers because the faults are radial in the central region within the inner ring, according to the Lance-Onat data.

Figure 37 is an interpretation of a freshly-formed basin in the spirit of the Lance-Onat data. The basin has formed and immediately infilled with breccia and rubble (additional rubble is built up to the extent of roughly a hundred meters per  $10^8$  years by the intense early bombardment). The Moon's interior may already be partially molten, but in any case the removal of the overburden encourages melting under the basin at a depth where the isotherms are appropriate. Some lava may gain access to the surface and begin flooding the basin interior or margins. At this point, diagrammed in Figure 37, we have a crust trying to sag into a partly melted substratum – a scaled-up analog of the Lance-Onat rigid plate sagging from a supported margin.

The Lance-Onat data accounts for inner rings better than outer rings. To be consistent in this model we would have to hypothesize that once the basin rim defines a radius  $R$ , whether or not fracturing has occurred at  $2^{-1/2} R$ , fracturing is also promoted outside  $R$  at  $2^{1/2} R$ ,  $2 R$ ,  $2^{3/2} R$ .... This problem is not dealt with by Lance and Onat.

Another unresolved problem is whether the lunar surface outside the basin immediately following the basin-forming event was homogeneous or was already markedly stressed and fractured at the points  $2^{1/2} R$ ,  $2 R$ ,  $2^{3/2} R$ ... by the impact. Figure 37 shows more or less homogeneous local fractures produced by the shock wave as it expanded outside the basin rim. H/K (1962) assumed that the formation of rings occurred simply by sagging motions along these pre-existing concentric 'microfractures' created during basin formation. However, the thrust of the work by Baldwin, Van Dorn, and Chadderton *et al.* (cf. Section 3) is that interference, standing waves, or some other shock phenomenon *during basin formation* concentrates these fractures at the points  $2^{1/2} R$ ,  $2 R$ ,  $2^{3/2} R$ .... A choice between these two models – passive sagging with homogeneous fracturing or concentrated fracturing – is not possible at this time.

*Conclusions.* The basin-forming event produces a fractured crust. It is unclear whether the fractures are either concentrated in concentric rings at  $\sqrt{2}$  intervals or are uniform. Partial melting below the basin, possibly produced in part by the overburden removal but possibly intrinsic to the Moon, allows sagging of the crust. Because of point symmetry in the basin fracture system, and because of increased melting by pressure-release under the basin center, and because large volumes of lava may extrude onto the surface (especially on the front side), the sagging of the crust shows point symmetry and produces faults and fractures concentrated in  $\sqrt{2}$  spacings by the mechanism of Lance and Onat. Intrusive and extrusive volcanic activity may occur along the tectonic fractures so produced.

## 8. Test of Formation Date of Concentric Rings

According to our hypothesis, the concentric scarps may have formed either during or significantly after basin formation. A test will distinguish between these alter-

natives. If the ring is a fault that formed significantly *after* basin-forming activity, then it should have a significantly *lower* fraction of its length obliterated by post-basin craters on the ejecta blanket nearby. This is a straightforward test.

However, our hypothesis of basin formation implies that a basin ring – no matter when it formed – may have been much affected by volcanism. Therefore the ring may be obliterated by a *higher* density of craters than appears nearby.

We propose the following two-step test. First, we define a narrow annular zone containing the ring, for example a zone 100 km wide along the Altai scarp. The crater density is determined in this area in the normal manner and compared to the crater density in a non-ring annulus on the nearby post-basin ejecta blanket. If there are more craters along the ring we conclude volcanism along the ring-fault produced them, just as we observed in the case of Korolev (Part 4). If there are the same or

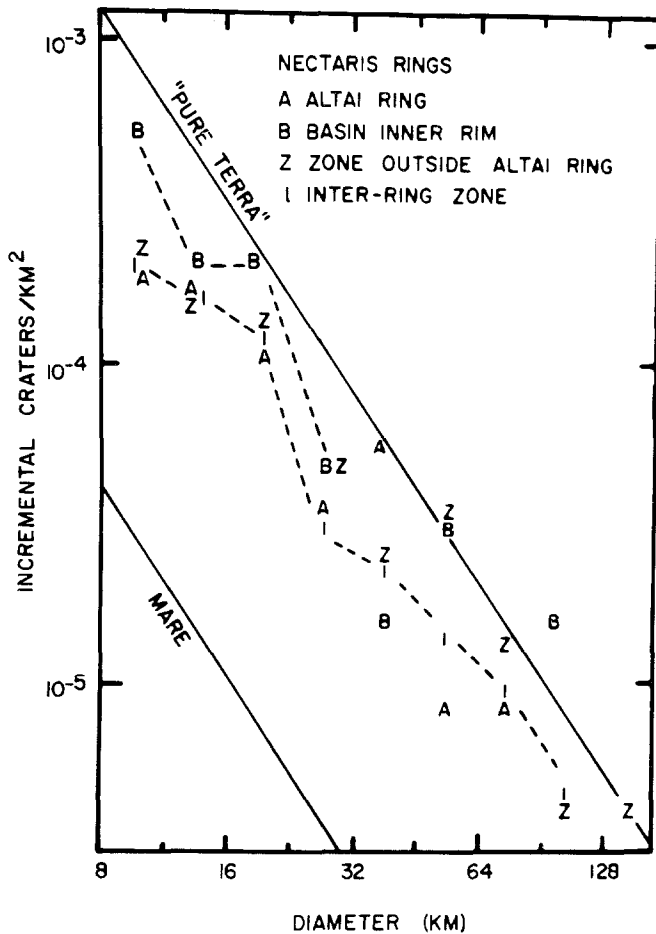


Fig. 38. Crater diameter distribution in annular arcs of Nectaris ring system – a test of ring age (see text).

fewer craters per unit area along the ring, the test is inconclusive and we go on to step two.

Step 2 tests whether the fault itself is younger than the surrounding surface. The percentage area covered by post-basin craters of various sizes in the ejecta blanket or interior is measured. Then the best-defined part of the scarp is searched for post-ring craters that obliterate the scarp. The percent length of the scarp obliterated is found. The figures are compared. For example, if '50 km craters' (craters in a diameter interval centered on  $D=50$  km) obliterate 50% of the area of the ejecta blanket, but only 10% of the scarp, the scarp must be younger than the basin.

*Nectaris*. The Nectaris basin seems ideal for such a test since the basin is old but the Altai scarp appears young. Figure 38 shows the first part of the test. Points A and B plot the crater density in annuli along the Altai scarp and hilly inner basin rim. Z is a zone in the presumed ejecta blanket outside the Altai ring, and I is an inter-ring zone. Z points should correspond to the age of the basin. I, however, is a partly flooded zone and at  $D < 32$  km it can be seen that it forms a lower envelope to the curves. That is, I is the youngest of these annuli. Z and A are indistinguishable, indicating that the Altai scarp does not have an over-abundance of craters. The inner

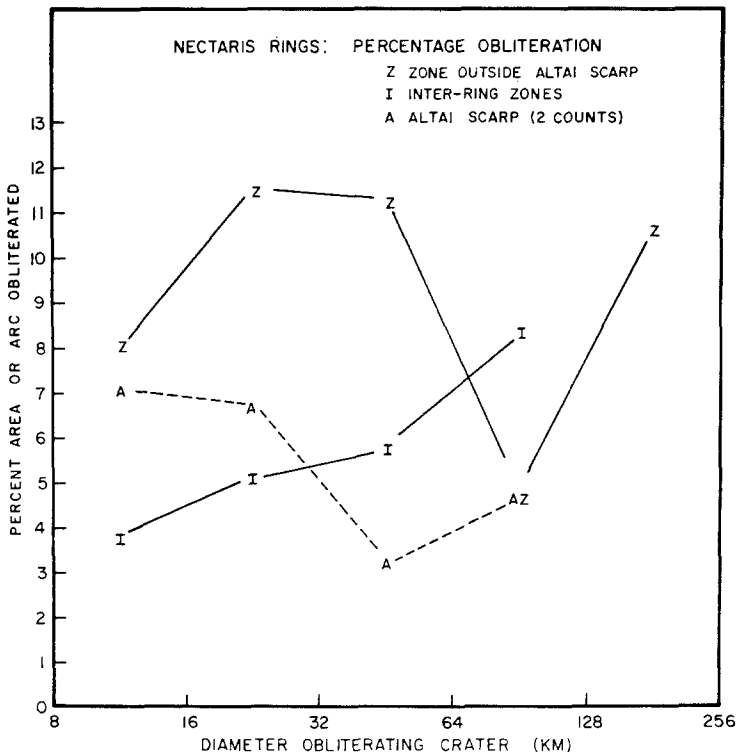


Fig. 39. Percentages of arcs obliterated by craters in the Nectaris ring system – a test of ring age (see text).

ring B, however, averages roughly 60% more craters of  $D < 32$  km per unit area than the normal post-basin surfaces. This suggests that the Nectaris inner ring has been the site of volcanic activity producing craters equal in size to terrestrial calderas.

The second part of the test, performed on the southern part of the Altai ring, is shown in Figure 39. Again we see that the inter-ring zone *I* is deficient in craters of  $D < 32$  km or somewhat larger, as accounted for by the partial flooding. At  $D > 64$  km, however, the inter-ring zone has a crater density comparable to the terra zone, *Z*. This supports the assertion that the *Z* curve illustrates roughly the area obliterated by post-basin craters, averaging about 10% in Figure 39.

The obliterated percentage of the Altai scarp (*A*) appears to be significantly less, averaging about 5 to 6%. The *A* curve is based on two independent counts, but is rather highly dependent on the observer's determination of the course of the scarp face. Uncertainties in individual *A* points are probably about  $\pm 4$  percent-units. This

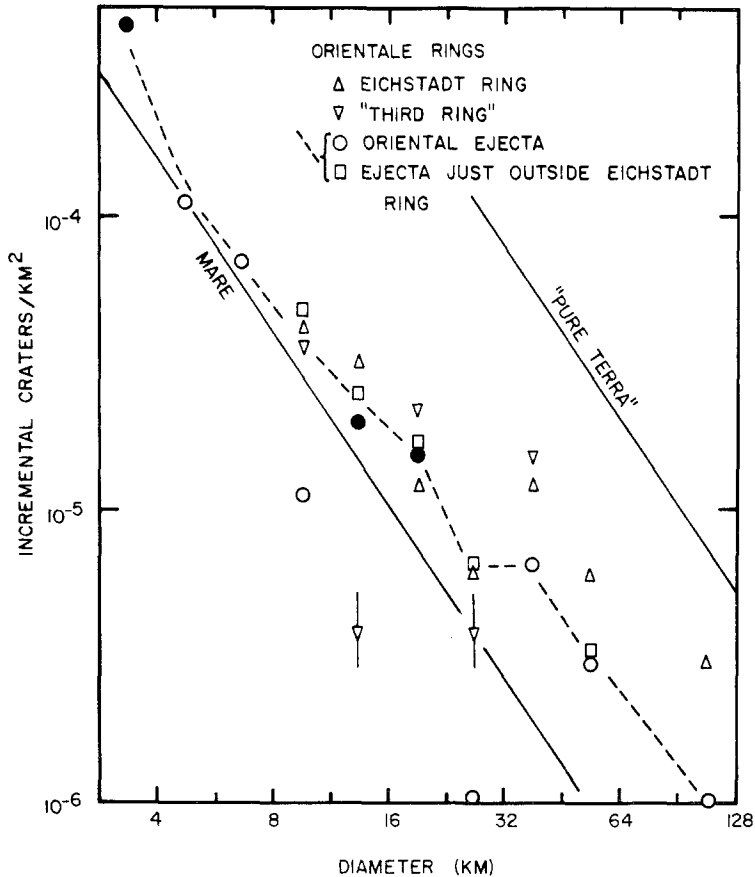


Fig. 40. Crater diameter distribution in annular arcs of Orientale ring system – a test of ring age (see text).

somewhat marginal evidence, then, suggests that the Altai fault scarp formed after the Nectaris Basin was created.

*Oriente.* Figure 40 shows the application of the test to the Eichstadt ring and so-called ‘third ring’ – next interior to the Eichstadt ring. Both appear to be fault scarps. Figure 40 indicates that there is no clear difference in crater density between the ring regions and the ejecta blanket (dashed line). However, there is some indication that craters larger than 32 km diameter are overabundant along the Eichstadt scarp.

The second part of the test – a figure comparable to Figure 39 – produced only a considerable scatter, with some evidence that the Eichstadt ring is cut by more craters than expected on the basis of areal obliteration in the ejecta blanket. We conclude that there is some poor evidence for volcanic crater-forming activity along the Eichstadt ring. Certainly there is abundant evidence in the arcuate maria at the foot of the scarp that lava extruded along this fault. However, the largest craters, which are responsible for the crater overabundance in Figure 40 – craters like Eichstadt, Shaler, and Schlüter A give no immediate proof of being endogenic rather than meteoritic.

*Conclusions.* Probably the inner ring of Nectaris and possibly the Eichstadt ring of Oriente are dotted with calderas of  $D < 32$  km in the first case and  $D > 32$  km in the second case. The Altai ring of Nectaris shows marginal evidence of being younger than the basin.

## 9. Origin of Wrinkle Ridges, Inner Peak-Rings and Central Peaks

Basins, wrinkle ridges and central peaks have usually been regarded as independent phenomena. Wrinkle ridges have been often regarded as a direct result of some process of mare flooding, such as contraction of the cooling lava. Our analysis of the rings of peaks in far-side unroofed basins leads us to propose a single genetic relationship embracing basin ring systems, wrinkle ridges, peak-rings, and central peaks.

‘*Peak-Rings*’. Basins such as Schrödinger, Compton, and Antoniadi exhibit rings composed of interconnecting peaks. These rings appear to be markedly different from the normal inner rims of craters. They are symmetric on their inner and outer slopes while crater rims are asymmetric. In each of the three examples named above, the peak-ring is surrounded by a massive, higher ring which appears to be a normal crater rim.

Peak-rings were unknown before Orbiter photography, because front-side basin floors are covered by mare material. The inner ring of the Imbrium basin, however, is a well-known ring of isolated peaks and now appears to be either a barely-protruding peak-ring, or the high crest of the original true rim.

Peak-rings appear to be constructional features formed on initially flat basin floors, and are probably extrusive.

*Wrinkle Ridges and Concentric Graben.* In earlier discussions of basins, wrinkle

ridges were not linked to the concentric scarps. However, the examples of constructional rings on the floors of far-side basins suggest a re-examination of concentric wrinkle-edge systems long known on the front side mare. Quaide (1964) cogently argued from pre-Orbiter data, that the wrinkle ridges were "volcanic structures which grew above dike feeders during the last stages of maria filling." Strom (published by Kuiper, 1966) showed that individual flows could be mapped in Mare Imbrium, running perpendicular to and apparently originating in the middle ridges. High resolution Orbiter photographs show the ridges to be complex positive features with lobate segments. It has long been known that individual wrinkle ridge segments are often arranged *en echelon*, as if following subsurface faults. Our observations of Birkhoff show that a wrinkle ridge can renew an obliterated rim, again indicating subsurface tectonic control.

This evidence, combined with the evidence for concentric ring-pattern extrusive activity in basin floors, led us to conclude that the circular concentric wrinkle ridges in many flooded basins are just one more manifestation of intrusion and extrusion along circular ring-faults produced by sagging and faulting in the large basin systems.

TABLE VI  
Wrinkle ridge systems

Basin	Ring description	Radius (km)	Ratio
Basins already listed in Table II			
Imbrium	Wrinkle ridge	640	0.48
	Inner ring of peaks	670	0.50
	Main rim (Apennines)	1340	1.0
Moscoviense	Wrinkle ridge	90	0.44
	Rim	205	1.0
Nectaris	'Shelf' or monocline	260	0.65
	Rim	400	1.0
Crisium	Wrinkle ridge	330	0.73
	Rim	450	1.0
Humorum	Wrinkle ridge	195	0.46
	Rim	425	1.0
Other basins identified by wrinkle ridge pattern			
Serenitatis (18.5°E 5.0°N)	Wrinkle ridge	445	0.65
	Rim?	682	1.0
SW Tranquillitatis (23.2°E 5.0°N)	Wrinkle ridge	84	0.24
	Wrinkle ridge	172	0.49
	Peaks (rim?)	350	1.0
W. Nubium (22.0°W 23.5°S)	Wrinkle ridge	195	0.46
	Rim (?)	425	1.0
Fecunditatis (48.2°W 3.2°S)	Wrinkle ridge	234	0.45
	Rim (?)	520?	1.0

Confirmation of this hypothesis is found in the statistics of wrinkle ridge spacings, Table VI. Just as Figures 27 and 34 show  $\sqrt{2}$  spacings in the case of the scarp and interior peak-ring systems, Table VI shows that wrinkle ridges are spaced according to the  $\sqrt{2}$  rule with respect to the nearest basin scarp or peak-ring.

Table VI adds four ancient front-side systems now identified as basins by their concentric wrinkle ridges, with characteristic diameter ratios. H/K (1962) did not list these as basins because the rim structure is only marginally detectable and no additional outer concentric scarps could be found. However, the four systems all show circular wrinkle ridges, and nearly-obliterated concentric rims. All of these features we now find to be explicable if these are ancient basins flooded during a post-basin mare-forming period.

*Origin of Inner Rings.* The relation we hypothesize between peak rings and wrinkle ridges will be made clear from Figure 41. Whereas Figure 37 showed a basin cross-section shortly after formation as flooding begins, Figure 41 shows the final stages of flooding.

By the Lance-Onat mechanism, the basin has fractured at  $0.7 R$ . These fractures allow access of magma to the surface as is proved by the maria Veris and Autumni in the Orientale system. If the lava is viscous, intrusions or extrusions may form hills

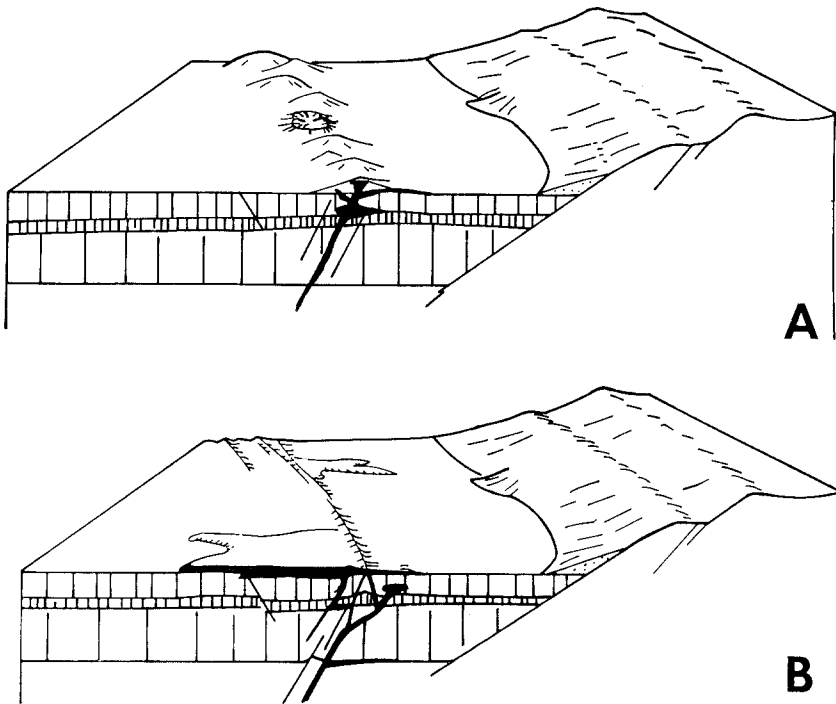


Fig. 41a and b. Cross-sections of lunar basin interiors, showing interpretations of peak-rings and crater-rings (a) and wrinkle ridges (b). Both types of feature are products of volcanic activity along ring fractures corresponding to the Lance-Onat fractures at  $0.7 R$ . In case A the magma is more viscous; in case B it is more fluid and produces flows observed to extend from wrinkle ridges.

as in Schrödinger; if the lava is gas-charged, maar-like craters may form along the fracture line as in Korolev. These are illustrated in Figure 41a. If the lava is very fluid, fissure eruptions may form vast flows emanating from low ridges – the wrinkle ridges – as in Imbrium. This is shown in Figure 41b.

In Poincaré, and the basin near Schiller, the inner, fragmentary ring of ridges is darker than the rest of the mare floor, possibly indicating more recent extrusive activity along the ring. These two basins may be an intermediate case between peak-rings and wrinkle ridges.

If there is a dearth of magma when the fractures form, no constructional features may be formed, and a complex network of graben may mark the site of the faulting. This occurred in the NE part of the Orientale inner basin, where the inner ring is extended as a rille through unflooded uplands – in itself a strong proof of the fault-nature of the inner rings.

The data suggest a possible time-dependence of volcanic products involved in mare filling. Schrödinger, Compton, Antoniadi, and Korolev – the basins best exemplifying the peak-ring of Figure 41a – all except Antoniadi lack young, dark maria, but contain smooth, light-toned material. In Antoniadi the dark mare is limited by and appears to post-date the ring. This suggests that the peak-ring phenomenon, when it occurs, may occur prior to or early in a basin's flooding. Fluid flows of dark basaltic lava, on the other hand, are the last stages, and wrinkle ridges are clearly features of the upper stratigraphic column, although their underlying fractures may have long served as dike channels.

The chemical implication – admittedly speculative – is that earliest magma extruded into the basins was more siliceous or richer in volatiles than the last flows (c.f. Rittmann, 1962, Tables 4 and 5, and Figure 57).

The structural implication is that the inner ring and wrinkle ridge complexes may resemble ring dike and cone sheet structures, known on the Earth, with extrusions along them. Flamsteed, which we do not class as a basin because there is no main crater-like rim, has a low ring of light-toned hills surrounding a mare floor with a wrinkle ridge at about  $0.76 R$ . The hills appear to be superimposed on the mare.

Thus the Flamsteed feature appears to match the characteristics we have found for peak rings and wrinkle ridges.\*

Both O'Keefe *et al.* (1967) and Fielder (1967) concluded that the Flamsteed ring was an extrusive feature of viscous lava, more acidic than mare lavas, and the former authors described Flamsteed as a ring dike and computed the viscosity of the lava. Details of the logic of these authors was criticized in several subsequent papers, including one by one of us (W.K.H.) but our present work adds support for their general conclusion – that extrusive ring features do occur on the Moon.

The relation of wrinkle ridges and peak-rings to ring dikes and cone sheets is not certain. Ring dikes result from subsidence of circular or more often oval crustal blocks while cone sheets result from upward pressure of intruding magma reservoirs (Richey,

\* As in the Imbrium system, the peak ring lies just outside the wrinkle ridge.



1961). We have proposed above that both subsidence and upward magma intrusion occurs in basin floors.

*Central Peaks.* Wood (1968) showed that central peaks increase in frequency from craters of about 10 km diam. to craters of about 100 km, yet Baldwin noted as long ago as 1949 that the largest craters and the basins lack central peaks.

The evidence for a genetic relation between basin ring-scarps, peak rings, and wrinkle ridges leads us to infer that central peaks of lunar craters are in some sense an extension of the same phenomenon, occurring at somewhat smaller-scale craters up to diameter 150 km. Baldwin (1969) expressed this idea by suggesting that inner rings are the basin equivalent of central peaks. The transition from central peaks to peak rings occurs at diameters of 140 to 175 km – the diameters of Antoniadi and Compton, the only two craters of the entire Moon known to exhibit both structures.

We do not have evidence indicating whether the central peak is a feature that is formed at once during the crater-forming event, or whether it evolves after the crater forms, by utilizing or creating fractures related to the concentric ring fracture system.

Drilling and shatter-cone mapping of the central uplift at Sierra Madera (Wilshire and Howard, 1968; Howard and Offield, 1968) indicate that the central uplift in this case dies out with depth and evolved from mutually flat-lying beds in the initially flat-floored crater. Such evidence indicates that central peaks are evolutionary isostatic rebound features, fairly sharply defined by faulting and distortion of strata and possibly involving incidental intrusive or extrusive activity.

#### SEQUENCE OF BASIN INTERIOR PROFILES







PROFILE	EXAMPLE	DIAMETER
	CENSORINUS	4 Km.
	LANSBERG	40
	BULLIALDUS	59
	GASSENDI	100
	COMPTON	175
	SCHRÖDINGER	300

Fig. 42. Schematic size sequence of crater forms, from no central peak (top), through progressively more complex and extended peaks, to peak-rings (bottom).

*Sequence of Crater Forms.* Figure 42 shows a possible size sequence of crater forms, based on our hypothesis of a relation between central peaks, wrinkle ridges, and peak rings. The categories are not mutually exclusive but there is a tendency to pass from bowl-shaped craters to simple central peaks, multiple central peaks, ring-shaped central peaks darker in the center at noon lighting, central peaks with peaks ring, and finally peak-rings and/or wrinkle ridges alone.

## 10. Mare Formation

We will now consider the final stages of evolution of the basin, their flooding by mare material.

*The earliest flooding.* Normal usage of the term 'mare' implies dark material. Our crater counts show that such surfaces usually fall in the relative age zone from about 1.6 to 0.6, defining a 'mare epoch'. Yet we have cited many examples of old, light-hued, mare-like surfaces which show characteristics of maria. For example, Schrödinger, Hertzprung, and the basin near Schiller contain old surfaces with flooded craters, wrinkle ridges, and other mare-like features. Grimaldi's inter-ring zone was flooded at about  $3.5 \pm 1$  (Figure 14). Poincaré shows a multi-stage history with inter-ring flooding at  $7 \pm 2$  and interior basin flooding at  $2.6 \pm 0.9$ . Inter-ring zones around Imbrium (Archimedes plateau), Crisium, and Nectaris show early flooding associated with orthogonal faults that make a lattice-work of ridges and graben. In general, inter-ring zones appear to have finished their flooding earlier than basin interiors.

Such data suggest that mare flooding has an extensive history reaching well back into early lunar time, and is not confined to an epoch from 1.6 to 0.6.

Was this early flooding the first part of a two-phase or episodic flooding history, or was it part of a single continuum in flooding? Figure 43 shows schematically the flooding sequence in the basins studied by us, combined with data on non-basin mare units (Hartmann, 1968b). The hatched bars show low-albedo mare units. The open bars show high-albedo plains-forming units which may be either early volcanic flooding or filling by ejecta from nearby craters and basins.

Although a concentration of mare surfaces exists at crater density 1.0, flooding occurred many times in the past, with the older flooding being light-hued. 'Upland plains-forming units' are familiar examples of the older flooding.

What is the nature of the ancient flooding? Judging by the high albedo, these regions are either (1) ancient mare lavas covered with a thin veneer of pulverized, high-albedo ejecta (Minnaert, 1970) or (2) a kind of volcanic product different from the crystalline basaltic lavas picked up in Tranquillitatis and Procellarum. We do not rule out (2), as we have already suggested that the earliest basin-filling lavas may have been more acidic than the last mare lavas (Section 9).

*Evolution of Mare Surfaces.* It appears, nonetheless, that some mare surfaces have been lightened with the passage of time (model 1). This idea, and the related concept that recently formed bright craters are darkened with time (Willey and Pohn, 1964), are supported by Figure 44, showing the normal albedo plotted against crater density

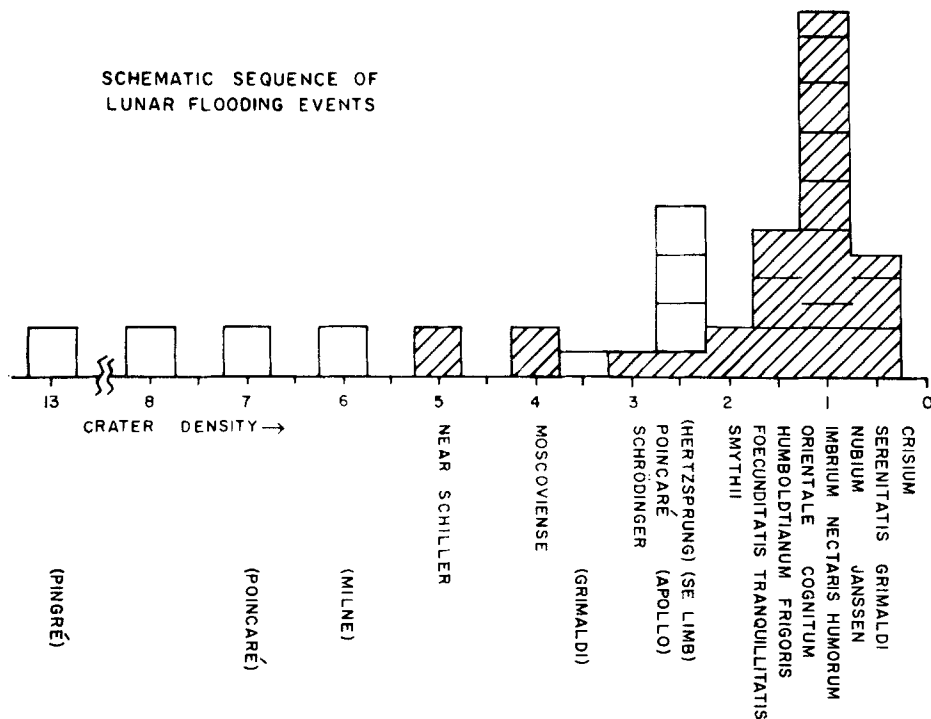


Fig. 43. Frequency histogram of dated flooding and blanketing events, distinguishing between dark mare surfaces (hatched) and lighter-hued surfaces (open).

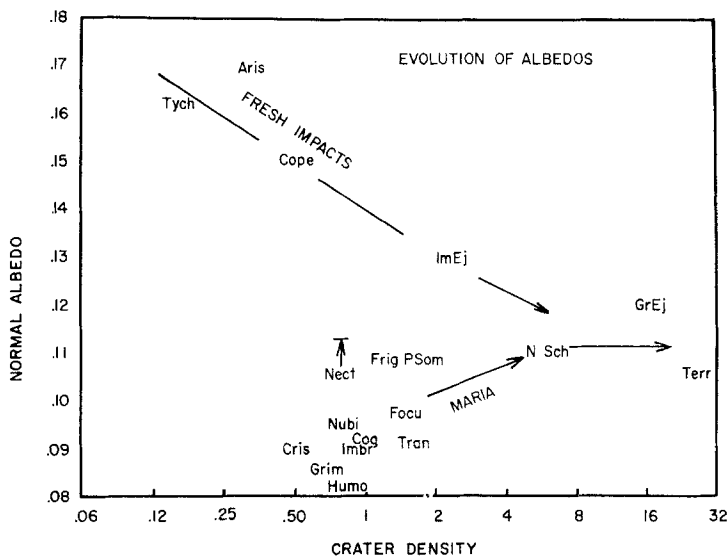


Fig. 44. Y-shaped evolutionary sequence for evolution of albedos of lunar terra and mare surfaces. Both albedos and crater densities are empirical data. Crater densities indicate age sequence.

for various surfaces. As the normal albedo has been visually estimated from Pohn and Wildey's albedo map (1970) and the crater densities have significant uncertainties, the figure indicates only first-order relations.

Figure 44 shows a Y-shaped evolutionary sequence for lunar surface materials. The freshest lunar materials are usually either very bright pulverized (and glass-bead-strewn?) ejecta or are dark fresh lavas. These units in general have crater densities less than 1.5. Regions from crater density 2 to about 10 are being converted into upland surface, as with Gault's (1969) 'mare exemplum' experiment, with a substantially mixed regolith whose albedo is approaching the lunar average. Regions of crater density 20 are old terra regions which have achieved a more or less homogeneous regolith near the average lunar albedo. The mechanism for evolution is horizontal and vertical mixing and pulverization of ejecta. Apollo results give evidence for horizontal mixing, and the Pohn-Wildey map shows a tendency for high albedos to encroach into maria, and low albedos to encroach into terrae at mare/terra contacts.

We conclude that major early volcanic extrusions – probably basaltic lavas – occurred prior to the formation of the large front-side maria, i.e., prior to relative age 2, and that these have been lightened.

*Lava Route to Surface.* We have already noted that mare material utilizes ring-faults around basins to gain access to the surface. Maria Veris and Autumni – arcs around Orientale – are examples, and we can also recall that much of the older maria on the front side are associated with inter-ring zones of basins such as Crisium, Nectaris, and Humorum. The same holds for partially flooded craters: frequently, the lava lies in arcs or patches along the inner base of the wall. Galvani, Lavoisier, Hercules, Atlas, Posidonius, Julius Caesar, Condorcet, Schlüter, Petavius, Humboldt, Schickard, and the Nectaris N rim illustrate this. These evidences show that the lunar 'crust' under the rims of many large craters is a preferential site for magma feeders. The resurgence of the rim of Birkhoff as a wrinkle ridge is another testimony to this effect. The explanation presumably is that the crater rims are favored sites of faulting due to the isostatic imbalance of excavation on the inside and ejecta deposition on the outside.

*Recent Flooding.* The familiar dark maria should probably be considered as the last major, but not necessarily the most extensive, episode of flooding, as shown in Figure 43. Numerical crater densities of some of these units are given in Table II.

Long-known evidence, which we have to some extent quantified, shows that the dark mare lavas formed *significantly* later than the basins. Among various evidence to this effect are (1) the maria have significantly lower densities of impact craters than the basin ejecta blankets, and (2) various basins have prominent 'Archimedian' craters that formed on the basin floor before the flooding. This proves that *the surface lavas were not immediately-produced impact melts* as has often been assumed. The Archimedian time intervals are 'significant' in terms of measurable crater density differences but may be short in terms of absolute time, since measurable crater-

density differences arose in intervals of less than  $10^8$  years during the intense early bombardment.

*Origin of Mare Lavas – Front- and Back-Side Asymmetries.* Substantial time intervals between basin formation and lava extrusion do not exclude the possibility that basin forming impacts encouraged the formation of maria. Ejection of the overburden may have substantially aided melting beneath the basins, producing lava that fed volcanic processes for a long time after the basin-forming impacts. Hartmann and Binder (1970) have proposed that this mechanism may explain in part the asymmetry of mare distribution on the front and far sides, as follows. The Moon was assumed to have an asymmetric isotherm distribution with the warmer side shifted toward the Earth as a result of the Moon's process of origin. In this case impacts on the front side would tap warmer layers and more easily cause pressure-release partial melting in the subsurface. This would account for the over-abundance of mare material on the front side. Because of such pressure-release melting, the partially melted region in Figure 37 was shown as shallower beneath the basin center.

There is no overabundance of impacts on the front side. We support this con-

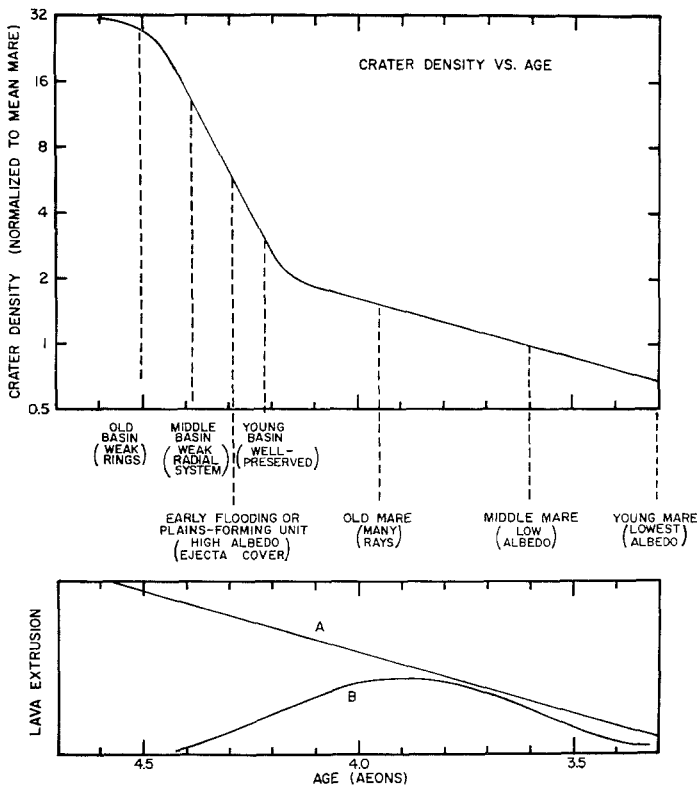


Fig. 45. Summary of lunar history. Upper chart shows crater density on various surfaces, plotted against age of surface – based on Apollo results. Lower chart shows two hypothetical early flooding sequences, between which no choice can now be made.

clusion of Stuart-Alexander and Howard (1970). Specifically, we found no longitude asymmetry distribution from front to back.

A misconception on this point has given rise to the oft-stated but unwarranted assertion that there is an asymmetry in basin distribution from front to back side. There is only an asymmetry in amount of lava. We find a related but marginal suggestion in our results that the age of the most recent flooding in different regions increases as a function of the distance from the Moon's center-of-face.

*Unanswered Questions.* The principal research area left open is the question whether (A) the rate of flooding was dying out during the mare-forming period (relative age 0.4 to 1.6) or whether (B) the rate of flooding was much higher during the mare epoch than in the beginning. This is equivalent to asking whether the subsurface temperatures (A) were always dropping since the Moon's formation, or (B) reached a peak and then subsided. This problem is illustrated in Figure 45.

Model (A) would imply that we see very little flooding before relative age 2 because it is so effectively masked by the frequent ejecta blankets of the large basins. For example, Figure 43 indicates a peak in blanketing at 2.4 due to Orientale ejecta which partially masks flooding in Hertzprung, Apollo, and the SE limb basin.

Model (B) would imply that we see very little flooding before relative age 2 because it only rarely occurred at that time.

We cannot as yet choose between models A and B for lunar flooding.

## 11. Relationships of Basins to Mascons

The last three columns of Table VII show that the morphological and age characteristics of the basins are *not* correlated with the size of their mascons.

Rather, a good correlation is found between the extent of mare (column 4) and the size of the mascon (column 2). This suggests that the mascon is due to the mare material itself. This would call for the mare material to be more dense than the ambient highland by an amount equal to the mascon mass/volume of flooding, column 5.

This model assumes that lunar magma, of lower density than the ambient lunar rock, rises to the surface and floods the basins. Upon reaching the surface it efficiently degasses and in its final crystalline form has a density higher than that of terra rocks. In Table VII we have estimated depths of the lava in the various basins (column 3) from morphology and number of partly-buried craters (Baldwin, 1970), rather than by theoretical crater depth-diameter extrapolations as used by some mascon analysts. The resulting correlation between mascons and mare volumes is not only reasonably close, but predicts a consistent and reasonable difference in density between the mare lavas and the ambient terra of the order of a few tenths  $\text{g/cm}^3$  (column 5).

The fact that mare volume is the only correlating parameter of basins and mascons supports theories of mascons which attribute them to the mare material itself (e.g., Conel and Holstrom, 1968), rather than to buried meteorites, etc. It will be of interest

TABLE VII  
Mascon-containing basins arranged by mascon mass

Basin	Estimated mascon mass ( $10^{20}$ g)	Estimated mean lava depth (km)	Mare volume ( $10^{20}$ cm <sup>3</sup> )	$\Delta\rho$ (Mare-Terra)	Relative age of mare <sup>a</sup>	Relative age of basin <sup>a</sup>	Clarity of concentric system
Imbrium <sup>b</sup>	7	4	47.0	0.1	0.9	Young (2.5)	Strong
Serenitatis <sup>b</sup>	4	3.5	13.2	0.3	0.6	V. old	Weak
Orientalis <sup>c</sup>	3.5	3	2.6	1.3	1.0	Young (2.4)	Strong
Smythii <sup>c</sup>	2.5	3.5	5.6	0.4	1.9	Old (27)	Weak
Crisium <sup>d</sup>	2	3.5	5.6	0.4	0.4	Mod. (17)	Moderate
Nectaris <sup>b</sup>	1.7	2.5	3.1	0.5	0.9	Mod. (16)	Moderate
Humboldtianum <sup>e</sup>	0.75	3?	1.0	0.8?			
Unnamed (C) <sup>e</sup>							
7°S, 27°E	0.75	2?	1.2	0.6?	—	V. old	V. weak
Humorum <sup>b</sup>	0.65	2	2.7	0.2	0.85	Old (25)	Weak
Grimaldi <sup>e</sup>	0.34	2.5?	0.40	0.8?	0.75	Mod (16)	Moderate
Unnamed (D) <sup>e</sup>							
17°S, 70°E	0.55	2.5?	0.93	0.6?	—	V. old	V. weak

<sup>a</sup> Crater density normalized to average mare.

<sup>b</sup> Kaula: 1969, *Phys. Earth Planet. Inst.* **2**, 123.

<sup>c</sup> Booker: 1970, *Nature* **227**, 56 (Surface mass).

<sup>d</sup> Gottlieb, Muller, and Sjogren: 1969, *Science* **166**, 1145.

<sup>e</sup> Kaula: 1969, *Science* **166**, 1581. Divided by e to accord with references b, c, d. These have less weight than b, c, d.

to see whether relatively unflooded basins lack mascons. Kaula (Table VII, note 1) shows that far-side mascon data is presently insufficient to answer this.

The concentric structure in the Orientale mascon, (Figure 2) can thus be interpreted as follows. The outer positive anomaly coinciding with the ejecta outside the Eichstadt scarp would result from the mass of the ejecta itself. The negative anomaly in the inter-ring zones would result from the subsidence of the fractured, flooded interior along concentric faults such as the Eichstadt scarp. The positive central anomaly would be due to the mass of the mare lava extruded in the inner basin.

## 12. Summary and Conclusions

We have reviewed theories of basin systems and compiled new data, which indicate significant differences in age among the basins (Sections 1–4). The basins with the clearest concentric and radial systems are youngest: older basins lack radial systems; the oldest multi-ring basins are nearly as old as the oldest lunar features, but are highly battered in appearance. Still older features, such as the Serenitatis basin, are recognized as true basins only through the symmetry and spacing of wrinkle ridge systems in their relatively young mare fill.

Table VIII summarizes our relative age data on the thirty-one basins (defined as large crater-like structures with concentric rings) identified in this paper. Table VIII also compares our basin data with those of other authors. In general, the age correspondence is good, with some confusion of results in the category we call ‘moderate age’, where age differences are scarcely detectable. The greatest discrepancy occurs for Crisium, which other authors list as younger than we find. Their finding may be affected by the fact that the mare fill in Crisium is unusually young. Other discrepancies occur in the case of the SE Limb Basin and Apollo. The other authors find higher ages than we do, probably as a result of the fact that these two basins have been highly damaged by Orientale ejecta and appear older than they are.

The basins are highly affected by faulting and other tectonic activity. The dominant symmetry of the radial and concentric fault pattern was set up during the impact, accounting for point symmetry. Rings apparently evolved as a result of basin formation. We leave open two possibilities for ring formation: (1) the impact produced a rather homogeneous system of ‘microfractures’ in a radial and concentric pattern, and these were later acted upon by internal lunar tectonism to emphasize systematic spacing of major faults at  $\sqrt{2}$  intervals; or (2) the impact process itself produced major fractures or fracture concentrations at  $\sqrt{2}$  intervals, which then led to faults. Sections 3 and 7 list a number of clear evidences of tectonic and faulting activity among various basins.

Although complex shock mechanics may have been involved in producing the concentric and radial fracture systems, we find a remarkable tendency for these enormous systems to have behaved as quite simple mechanical structures with highly-developed symmetry and with analogs to small-scale phenomena. The perturbing influences that make the systems differ from each other are, generally, less impressive



TABLE VIII  
Summary of 31 lunar basins<sup>a</sup> arranged by age and compared with other author's results

Basin	This paper		Stuart-Alexander and Howard (1970)		Baldwin (1969) <sup>b</sup>		Offield and Pohn (1969)	Hartmann (1964)
	Rel. crater density	Rel. age	'Age group'	Order by age	Rel. crater density	Rim class	Rel. age class	Rel. age
Orientele	2.4	V. Young	IV	1	4.4	2	4.8	V. Young
Imbrium	2.5	V. Young	IV	3	16	3	4.2	Young
Antoniadi	?	Young						
Compton	?	Young						
Schrödinger	5	Young	IV	2	0.95	1		
Milne	10	Moderate			12	5		
S.E. Limb	12	Moderate	II	19				
Apollo	12	Moderate	II	18	35	6		
Bailly	12	Moderate	III	8	14	7		
Moscoviense	14	Moderate	III	7	15	5	3.0	
Korolev	15	Moderate	III	6	15	7		
Humboldtianum	15	Moderate	II	20	26	5		Moderate
Hertzprung	15	Moderate	III	5	14	7		
Nectaris	16	Moderate	II	11	20	7	2.2	Moderate
Grimaldi	16	Moderate	II	16	7.9	6		Moderate
Planck	16	Moderate			29	7		
Poincaré	17	Moderate	II	12	29	8		
Crisium	17	Moderate	III	4	9.1	4	3.2	Moderate
Birkhoff	18	Moderate	II	15	25	5		
Unnamed (A)	21	Old			29	8		
Janssen	22	Old			15	6		Old
Lorentz	23	Old			32	7		
Humorum	25	Old	II	10	15	8	3.1	Moderate
Unnamed (B)	25	Old		21				
Pingré	25 ?	Old	II		29	10		
Near Schiller	26	Old	II	14	32	9	1.8	Old
Smythii	27	Old	I	22	28	9		
Serenitatis <sup>c</sup>	28	V. Old	II	17	24	8	2.7	Old
S. W. Tranquill.	30	V. Old	I	25				
W. Nubium <sup>c</sup>	30	V. Old	I	27				
Fecunditatis <sup>c</sup>	30	V. Old	I	23				

<sup>a</sup> Gassendi and Posidonius and other large craters show evidence of multi-ring basin structure but are not included here (see Table V). The other authors list additional large craters not included here because they lack multiple rings and other features diagnostic of basins.

<sup>b</sup> Baldwin's crater densities are counts of craters larger than 1.6 km diam. Generally, these craters are too small to give accurate data on basin age; they may include secondaries and endogenic craters. Baldwin's rim class is better representative of his age estimates.

<sup>c</sup> Classed as basins on strength of wrinkle ridge structure and spacing (see Table VI).

than the similarities. Experimental and theoretical work on sagging plates by Lance and Onat (1962) appears to offer insight into the mechanical processes that formed the rings, or at least the rings on basin floors, interior to what we identify as the original rim (Section 7).

There is some empirical evidence that certain outer rings may have developed by faulting significantly after the basin formed (Section 8). We find a genetic correlation relating wrinkle ridges, inner rings of peaks, inner rings of craters, and central peaks. All of these appear to develop as a result of concentric fracturing inside basins and are consistent with the Lance-Onat model of sagging plates. Concentric graben just inside basin rims also are explained by this model (Section 9).

Mare lavas extruded into basins significantly after they formed, and were not produced immediately by impact melting, although pressure-release partial melting may have been involved. There were major flooding episodes long before the familiar front-side mare formed. These have higher albedos than normal maria. They were probably extrusions of mare-like basalts that were later covered by veneers of ejecta, but they may have involved a different kind of volcanism (Section 10). There is a marginal suggestion in the wrinkle ridges and peak-rings that early lunar volcanics were more acidic than the last lunar lavas (Section 9). A question remains on the thermal history. We leave open two possibilities: Lunar interior temperatures, and rates of volcanism were (A) declining since the Moon's formation, or (B) peaked during the period of formation of the familiar front-side maria, about 3 to 4 aeons ago (Section 10).

The basins offer important keys to understanding the earliest history of the moon, and hence the formative processes of planets.

### Acknowledgements

We thank Drs E. Anders, A. Marcus, and H. Urey for helpful comments on portions of the manuscript. This work was supported by grants from NASA and by a NASA Institutional Grant through the University of Arizona.

**Note added in proof.** The designation Pingré was shifted to a crater within the basin here called Pingré.

### References

- Anders, E.: 1965, 'Fragmentation History of Asteroids', *Icarus* **4**, 399.  
 Arnold, J. R.: 1965, 'The Origin of Meteorites as Small Bodies, II', *Astrophys. J.* **141**, 1536.  
 Baldwin, R. B.: 1949, *The Face of the Moon*, Univ. of Chicago Press, Chicago.  
 Baldwin, R. B.: 1963, *The Measure of the Moon*, Univ. Chicago Press, Chicago.  
 Baldwin, R. B.: 1966, 'On the Origin of Ring Structures Concentric with Large Lunar Impact Craters', Private communication.  
 Baldwin, R. B.: 1969, 'Ancient Giant Craters and the Age of the Lunar Surface', *Astron. J.* **74**, 570.  
 Baldwin, R. B.: 1970, 'A New Method of Determining the Depth of Lava in Lunar Maria', *Publ. Astron. Soc. Pacific* **82**, 857.  
 Barricelli, N. and Metcalfe, R.: 1969, 'The Lunar Surface and Early History of the Earth's Satellite System', *Icarus* **10**, 144.

- Binder, A.: 1967, 'Stratigraphy and Structure of the Cleomedes Quadrangle of the Moon', Ph.D. thesis, Univ. Arizona.
- Booker, J. R.: 1970, 'Mare Orientale Gravity Anomaly', *Nature* **227**, 56.
- Chadderton, L., Krajenbrink, F., Katz, R., and Poveda, A.: 1969, 'Standing Waves on the Moon', *Nature* **223**, 259.
- Conel, J. and Holstrom, G.: 1968, 'Lunar Mascons: A Near-Surface Interpretation', *Science* **162**, 1403.
- Dence, M. R.: 1964, 'A Comparative Structural and Petrographic Study of Probable Canadian Meteorite Craters', *Meteoritics* **2**, 249.
- Dence, M. R., Innes, M., and Robertson, P.: 1968, 'Recent Geological and Geophysical Studies of Canadian Craters', *Cont. Dom. Obs. Ottawa* **8**, No. 25.
- Fielder, G.: 1961, *Structure of the Moon's Surface*, Pergamon Press, London.
- Fielder, G.: 1963, 'Nature of the Lunar Maria', *Nature* **198**, 1256.
- Fielder, G.: 1967, 'Volcanic Rings on the Moon', *Nature* **213**, 333.
- Gault, D.: 1969, 'Saturation and Equilibrium Conditions for Impact Cratering on the Lunar Surface: Criteria and Implications', *Radio Sci.* **5**, 273.
- Gilbert, G. K.: 1893, 'The Moon's Face', *Bull. Phil. Soc. Wash.* **12**, 241.
- Guest and Murray: 1969, 'Nature and Origin of Tsiolkovsky Crater, Lunar Farside', *Planetary Space Sci.* **17**, 121.
- Hartmann, W. K.: 1963, 'Radial Structures Surrounding Lunar Basins. I', *Comm. Lunar Planetary Lab.* **2**, 1.
- Hartmann, W. K.: 1964, 'Radial Structures Surrounding Lunar Basins. II', *Comm. Lunar Plan. Lab.* **2**, 175.
- Hartmann, W. K.: 1966, 'Lunar Basins, Lunar Lineaments, and the Moon's Far Side', *Sky Telesc.* **32**, 128.
- Hartmann, W. K.: 1968a, 'The Young Craters Tycho, Aristarchus, and Copernicus', *Comm. Lunar Planetary Lab.* **7**, 145.
- Hartmann, W. K.: 1968b, 'Post-Mare and Archimedian Variation', *Comm. Lunar Planetary Lab.* **7**, 125.
- Hartmann, W. K.: 1968c, 'Latitude Dependence and Sources of Impacting Bodies', *Comm. Lunar Planetary Lab.* **7**, 139.
- Hartmann, W. K.: 1970, 'Lunar Cratering Chronology', *Icarus* **13**, 299.
- Hartmann, W. K. and Hartmann, A. C.: 1968, 'Asteroid Collisions and Evolution of Asteroidal Mass Distribution and Meteoritic Flux', *Icarus* **8**, 361.
- Hartmann, W. K. and Kuiper, G. P.: 1962, 'Concentric Structures Surrounding Lunar Basins', *Comm. Lunar Planetary Lab.* **1**, 51.
- Hartmann, W. K. and Yale, F. G.: 1968, 'Mare Orientale and its Basin System', *Comm. Lunar Planetary Lab.* **7**, 131.
- Howard, K. and Offield, T.: 1968, 'Shatter Cones at Sierra Madera, Texas', *Science* **162**, 261.
- Innes, M. J. S.: 1964, 'Recent Advances in Meteorite Crater Research at the Dominion Observatory, Ottawa Canada', *Meteoritics* **2**, 219.
- Johnson, G. G., Vand, V., and Dachille, F.: 1964, 'Additional Rims around Ries Kessel Meteorite Crater', *Nature* **201**, 592.
- Kuiper, G. P.: 1965, 'Interpretation of the Ranger VII Records'. in *Ranger VII. Part II. Experimenters' Analyses and Interpretations*. JPL TR 32-700, 9.
- Lance, R. and Onat, E.: 1962, 'A Comparison of Experiments and Theory in the Plastic Bending of Circular Plates', *J. Mech. Phys. Solids* **10**, 301.
- Lipsky, Y. N.: 1965, 'Zond-3 Photographs of the Moon's far Side', *Sky Telesc.* **30**, 338.
- Marcus, A.: 1965, 'Positive Stable Laws and the Mass Distribution of Planetesimals', *Icarus* **4**, 267.
- Masursky, H.: 1969, 'Preliminary Geologic Interpretations of Lunar Orbiter Photography', in *1969 NASA Authorization*, Ninetieth Congress, 2nd Session, on H.R. 15086, Feb. 19-21, 26-29, 1968, part 3, p. 664.
- Minnaert, M.: 1970, 'The Effect of Pulverization on the Albedo of Lunar Rocks', *Icarus* **11**, 332.
- O'Keefe, J., Lowman, P., and Cameron, W.: 1967, 'Lunar Ring Dikes from Lunar Orbiter I', *Science* **155**, 77.
- Öpik, E. J.: 1966, 'The Stray Bodies in the Solar System, II', in *Adv. Astron. Astrophys.* **4**, 301.

- Pohn, H. A. and Wildey, R. L.: 1970, 'A Photoelectric-Photographic Study of the Normal Albedo of the Moon', *USGS Prof. Paper* 599-E.
- Richey, J. E.: 1961, *Scotland: The Tertiary Volcanic Districts*, 3rd ed. Her Majesty's Stationery Office, Edinburgh.
- Rittmann, A.: 1962, *Volcanoes and their Activity*, Wiley, New York.
- Shemyakin, M. M.: 1969, 'Regularities in Disposition and Dimensions of Lunar Crater Chains', *Solar Syst. Res.* **3**, 53.
- Stevenson, W. H.: 1919, 'The Lunar Furrow', *JBAA* **29**, 164.
- Strom, R. G. and Fielder, G.: 1970, 'Multiple Eruptions Associated with Tycho and Aristarchus', *Comm. Lunar Planetary Lab.* **8**, 235.
- Stuart-Alexander, D. and Howard, K.: 1970, 'Lunar Maria and Circular Basins - a Review', *Icarus* **12**, 440.
- Sukhanov, A. L.: 1968, 'The Mechanism of Origin of the Lunar Seas with Comments by E. Hope and G. Jones', *Dokl. Akad. Nauk. SSSR* **181**, 309, Transl. Def. Scien. Inf. Serv., DRB, Canada, T-507 R.
- Taylor, F. and Dence, M.: 1969, 'A Probable Meteorite Impact Origin for Mistastin Lake, Labrador', *Can. J. Earth Sci.* **6**, 1.
- Urey, H. C.: 1952, *The Planets*, Yale University Press, New Haven.
- Van Dorn, W. G.: 1968, 'Tsunamis on the Moon?', *Nature* **220**, 1102.
- Van Dorn, W. G.: 1969, 'Lunar Maria: Structure and Evolution', *Science* **165**, 693.
- Wilshire, H. and Howard, K.: 1968, 'Structural Patterns in Central Uplifts of Crypto-Explosion Structures as Typified by Sierra Madera', *Science* **162**, 258.
- Wood, C. A.: 1968, 'Statistics of Central Peaks in Lunar Craters', *Comm. Lunar Planetary Lab.* **7**, 157.
- Zabelin, E. I. *et al.*: 1968, 'Statistical Classification of Ring Structures on the Moon and Mars and Their Diameters', *Solar Syst. Res.* **2**, 176.